8-14-2020 11:00 AM

A Clinically Representative Rat Model of Hip Hemiarthroplasty

Adam DM Paish, *The University of Western Ontario*

Supervisor: Holdsworth, David W, *The University of Western Ontario*

A thesis submitted in partial fulfillment of the requirements for the Doctor of Philosophy degree in Medical Biophysics

Abstract

Joint replacement is an increasingly common surgery with over 130,000 procedures performed annually in Canada. Although joint replacement surgery is highly successful, implants do not last a lifetime, and often have to be replaced via costly revision surgeries. Before innovations aimed at extending the life of implants are applied to the clinic, testing must be performed in animal models. Clinically representative small-animal models of joint replacement would be ideal in the initial stages of research and development, due to ease of handling and low costs, but few such models have been established in the literature. Thus, we describe the development of a clinically representative rat model of hip hemiarthroplasty.

A database of micro-computed tomography volumes of skeletally mature male Sprague-Dawley rats was analyzed to quantify the dimensions of the proximal rat femur. This was done in order to guide the creation of a parameterized rat-hip implant in computer-aided design software. Sets of rat-specific femoral implants were then produced in medical-grade alloys using additive manufacturing. Implants were then installed into cadaveric, and then live rats. Micro-computed tomography imaging was used to evaluate the position of the implant within the proximal femur longitudinally. Animals also underwent a gait analysis protocol using a commercially available CatWalk XT system, in parallel with an X-ray fluoroscopy protocol, whereby animals were imaged while running on a custom made radiolucent treadmill.

Surgeries were successful in live animals; rats were able to tolerate the procedure and were observed ambulating on their affected limbs immediately following recovery from anaesthesia. Micro-CT imaging revealed clinically representative complications (implant subsidence) in some animals that mimic complications found in larger models. Functionally

loaded implants were observed in the remaining animals at twelve weeks, postoperative. Rats were successful in completing gait analysis protocols on both the Catwalk and fluoroscopic treadmill systems. Animal gait was restored following hemiarthroplasty.

We report the first clinically representative rat hip hemiarthroplasty surgeries using custom 3D-printed metal implants. This thesis supports the feasibility of this model as a preclinical platform for basic scientists to study osseointegration, metal-on-cartilage interactions, and joint infection around a functional implant.

Keywords

Hip; hemiarthroplasty; arthroplasty; clinically representative animal model; micro-computed tomography; additive manufacturing; selective laser melting; titanium; cobalt-chrome; stainless steel; computer-aided design; gait analysis; x-ray fluoroscopy; laser powder-bed fusion; rat; Sprague-Dawley

Summary for Lay Audience

Joint replacement surgery is an increasingly common procedure, performed to relieve the pain of cartilage damage caused by osteoarthritis, or to restore joint function following a traumatic injury. While joint replacement surgery is highly successful, implants don't always last a lifetime. When implants fail to function properly, they must be replaced via revision surgeries; these procedures are higher-risk, more complex and more costly compared to initial joint replacement surgeries, and therefore are to be avoided or delayed if possible. Consequently, scientists continue to research new ways to extend the life of implants, and reduce the burden of revision surgeries. However, before new innovations can be applied to the clinic, testing in animal models is often required. Historically, large animals (such as sheep) have been used to test joint implants, but these trials are expensive to conduct, and there are sometimes ethics concerns of testing in more sentient species. Small lab animals are more readily available, but joint implants are not easily manufactured in the sizes required for small animal testing. In this thesis we describe an approach to create custom small-animal implants, through the use of image-based design and 3D-metal printing. We also demonstrate the installation of these implants in rats, followed by 3D imaging and analysis of animals walking after surgery. Our rat hip implant model presents a new research tool for scientists who are looking to find ways to extend the life of implants, so that patients can maintain lifelong mobility with fewer surgical interventions.

Co-Authorship Statement

The following thesis contains three manuscripts that range from "in press" to "in preparation" for a peer-reviewed scientific journal. Chapter 2 is an original research article entitled "Image-based design and 3D-metal printing of a rat hip implant for use in a clinically representative model of joint replacement" and was published online ahead of print in the Journal of Orthopaedic Research, May 2020. Permission to reuse this article in this thesis was obtained from John Wiley and Sons (see Appendix). This manuscript was co-authored by Adam DM Paish, Hristo N Nikolov, Ian D Welch, Alexander O El-Warrak, Matthew G Teeter, Douglas DR Naudie and David W Holdsworth. Author contributions were as follows: ADMP: substantial contributions to research design, image analysis, implant design, performing surgery, and the acquisition, analysis and interpretation of data, in addition to overall management and execution of the research project. HNN: substantial contributions to analysis or interpretation of data, component design and manufacturing. IDW and AOE-W: substantial contributions to research design, performing surgery, and the acquisition, analysis or interpretation of data. MGT: contributions to research design. DDRN: contributions to research design, implant design, and surgical approach. DWH: substantial contributions to research design, and analysis and interpretation of data, and was responsible for the project's inception and funding. All authors were involved in drafting the paper, revising it critically, and approving the submitted and final versions.

Chapter 3 is an original research article entitled "Longitudinal micro-computed tomography of a rat model of hip hemiarthroplasty using 3D-printed titanium implants" and is in preparation for the Journal of Orthopaedic Research. This manuscript was co-authored by Adam DM Paish, Emily A Truscott, Hesham Abdelbary, Matthew G Teeter, Douglas DR

Naudie and David W Holdsworth. Author contributions were as follows: ADMP: substantial contributions to research design, image analysis, implant design, performing surgery, implant manufacturing, and the acquisition, analysis and interpretation of data, in addition to overall management and execution of the research project. EAT: substantial contributions to research design, performing surgery, and the acquisition, analysis or interpretation of data. AH: contributions to surgical approach and research design. MGT: contributions to research design. DDRN: contributions to research design, implant design, and surgical approach. DWH: substantial contributions to research design, and analysis and interpretation of data, and was responsible for the project's inception and funding.

Chapter 4 is an original research article entitled "Post-operative gait analysis in a rat model of hip hemiarthroplasty" and is in preparation for the Journal of Orthopaedic Research. This manuscript was co-authored by Adam DM Paish, Emily A Truscott, Steven S Pollman, Matthew G Teeter, Douglas DR Naudie and David W Holdsworth. ADMP: substantial contributions to research design, image analysis, gait protocol creation, image edge enhancement design, performing surgery, implant manufacturing, treadmill design, and the acquisition, analysis and interpretation of data, in addition to overall management and execution of the research project. EAT: substantial contributions to research design, performing surgery, treadmill safety evaluation, and the acquisition, analysis or interpretation of data. SSP: substantial contributions to treadmill design, manufacturing and implementation, imaging protocol implementation and data acquisition. MGT: contributions to research design. DDRN: contributions to research design, implant design, and surgical approach. DWH: substantial contributions to research design, and analysis and interpretation of data, and was responsible for the project's inception and funding.

Acknowledgments

I would first like to thank and acknowledge my primary supervisor, Dr. David W Holdsworth. David is a pioneer in preclinical imaging, who has boundless energy and insight that has lead him towards substantial contributions to the fields of Medical Imaging and Musculoskeletal Health Research over many years. I will always be grateful for his guidance, candor, and for taking a chance on a "Baseball Player" who wanted to become a Medical Biophysicist. From him I have learned how to plan and execute research at the highest level, problem solve effectively, and communicate scientific information in an accessible way. In addition to Dr. Holdsworth, I would also like to my other advisory committee members and mentors, Dr. Matthew G Teeter and Douglas DR Naudie for their continued patience, support and advice over the many years of trial and error that it took to develop this model. Dr. Teeter and Dr. Naudie always took the time to advise me on both academic and personal goals, which helped me to develop confidence as a young scientist. Dr. Teeter in particular was always the first to add edits and insight to my written works, and Dr. Naudie was essential for helping me to generate and communicate work that was relevant to orthopaedic surgery, and even let me observe several surgeries in the OR. I would also like to thank Dr. Aaron D Ward, who both in his capacity as Graduate Chair of Medical Biophysics and as my Pedagogy Professor, helped to ensure my work was completed at the highest level. Dr. Ward is one of the most organized and scientists I have ever had the fortune of knowing. Learning from how he conducts himself was critical to my professional and personal development, particularly in this final year of my PhD candidacy, where I had to also balance responsibilities of being a Western Medical Innovation Fellow and a new father.

Next I would like to thank the members Holdsworth Imaging group at the Robarts Research Institute for their many years of advice, help and support. I will be forever appreciative of the support, insights, criticism and friendships I gained from this group over my graduate training. In particular, I would like to acknowledge the technical support I received from Hristo N Nikolov, Steven S Pollamn, Dr. Joseph U Umoh, Chris Norley, Dr. Danny Poinapen, Alex Kopacz, Dr. Sarah Detombe and Tom Chmiel, which made this work possible. I would also like to mention two of my peers, Dr. Justin J Tse and Dr. Daniel Lorusso, with whom I shared the majority of my graduate training within the Bone and Joint Institute. I will be forever grateful that I got to share this journey with you both, and will fondly remember our daily discussions, conference trips, and afternoons spent at the Grad Club together.

I must also acknowledge the team at Western Animal Care and Veterinary Services, who made my countless trips to both Medical Sciences and West Valley Buildings a pleasure. In particular Dr. Ian D Welch and Dr. Alex O El-Warrak both provided me with many hours of advice and time that were essential to both the development of this model and me as a person over the initial years of this project. Heather-Anne Cadieux-Pitre and the veterinary technician staff at ACVS were always most helpful and contributed to the highest-level surgery and animal care that our rats received. Dr. Patti Kiser graciously provided her time in conducting post-mortems and histopathology. Finally, I could not have completed this work without Dr. Emily A Truscott, with whom I hope to be a lifelong collaborator. Your surgical prowess helped make this refined model a reality, and I enjoyed all of our discussions over apple sandwiches. We should also acknowledge the rats, from “Arnold” to “Q-tip”, who were sacrificed to allow this work to be possible.

I will also be grateful to Dr. Hesham Abdelbary and Dr. Mariam Taha from the Ottawa Hospital, who recognized the value in this model and helped us to refine the surgical approach to permit repeated installation of implants. I appreciate our continued collaboration to optimize this model for periprosthetic joint infection research. Many thanks as well go out to Milko Lamos and Pavel Belenkov from Schulich Dentistry for the time and expertise they gave me regarding implant polishing and post-processing.

Financial support of my graduate training was graciously provided by Western University, through a Western Graduate Research Scholarship, Schulich Graduate Scholarship, and a Transdisciplinary Training Award from the Bone and Joint Research Institute. I also was supported by a Canadian Institutes of Health Research Strategic Training Initiative in Health Research Award, administered through the Joint Motion Program at Western. Thanks as well to Shannon Woodhouse and team for all of their work in administrating the Collaborative Training Program in Musculoskeletal Health Research, which I was fortunate to be a part of throughout my graduate training.

Finally, I would like to acknowledge the support of my family and friends for their constant support and encouragement during my PhD training, especially my parents, David G Paish and Carolyn R McCready, my siblings Annie, Andrew and Alexander, and Grandparents Donald, Arlene, David and Rosemarie. And to my partner Emily and daughter Hailey – no words can express how much your love and support mean to me, and I will be forever grateful to this work for bringing us together. There is no doubt, that the greatest results to come out of this thesis work were both of you.

Table of Contents

List of Tables

List of Figures

List of Appendices

List of Abbreviations

2D	two-dimensional
3D	three-dimensional
AM	additive manufacturing
AP	anterior-posterior
CAD	computer-aided design
cm	centimeter
CT	computed tomography
Fig.	Figure
FOV	field-of-view
Gy	Gray (dose)
Hz	Hertz (1/s)
kVp	peak kilovoltage
mA	milliamperage (tube current)
mGy	milli-Gray
Micro-CT	micro-computed tomography
ML	medial-lateral
mm	millimeter
OA	osteoarthritis
PJI	periprosthetic joint infection
PJR	partial joint replacement
s	second
SS	stainless steel
SLM	selective laser melting
Ti6Al4V	titanium-6-alumnium-4-vanadium
TJR	total joint replacement
V	volts

Dedication

This thesis is dedicated to my late Grandfather, Dr. Donald G Paish Jr., MD, who grew up poor, served in the United States Army, and became an outstanding Orthopaedic Surgeon. Dr. Paish dedicated his professional life to patient care, above all else. He never required payment from any of his patients, insisting that those who required help should be given it. This philosophy of care put him at odds with a certain healthcare center in Chicago that he was practicing at during his residency. A man of principle, he left and started a clinic in the Bronx, NY, serving many patients who were not well off. A man of faith, he had a particular affection for members the clergy, whom he never once charged for care. Eventually he moved his practice upstate, where he continued to serve the NY capitol region for many years, and raised a family of four children with his wife Arlene. Eventually his career was cut short when he developed Parkinson's disease, which eventually contributed to his death in 2011. However, his life-long passion of caring for and serving others, particularly his love of Orthopaedic Medicine, endures through the works presented in this thesis.

During the difficult years of my training, where nothing seemed to be going right, I found resilience by recalling how he would describe difficult cases, emphasizing that it is a surgeon's responsibility to "get it right", to the best of their ability. Without the love and support he gave me during his life, this work would not have been possible. Thank you Grandpa for your enduing legacy of care. You truly were a hero to so many, especially me.

Chapter 1

1 Introduction

1.1 Hip Joint Replacement in Canada

Each year approximately 130,000 Canadians undergo joint replacement surgery, and of these, approximately 58,000 are hip replacement procedures.[1] Joint replacement is predominantly performed as a last resort to alleviate joint pain caused by degenerative osteoarthritis (OA).[1] Total joint replacement (TJR) surgery, also known as total joint arthroplasty, is the most common surgery performed, to alleviate OA pain.[1] This procedure involves the installation of implants into the bone on either side of a joint surface, which serve to replace painful, worn-out cartilage. The most common TJR approach in the hip is to install a titanium-alloy prosthesis (stem) into the proximal femur via a press-fit (cementless) approach.[1-3] The stem is attached via a tapered fit to a smooth ball, typically made of either cobalt-chrome alloy or ceramic (as titanium does not have favourable wear properties), which acts as a bearing surface within the acetabular component (cup).[3] The cup's shell is typically made of titanium alloy, which houses a highly cross-linked ultra-high molecular weight polyethylene (XLPE) liner on the inner surface that articulates with the ball.[3] Cups serve to replace worn acetabulum cartilage, and are also commonly installed via an uncemented approach into the pelvic bone.[4] The annual cost of joint replacement surgery in Canada is 1.2 billion dollars, with an average cost of 11,500 dollars per procedure for primary hip replacement surgery.[1]

Patients who have experienced a traumatic injury to bone, such as a femoral neck fracture, may also require joint replacement surgery, but may not undergo TJR if their cartilage is intact.[5-7] In these cases, a hemiarthroplasty, or partial joint replacement (PJR) may be performed, whereby an implant is installed that articulates with cartilage, replacing only the injured side of the joint. In fact, the first modern hip implant was a hemiarthroplasty implant that replaced the femoral head, made of "Vitallium", a cobalt-chrome alloy.[8] Currently, hip hemiarthroplasty is most commonly performed to replace the proximal femur, in patients who have suffered an acute femoral neck fracture.[1; 5-7; 9]

While primary joint replacement surgeries are highly successful, with a success rate of approximately 97% at five post-operative years,[1] implants do not last a lifetime. At ten post-operative years, 85% of uncemented hip implants remain functional, but this number drops to 70% at 15 post-operative years.[2; 10] Implants can fail for various reasons; the most common reasons for failure are aseptic loosening (Figure 1.1), implant instability, infection, and periprosthetic fracture.[1; 2] As an implant fails, it becomes increasingly painful, and eventually must be removed to preserve the patient's quality of life. Procedures to remove failed components are known as revision surgeries, which account for around 10% of all hip replacement surgeries in Canada, costing approximately 163 million dollars annually.[1] Revision surgeries are more complex than primary joint replacement surgeries, have higher morbidity, and are more expensive to manage than primary TJR cases.[1; 11; 12] Patients are typically older, and there is less bone for the surgeon to work with, as more bone must be removed with each successive surgery to remove and re-install implants. These factors contribute to why revision

surgeries are to be avoided whenever possible, and why extending the longevity of primary joint replacement implants remains an active area of research.

Figure 1.1: An uncemented total hip replacement implant *in situ*. Black arrows reveal radiolucency zones at the femoral stem, indicating aseptic loosening. Image is reused from Apostu et al, 2017,[2] an open-source article published by Sage Journals, distributed under the terms of the Creative Commons License CC BY-NC 4.0 (see: creativecommons.org/licenses/by-nc/4.0/) (copyright license not required to reuse in this thesis).

In the case of PJR, originally intact cartilage can begin to wear out over time, leading to OA as it is cyclically loaded against the often harder, metal surface of the

implant. In this scenario, the PJR must be revised to a TJR to replace the worn-out cartilage. Implants can also fail from periprosthetic joint infection (PJI), which incurs especially high associated costs and morbidity.[11] Although PJI is relatively rare, affecting only around 1% of patients who undergo primary joint arthroplasty, PJI is the most common source of surgery-contracted infections in hospital inpatients in the industrialized world, due largely to the high volume of joint replacement surgeries performed annually.[11; 13] Infected implants must be removed and replaced, requiring one or more revision surgeries, in addition to aggressive antibiotic therapy.[11; 13]

Because joint replacement surgery is so common in the industrialized world, even a low failure rate of a few percent translates to thousands of patients annually who experience complications from failed components.[1] For this reason, the development of innovations that can improve the function and longevity of joint replacement implants remains an active area of research in the medical sciences.

1.2 Animal Models in Preclinical Orthopaedic Research

Before innovations can be applied to the clinic, preclinical development and testing is required in animal models. Numerous factors can be considered when selecting an appropriate animal model for preclinical orthopaedic research and development, including joint biomechanics, physiological parameters (lifespan, metabolic rate, age, sex, weight, healing rate, etc.), post-operative function, cost and ease of handling.[14] The type of implant or feature that is being tested and the stage in the development pipeline are also important to consider, where more clinically representative models should be

chosen to immediately precede human trials. Typically there are two classes of animal models to select from, small and large, each with its own advantages and disadvantages.

1.2.1 Large-Animal Models of Joint Replacement

Traditionally, large-animals have been utilized as clinically representative models of joint replacement, to investigate research questions related to the bone-implant interface, prosthetic material composition, implant design and mechanics, tribology and systemic effects secondary to joint replacements.[14; 15] Examples of large-animal models of joint replacement include sheep,[16-21] pigs,[22; 23] goats,[24; 25] dogs,[26-29] horses,[30] and non-human primates.[24] Large animal models are often utilized because their joints are of similar size to humans; this allows hardware to be installed that either mimics, or is equivalent to, the implants used in human joint replacement surgery. However, large-animal studies are expensive to conduct, incurring high procurement and housing costs, and require specialized facilities that are not available at all institutions. There are also ethical concerns around the use of large-animal models that may hinder knowledge translation beyond the research and medical communities.[31] For these reasons, large-animal studies are commonly conducted in the later stages of preclinical research and development, where the efficacy of a given innovation has already been supported in small-animal studies, which are comparably lower in costs and have fewer ethics barriers to overcome.

1.2.2 Small-Animal Models in Preclinical Orthopaedic Studies

Small-animal models, such as mice,[32-35] rats,[14; 36; 37] rabbits,[37; 38] and guinea pigs[39-41] have several advantages compared to large-animal models that make them more

attractive options in the initial stages of research and development. These advantages include low procurement and housing costs, higher throughput potential, less variability between subjects, and broad use across medical science research disciplines. Small-animal models have been used to study concepts such as osseointegration,[36-38; 42] the integration of new bone into the surface of an implant, and peri-prosthetic joint infection (PJI),[11; 32; 35; 43] the pathologic growth of bacteria around an implant within the joint. Historically, small-animal implant studies utilize devices that that are non-functional, such as intracortical rods,[36; 42] pins,[44-46] and screws,[47] which do not articulate within the joint space, unlike clinical joint replacement implants. This discrepancy is largely due to the fact that simple metal implants are easier to manufacture in the sizes required for small-animal testing, compared to the more complex geometry of joint replacement implants. Consequently, small-animal models are typically not used as clinically representative models of joint replacement, unlike their large-animal counterparts; however, this could be overcome if joint replacement hardware could be developed in the sizes required for small animal testing.

The first small-animal model that utilized a functional joint implant was described by Powers *et al*., who piloted a cemented model of hip arthroplasty in the rat, using custom rat-specific implants.[14] This study demonstrated that the creation and installation of components in the sizes required for small-animal testing was feasible and that animals could recover ambulation post-operatively, but had limitations that have prevented this rat model from being widely adopted, including: (i) resection of the greater trochanter to access the proximal medulla of the femur, compromising post-operative functionality of the hip joint, (ii) low rates of stability of the screw-fixed acetabular component due to the

thin rat pelvis, and (iii) the use of a non-conformal implant inside the proximal femoral anatomy, which required bone cement to be used for fixation – a less commonly performed procedure in the present day.[1; 14]

While the development and surgical implantation of implants in a small-animal model such as the rat hip model is inherently challenging, the advantages of its potential use in preliminary orthopedic research have warranted further investigation in recent years. The orthopaedic community has also recently called for more clinically representative small-animals models to facilitate an increase our in understanding of PJI in particular, as efforts to prevent cases of infection have become a major priority in joint arthroplasty research.[11; 35; 43] Ideally the implant used in a small-animal study should be designed specifically to the species' joint anatomy, in the same way that human and large-animal components are tailored to fit precisely in the joint of interest. To create and test custom implants in the scale required to be anatomically conformal to small animal models, a non-traditional approach to manufacturing, such as additive manufacturing should be explored.

1.3 Additive Manufacturing for Rapid Prototyping of Implants

Carli *et al.* recently described a mouse model of knee hemi-arthroplasty for PJI studies that utilized additive manufacturing (AM) to develop a mouse-specific knee implant in medical-grade titanium alloy.[32; 35] AM is a technique that produces objects in a layer-by-layer fashion, whereby material is added on top of the previously built layer until the full volume of the object is created.[48] This technique relies on computer-

generated three-dimensional (3D) models to manufacture parts, and does not require part-specific moulds or specialized cutting tools to remove material from a block like in sculpting (subtractive manufacturing), reducing tool costs.[48] A multitude of different components can also be manufactured concurrently within a given build volume, with a negligible amount of wasted material (support structures to secure parts during construction, like scaffolding). AM has been widely explored for surgical applications in recent years;[48-50] implants and surgical tools can be made to be highly conformal to the anatomy of interest (patient-specific), which is beneficial for both the surgeon and the patient.[48] Other advantages of AM include: (i) reduced component weight, since material only needs to be placed where essential to construct a part; (ii) rapid design iterations, since design changes to a part are made digitally and can be easily re-printed as needed; (iii) complex geometries can be built, such as thin walls and internal structures like lattices and pores that would be virtually impossible to produce via conventional manufacturing techniques; and (iv) increased design freedom, since AM parts are not constrained by traditional manufacturing and design rules.[48; 50-52] AM options exist for a wide variety of materials, but the most pertinent to preclinical orthopaedic research is additive manufacturing in medical-grade alloys including 316L stainless steel, ASTM F75 cobalt-chrome, and Ti6Al4V titanium alloy, which have the same biocompatibility as human orthopaedic implants.[48; 53]

1.3.1 Selective Laser Melting

As mentioned above, AM machines produce objects in a layer-by-layer fashion, whereby material is added on top of the previously built layer until the full volume of the object is created[48] (Figure 1.2). Selective Laser Melting (SLM) is an AM technique that

relies on a high-powered infrared laser, which is directed by a computer-controlled lens to heat and melt specific sites on a single layer of metal powder, creating small pools of molten metal. As the metal cools it adheres to the metal layer below and solidifies. The initial layer of an SLM build is constructed on a solid metal platform, which drops down by a specified distance to allow a second layer of metal powder to be placed above the first layer. The laser then selectively melts sections of the second layer, which adheres to material from the first layer. This process is then repeated until all parts are constructed. The metal powder that surrounds the solid metal parts is then removed and can be reused in future builds. The metal platform and build parts are then removed together from the SLM machine, which is an enclosed space with a controllable atmosphere (some metals react with oxygen and require an inert atmosphere such as Argon gas). Next, parts are often heat-treated to relieve stresses in the metal that accumulate during the building process.[55] Finally the parts and any support structures are removed from the metal platform. Parts then undergo whichever post-processing technique is required for them to meet their intended design specifications. SLM parts have an inherent surface texture that is related to the average grain size of the metal powder being used for their construction; the molten metal pools capture adjacent powder particles as they solidify. Sandblasting followed by polishing with a rotary tool is often required to create a smooth surface on SLM parts. SLM is capable of producing parts in a variety of medical-grade metal alloys, making this an ideal technique for creating novel orthopaedic implants and custom-surgical tools[48] that could be applied towards the development of novel small-animal models of joint replacement surgery.[35]

Figure 1.2: A Renishaw plc AM 400 selective laser melting 3D printer (ADEISS Canada, London, Ontario) capable of building parts in medical-grade metal alloys.

1.3.2 Computer-Aided Design of Implants

Computer-aided design (CAD) software facilitates the creation of 3D geometries that can be printed as parts through additive manufacturing.[48] Implants specifically, can be designed virtually to create a geometry that fits within the anatomical constraints of the species of interest. Once an initial implant prototype has been designed in CAD, changes can be made, based on feedback from surgeons and data collected from *ex vivo*

and *in vivo* trials, to further optimize the component. Custom surgical tools can also me made via the same approach, to help facilitate the installation of components. Since implants are not one-size-fits all, several sizes of an implants can also easily be produced to accommodate range of bone volumes, by utilizing a scaling feature that allows for percentage changes in the overall volume of the component. CAD ultimately allows for a high level of design freedom, which is optimal in iterative prototyping of a new custom implant for a small-animal model. This means that information obtained from cadaveric and live animal trials can inform design changes to both implants and surgical tools, to improve the surgical procedure. However, CAD models must first be parameterized so that implants fit precisely within the bone of interest and remain stable; for this to occur, accurate measurements of the bony anatomy of the joint of interest must first be made.

1.4 Micro-Computed Tomography

Micro-computed tomography (micro-CT) is well described and mature imaging technique that can facilitate the visualization and characterization of dense x-ray attenuating structures within the body, especially bone[56-59]. Micro-CT also allows for 3D imaging of implanted objects, particularly prosthetic devices,[60; 61] which are well represented within micro-CT volumes compared to other imaging modalities.[62] Briefly, micro-CT imaging involves the generation of X-rays (from an X-ray source) followed by the projection of x-rays through a sample at multiple angles. A detector then captures X-rays that make it through the sample; the x-ray absorption (attenuation) along each ray path is determined from the number of X-ray photons that are captured. More electron-

dense regions within the sample will attenuate more X-rays, giving each ray path a unique signal intensity value.

Micro-CT volumes are comprised of several hundred two-dimensional (2D) projections, collected at multiple angles around the specimen of interest. 3D volumes are then produced via the reconstruction of the scanned volume using established algorithms such as filtered back-projection; this algorithm is implemented on cone-beam scanners (Figure 1.3), where the detector is a 2D grid of elements that captures x-rays emitted from a focal point source.[63] Within the 3D volume, each volumetric element (voxel) is assigned a CT number, which is proportional to the linear attenuation coefficient of the material within that voxel.[64] Electron-dense objects like bone have a high CT number, and less dense objects, like soft tissues, have a low CT number.[65]

Figure 1.3: A Locus Ultra cone-beam micro-computed tomography scanner (GE Medical, London, Ontario, Canada) for preclinical animal imaging.

Sometimes extremely electron-dense objects like metal can present a problem (beam-hardening) when imaged on most biomedical micro-CT scanners.[66] Beam hardening is a process that occurs when an emission of polychromatic x-ray photons passes through an electron-dense material of relatively high atomic number, resulting in the selective attenuation of lower energy photons. This leads to bright and dark artifacts in the image volume that can compromise the ability to interrogate the tissue around

metal objects. However, the implementation of a modern beam-hardening correction algorithm during image reconstruction can help to mitigate this problem and preserve image quality around a metal implant.[66]

Another benefit of micro-CT is that an animal can be imaged longitudinally at several time-points during the course of a study; this is advantageous as animals do not need to be sacrificed at each time-point, as would be required for conducting a conventional histological analysis of bone. Imaging software also exists that facilitates the ability to take precise quantitative measurements of the anatomy of interest from micro-CT image volumes.[65; 67] Thus, micro-CT is an ideal imaging modality for quantifying the bony anatomy of a small animal species, with the intent of creating a parameterized CAD model of an implant.

1.5 Surgical Procedure Considerations

When creating a novel implant, via 3D CAD design and additive manufacturing, it is necessary to consider the constraints of the surgical procedure that will be used to install the component.[48] Hip replacement first requires that the surgeon access the hip by retracting the surrounding muscle layers in order to create a visual field of the femoral-acetabular joint. An incision is then made into the joint capsule to allow the hip to be dislocated. The femoral head and neck are then resected to permit access to the proximal femoral medulla, so that it can be incrementally widened to the proper size to accommodate an implant.[68; 69] The femoral component is then inserted and fixed to the bone using bone cement, or via a press-fit (uncemented/cementless) approach.[9; 10; 70] Choice of technique is determined by surgeon preference, but is influenced by the quality

and amount of available bone (lower quality medullary bone often requires a cemented approach).[71] For a total hip arthroplasty, the acetabulum is reamed and a metal cup is either press-fit or cemented into the pelvis to articulate with the femoral implant; for a hip hemiarthroplasty, the femoral implants' head is left to articulate with the native acetabulum.[6-8; 71] The joint capsule is then sutured closed followed by deep to superficial muscle layers and the incision site.

A technically challenging part of hip arthroplasty is the precise shaping of bone to accommodate the femoral implant.[68; 72-74] In human surgery this process relies on specialized tools that can now be guided by computer-assisted surgery devices or surgical robots.[72-74] Unfortunately this equipment is not available for small-animal applications. Coupled with the need to access a proportionally smaller joint during small animal surgery, it is critical to try and establish a surgical field that makes preparation of the proximal femoral medulla as easy as possible, in order to ensure implants are installed properly. Thus, achieving a surgical approach that is repeatable will likely require the development of specialized tools, and will certainly involve the trial of different approaches to access the hip in both ex vivo and in vivo subjects. Implants must also be designed appropriately so that it they can be installed consistently within the bone and preserve the bony and muscular anatomy in order to facilitate functional motion on a stable implant, post-operatively.

1.6 Rodent Gait Analysis

Once implants are customized to accommodate the small-animal hip joint, and can be installed consistently into live animals, recovery of ambulation should be assessed,

in order to verify that implants are serving their intended purpose of being functionally loaded post-operatively. Commercial optical imaging systems exist (CatWalk XT) that provide quantitative measurements that can be used to assess gait in rats[75-79] and mice.[80-82] CatWalk XT systems incorporate a long rectangular enclosure that the animals can run through, with a camera system that can track their paw prints from underneath the floor. The enclosure has a ceiling that emits red light, and a glass floor that encases green light, emitted in parallel along the floor. When animals step on the glass surface, the green light, which is normally internally reflected within the glass, is reflected down, creating a green paw print that is easily viewed against the red backdrop by the camera mounted at a prescribed distance underneath the glass.[83; 84] Steps within the cameral field-of-view (FOV) are recorded via digital video by the camera system. Relative print intensities, step frequency and print area are a few of the many metrics that such systems are able to collect. CatWalk XT gait analysis is commonly used in neurological studies investigating phenomena such as pain,[85] stroke,[80] and spinal cord injury[86], as well as in musculoskeletal studies involving conditions such as compartment syndrome[87] and osteoarthritis.[79]

Figure 1.4: CatWalk XT system (Noldus, Leesburg, Virginia) for murine gait analysis. The system includes a glass-floored walkway, with one open end; the other end contains an enclosure that houses the animal's cage. A camera captures fluorescent light that is reflected downward when the animal makes contact with the glass floor. Image is reused from Kappos et al 2017;[84] an open-source article published by John Wiley and Sons and distributed under the terms of the Creative Commons License, CC BY (see: creativecommons.org/licenses/) (copyright license not required to reuse in this thesis).

Utilizing this well-established approach would be ideal for determining to what extent animals are able to recover their gait following hip replacement surgery. However, one deficit of optical imaging techniques, as it pertains to studying joint replacement, is that they are unable to facilitate visualization of the implant as it articulates within the

joint space; this ability is important as it can provide useful insight into implant function during movement. In some cases, quadrapedal animals are able to ambulate without a functional hip joint, due to compensation by surrounding muscles.[27] If an implant were to become unstable during a longitudinal study (a common complication is implant loosening within the femur),[1; 2] optical gait analysis alone may not be sensitive enough to detect subtle changes at the hip joint that could influence whether or not an implant is functional.

X-ray fluoroscopy is a well-established technique for collecting sequential images of internal anatomic structures for a variety of indications in both humans[88-90] and animals.[91; 92] Fluoroscopy machines consist of an x-ray source and a detector that can generate and store many x-ray images per second that can be compiled to create an x-ray video of the structure of interest. This technique is especially useful when investigating the cyclic loading of joints, which are difficult to observe using static imaging. Treadmills are often used in conjunction with X-ray fluoroscopy systems, so that several gait cycles can be collected consecutively while the subject remains in the field of view between the x-ray source and the detector. Treadmills are commonly used in preclinical research, but an ideal treadmill would be made of materials that are radiolucent so that the subject of interest could be imaged within an unimpeded FOV.[91] Such a setup would provide data that when used in concert with optical imaging, can be used to create a complete picture of gait recovery following hip replacement surgery in a small-animal model.

1.7 Thesis Objectives and Hypotheses

In this thesis, we present the methodologies required to: (i) design a novel, preclinical hip implant for use in a rat model of hip hemiarthroplasty; (ii) consistently install rat hip implants and longitudinal track implant position post-operatively using micro-CT imaging, and; (iii) ascertain the extent to which a cohort of rats with femoral implants recover their gait at several post-operative timepoints following hip hemiarthroplasty. The key content described in each Chapter is summarized as follows.

In Chapter 2 our aim was to obtain micro-computed tomography derived measurements of the rat proximal femur, to create parameterized rat hip implants that could be surgically installed in a clinically representative small animal model of joint replacement. The proximal femoral anatomies of N=25 rats (male, Sprague-Dawley, 390-605g) were quantified and averaged. Key anatomical measurements were used to parameterize computer-aided design models of monoblock rat femoral implants. Linear regression analysis was used to determine if rat hip dimensions could be predicted from animal weight. A correlation analysis was used to determine how implants could be scaled to create a range of sizes. Additive manufacturing (3D printing) was used to create implants in medical-grade metal alloys. Linear regressions comparing rat weight to Femoral Head Diameter and Neck-Head Axis Length revealed a significant non-zero slope ($p<0.05$). Pearson's correlation analysis revealed five significant correlations between key measurements in the rat femur ($p<0.05$). Implants were installed into both cadaveric and live animals; iterative design modifications were made to prototypes based on these surgical findings. Animals were able to tolerate installation of implants, and

were observed ambulating on their affected limbs post-operatively. Overall, we established a preclinical joint surgery model using image-based and iterative design techniques to create 3D-metal printed implants in medical-grade metal alloys for a small-animal model. Our findings support further development of this functional rat hip model for use as a low-cost translational test platform for preclinical orthopaedic research into areas such as osseointegration, metal-on-cartilage wear and peri-prosthetic infection.

In Chapter 3 we describe the surgical installation of custom-designed unipolar rat femoral implants, which were created in five sizes and 3D-printed in titanium alloy. The cementless components were press-fit into the medullary canal of skeletally mature male Sprague-Dawley rats (N=6), using a posterior approach to access the hip joint. Animals were evaluated post-operatively (day 1) and at six time-points following surgery with in vivo micro-computed tomography to assess implant stability. Animals were sacrificed after 12 weeks and post-mortem analysis was conducted to assess fixation of each implant. Surgery was successful in all animals, and micro-CT imaging revealed stable implant positioning at 1 day and 1 week, post-operatively. Return to gait was observed in all cases, and rats remained ambulatory throughout the study. No incidences of implant failure were observed through the 3-week time-point. Micro-CT did, however, reveal implant subsidence in three of six animals at the 6-week time-point, resulting in hip subluxation. Post-mortem analysis revealed variable amounts of micro-motion when implants were manipulated with forceps, with more gross movement detected in subsided implants. We report the first clinically representative rat hip hemi-arthroplasty surgeries using custom 3D-printed titanium alloy implants. Clinically relevant complications were observed (subsidence) that mimic complications of larger joint models. These findings

support the use of this model as a preclinical platform that could be expanded for studies of osseointegration, metal-cartilage interactions, and joint infection around a functional implant.

In Chapter 4 we describe the post-operative gait of five rats (male, Sprague-Dawley) following hip hemiarthroplasty. Rats were trained to walk across a CatWalk XT system, incentivized by cereal treats. Pre-operative data were collected prior to surgery and at 3, 6, 9, and 12 weeks postoperatively. Rats were also taught to run on a radiolucent treadmill, compatible with a commercially available micro-CT system that was modified to perform X-ray fluoroscopy at 62.5Hz. The ratio of affected and unaffected hind limbs was compared for multiple metrics. Post-operative videos were collected at a low treadmill speed (12cm/s) to qualitatively assess implant articulation within the acetabulum. Duty cycle % was significantly different at 6 post-operative weeks compared to baseline, but no other timepoints were significantly different to baseline. X-ray fluoroscopy revealed that implants in 2 of 5 animals had subsided at the 6-week timepoint; subsidence progressed for both animals until post-operative week 12. These findings indicate that rats are able to recover functional use of their affected limbs following the hip hemi-arthroplasty surgery, even if complications at the level of the joint are present. These findings also support that a complimentary imaging technique to optical gait tracking might be necessary to detect abnormal joint mechanics, since animals appear to be able to compensate for a failed implant, only partially detectable on CatWalk XT trials.

In Chapter 5 we present a summary of the main objectives and findings from Chapters 2-4. We also overview the research implications and future directions that this work could take within the field of preclinical orthopaedic research.

Overall, this thesis demonstrates, for the first time, the development of a clinically representative model of rat hip hemiarthroplasty, including (i) implant design manufacturing and optimization; (ii) surgical design and optimization; and (iii) post-operative care, imaging and gait assessment protocols, including the development of a novel radiolucent treadmill. This model provides basic scientists with a translation test platform for studying new innovation aimed at improving the longevity and outcome of joint replacement surgery.

1.8 References

1. 2019. Canadian Joint Replacement Registry Annual Report: Hip and Knee Replacements in Canada, 2017-2018. Ottawa, ON: Canadian Institute for Health Information.

2. Apostu D, Lucaciu O, Berce C, et al. 2018. Current methods of preventing aseptic loosening and improving osseointegration of titanium implants in cementless total hip arthroplasty: a review. The Journal of international medical research 46:2104-2119.

3. Hu CY, Yoon TR. 2018. Recent updates for biomaterials used in total hip arthroplasty. Biomaterials research 22:33.

4. Bjerkholt H, Høvik O, Reikerås O. 2010. Direct comparison of polyethylene wear in cemented and uncemented acetabular cups. Journal of orthopaedics and traumatology : official journal of the Italian Society of Orthopaedics and Traumatology 11:155-158.

5. Alazzawi S, Sprenger De Rover WB, Brown J, et al. 2012. The conversion rate of bipolar hemiarthroplasty after a hip fracture to a total hip arthroplasty. Clin Orthop Surg 4:117-120.

6. Bhandari M, Einhorn TA, Guyatt G, et al. 2019. Total Hip Arthroplasty or Hemiarthroplasty for Hip Fracture. The New England journal of medicine 381:2199-2208.

7. Guyen O. 2019. Hemiarthroplasty or total hip arthroplasty in recent femoral neck fractures? Orthopaedics & traumatology, surgery & research : OTSR 105:S95-s101.

8. Hernigou P, Quiennec S, Guissou I. 2014. Hip hemiarthroplasty: from Venable and Bohlman to Moore and Thompson. Int Orthop 38:655-661.

9. Parker MJ, Cawley S. 2020. Cemented or uncemented hemiarthroplasty for displaced intracapsular fractures of the hip: a randomized trial of 400 patients. The bone & joint journal 102-b:11-16.

10. Hailer NP, Garellick G, Kärrholm J. 2010. Uncemented and cemented primary total hip arthroplasty in the Swedish Hip Arthroplasty Register. Acta orthopaedica 81:34-41.

11. Taha M, Abdelbary H, Ross FP, et al. 2018. New Innovations in the Treatment of PJI and Biofilms-Clinical and Preclinical Topics. Current reviews in musculoskeletal medicine 11:380-388.

12. Gwam CU, Mistry JB, Mohamed NS, et al. 2017. Current Epidemiology of Revision Total Hip Arthroplasty in the United States: National Inpatient Sample 2009 to 2013. J Arthroplasty 32:2088-2092.

13. Kapadia BH, Berg RA, Daley JA, et al. 2016. Periprosthetic joint infection. Lancet (London, England) 387:386-394.

14. Powers DL, Claassen B, Black J. 1995. The rat as an animal model for total hip replacement arthroplasty. J Invest Surg 8:349-362.

15. Wancket LM. 2015. Animal Models for Evaluation of Bone Implants and Devices: Comparative Bone Structure and Common Model Uses. Vet Pathol 52:842-850.

16. El-Warrak AO, Olmstead M, Apelt D, et al. 2004. An animal model for interface tissue formation in cemented hip replacements. Vet Surg 33:495-504.

17. El-Warrak AO, Olmstead M, Schneider R, et al. 2004. An experimental animal model of aseptic loosening of hip prostheses in sheep to study early biochemical changes at the interface membrane. BMC musculoskeletal disorders 5:7.

18. Jakobsen T, Kold S, Baas J, et al. 2015. Sheep Hip Arthroplasty Model of Failed Implant Osseointegration. The open orthopaedics journal 9:525-529.

19. Bloebaum RD, Willie BM, Mitchell BS, et al. 2007. Relationship between bone ingrowth, mineral apposition rate, and osteoblast activity. J Biomed Mater Res A 81:505-514.

20. Egermann M, Goldhahn J, Schneider E. 2005. Animal models for fracture treatment in osteoporosis. Osteoporos Int 16 Suppl 2:S129-138.

21. Field JR, Callary SA, Solomon LB, et al. 2016. Early acetabular cartilage wear following hemiarthroplasty: An ovine model. Vet Comp Orthop Traumatol 29:125-130.

22. Hunt S, Stone C, Seal S. 2011. Timing of femoral prosthesis insertion during cemented arthroplasty: cement curing and static mechanical strength in an in vivo model. Can J Surg 54:33-38.

23. Pawaskar SS, Grosland NM, Ingham E, et al. 2011. Hemiarthroplasty of hip joint: An experimental validation using porcine acetabulum. J Biomech 44:1536-1542.

24. Cunningham BW, Hu N, Zorn CM, et al. 2009. Bioactive titanium calcium phosphate coating for disc arthroplasty: analysis of 58 vertebral end plates after 6- to 12-month implantation. Spine J 9:836-845.

25. Harboe K, Ellingsen CL, Sudmann E, et al. 2015. Can bone apposition predict the retention force of a femoral stem? An experimental weight-bearing hip-implant model in goats. BMC musculoskeletal disorders 16:102.

26. DiVincenzo MJ, Frydman GH, Kowaleski MP, et al. 2017. Metallosis in a Dog as a Long-Term Complication Following Total Hip Arthroplasty. Vet Pathol 54:828-831.

27. Harper TAM. 2017. Femoral Head and Neck Excision. The Veterinary clinics of North America Small animal practice 47:885-897.

28. Ireifej S, Marino D, Loughin C. 2012. Nano total hip replacement in 12 dogs. Vet Surg 41:130-135.

29. Liska WD, Doyle ND. 2015. Use of an Electron Beam Melting Manufactured Titanium Collared Cementless Femoral Stem to Resist Subsidence After Canine Total Hip Replacement. Vet Surg 44:883-894.

30. Husby KA, Reed SK, Wilson DA, et al. 2016. Evaluation of a Permanent Synthetic Osteochondral Implant in the Equine Medial Femoral Condyle. Vet Surg 45:364-373.

31. Robinson NB, Krieger K, Khan FM, et al. 2019. The current state of animal models in research: A review. International journal of surgery (London, England) 72:9-13.

32. Carli AV, Bhimani S, Yang X, et al. 2017. Quantification of Peri-Implant Bacterial Load and in Vivo Biofilm Formation in an Innovative, Clinically Representative Mouse Model of Periprosthetic Joint Infection. J Bone Joint Surg Am 99:e25.

33. Li Z, Kuhn G, Schirmer M, et al. 2017. Impaired bone formation in ovariectomized mice reduces implant integration as indicated by longitudinal in vivo micro-computed tomography. PLoS One 12:e0184835.

34. Yang SY, Yu H, Gong W, et al. 2007. Murine model of prosthesis failure for the long-term study of aseptic loosening. J Orthop Res 25:603-611.

35. Carli AV, Ross FP, Bhimani SJ, et al. 2016. Developing a Clinically Representative Model of Periprosthetic Joint Infection. J Bone Joint Surg Am 98:1666-1676.

36. AbuMoussa S, Ruppert DS, Lindsay C, et al. 2018. Local delivery of a zoledronate solution improves osseointegration of titanium implants in a rat distal femur model. J Orthop Res 36:3294-3298.

37. Al-Jandan B, Marei HF, Abuohashish H, et al. 2018. Effects of sunitinib targeted chemotherapy on the osseointegration of titanium implants. Biomed Pharmacother 100:433-440.

38. Cai J, Li W, Sun T, et al. 2018. Pulsed electromagnetic fields preserve bone architecture and mechanical properties and stimulate porous implant osseointegration by promoting bone anabolism in type 1 diabetic rabbits. Osteoporos Int 29:1177-1191.

39. De Smet E, Jaecques SV, Wevers M, et al. 2013. Constant strain rate and peri-implant bone modeling: an in vivo longitudinal micro-CT analysis. Clin Implant Dent Relat Res 15:358-366.

40. Graca YL, Opolski AC, Barboza BE, et al. 2014. Biocompatibility of Ricinus communis polymer with addition of calcium carbonate compared to titanium. Experimental study in guinea pigs. Rev Bras Cir Cardiovasc 29:272-278.

41. Tang L, Zhao C, Xiong Y, et al. 2010. Preparation, antibacterial properties and biocompatibility studies on vancomycin-poly(D,L)-lactic loaded plates. Int Orthop 34:755-759.

42. Ruppert DS, Harrysson OLA, Marcellin-Little DJ, et al. 2017. Osseointegration of Coarse and Fine Textured Implants Manufactured by Electron Beam Melting and Direct Metal Laser Sintering. 3D Print Addit Manuf 4:91-97.

43. Bargon R, Bruenke J, Carli A, et al. 2019. General Assembly, Research Caveats: Proceedings of International Consensus on Orthopedic Infections. J Arthroplasty 34:S245-S253 e241.

44. Li K, Wang C, Yan J, et al. 2018. Evaluation of the osteogenesis and osseointegration of titanium alloys coated with graphene: an in vivo study. Sci Rep 8:1843.

45. He T, Cao C, Xu Z, et al. 2017. A comparison of micro-CT and histomorphometry for evaluation of osseointegration of PEO-coated titanium implants in a rat model. Sci Rep 7:16270.

46. Lindtner RA, Castellani C, Tangl S, et al. 2013. Comparative biomechanical and radiological characterization of osseointegration of a biodegradable magnesium alloy pin and a copolymeric control for osteosynthesis. Journal of the mechanical behavior of biomedical materials 28:232-243.

47. Huanhuan J, Pengjie H, Sheng X, et al. 2017. The effect of strontium-loaded rough titanium surface on early osseointegration. J Biomater Appl 32:561-569.

48. Javaid M, Haleem A. 2018. Additive manufacturing applications in orthopaedics: A review. Journal of clinical orthopaedics and trauma 9:202-206.

49. Choi JW, Kim N. 2015. Erratum: Clinical Application of Three-Dimensional Printing Technology in Craniofacial Plastic Surgery. Archives of plastic surgery 42:513.

50. Dall'Ava L, Hothi H, Henckel J, et al. 2019. Comparative analysis of current 3D printed acetabular titanium implants. 3D printing in medicine 5:15.

51. Cheong VS, Fromme P, Coathup MJ, et al. 2019. Partial Bone Formation in Additive Manufactured Porous Implants Reduces Predicted Stress and Danger of Fatigue Failure. Annals of biomedical engineering.

52. Gokuldoss PK, Kolla S, Eckert J. 2017. Additive Manufacturing Processes: Selective Laser Melting, Electron Beam Melting and Binder Jetting-Selection Guidelines. Materials (Basel, Switzerland) 10.

53. Wang H, Zhao B, Liu C, et al. 2016. A Comparison of Biocompatibility of a Titanium Alloy Fabricated by Electron Beam Melting and Selective Laser Melting. PLoS One 11:e0158513.

54. Xiang N, Xin XZ, Chen J, et al. 2012. Metal-ceramic bond strength of Co-Cr alloy fabricated by selective laser melting. J Dent 40:453-457.

55. Zhao ZY, Li L, Bai PK, et al. 2018. The Heat Treatment Influence on the Microstructure and Hardness of TC4 Titanium Alloy Manufactured via Selective Laser Melting. Materials (Basel, Switzerland) 11.

56. McErlain DD, Appleton CT, Litchfield RB, et al. 2008. Study of subchondral bone adaptations in a rodent surgical model of OA using in vivo micro-computed

tomography. Osteoarthritis and cartilage / OARS, Osteoarthritis Research Society 16:458-469.

57. Batiste DL, Kirkley A, Laverty S, et al. 2004. Ex vivo characterization of articular cartilage and bone lesions in a rabbit ACL transection model of osteoarthritis using MRI and micro-CT. Osteoarthritis and cartilage / OARS, Osteoarthritis Research Society 12.

58. Holdsworth DW, Thornton MM. 2002. Micro-CT in small animal and specimen imaging. Trends in Biotechnology 20:S34-S39.

59. Joseph UU, Arthur VS, Ian W, et al. 2009. In vivo micro-CT analysis of bone remodeling in a rat calvarial defect model. Physics in Medicine & Biology 54:2147.

60. Hindelang F, Zurbach R, Roggo Y. 2015. Micro Computer Tomography for medical device and pharmaceutical packaging analysis. Journal of Pharmaceutical and Biomedical Analysis 108:38-48.

61. Morrison RJ, Kashlan KN, Flanangan CL, et al. 2015. Regulatory Considerations in the Design and Manufacturing of Implantable 3D-Printed Medical Devices. Clinical and Translational Science 8:594-600.

62. Bushberg JT. 2002. The Essential Physics of Medical Imaging: Lippincott Williams & Wilkins;

63. Feldkamp LA, Davis LC, Kress JW. 1984. Practical cone-beam algorithm. J Opt Soc Am A 1:612-619.

64. Badea CT, Drangova M, Holdsworth DW, et al. 2008. In Vivo Small Animal Imaging using Micro-CT and Digital Subtraction Angiography. Physics in medicine and biology 53:R319-R350.

65. Tse JJ, Dunmore-Buyze J, Drangova M, et al. 2018. Dual-energy computed tomography using a gantry-based preclinical cone-beam microcomputed tomography scanner. Journal of medical imaging (Bellingham, Wash) 5:033503.

66. Edey DR, Pollmann SI, Lorusso D, et al. 2019. Extending the dynamic range of biomedical micro-computed tomography for application to geomaterials. Journal of X-ray science and technology 27:919-934.

67. McNiven AL, Umoh J, Kron T, et al. 2008. Ionization chamber volume determination and quality assurance using micro-CT imaging. Physics in medicine and biology 53:5029-5043.

68. Batailler C, Fary C, Servien E, et al. 2018. Influence of femoral broach shape on stem alignment using anterior approach for total hip arthroplasty: A radiologic comparative study of 3 different stems. PLoS One 13:e0204591.

69. Warth LC, Grant TW, Naveen NB, et al. 2020. Inadequate Metadiaphyseal Fill of a Modern Taper-Wedge Stem Increases Subsidence and Risk of Aseptic Loosening: Technique and Distal Canal Fill Matter! J Arthroplasty.

70. Abdulkarim A, Ellanti P, Motterlini N, et al. 2013. Cemented versus uncemented fixation in total hip replacement: a systematic review and meta-analysis of randomized controlled trials. Orthopedic reviews 5:e8.

71. Leighton RK, Schmidt AH, Collier P, et al. 2007. Advances in the treatment of intracapsular hip fractures in the elderly. Injury 38 Suppl 3:S24-34.

72. Banerjee S, Cherian JJ, Elmallah RK, et al. 2016. Robot-assisted total hip arthroplasty. Expert review of medical devices 13:47-56.

73. Kanawade V, Dorr LD, Banks SA, et al. 2015. Precision of robotic guided instrumentation for acetabular component positioning. J Arthroplasty 30:392-397.

74. Chang JD, Kim IS, Bhardwaj AM, et al. 2017. The Evolution of Computer-Assisted Total Hip Arthroplasty and Relevant Applications. Hip Pelvis 29:1-14.

75. Herold S, Kumar P, Jung K, et al. 2016. CatWalk gait analysis in a rat model of multiple sclerosis. BMC Neurosci 17:78.

76. Kameda T, Kaneuchi Y, Sekiguchi M, et al. 2017. Measurement of mechanical withdrawal thresholds and gait analysis using the CatWalk method in a nucleus pulposus-applied rodent model. Journal of experimental orthopaedics 4:31.

77. Miyagi M, Ishikawa T, Kamoda H, et al. 2011. Assessment of gait in a rat model of myofascial inflammation using the CatWalk system. Spine 36:1760-1764.

78. Miyagi M, Ishikawa T, Kamoda H, et al. 2013. Assessment of pain behavior in a rat model of intervertebral disc injury using the CatWalk gait analysis system. Spine 38:1459-1465.

79. Miyamoto S, Nakamura J, Ohtori S, et al. 2017. Pain-related behavior and the characteristics of dorsal-root ganglia in a rat model of hip osteoarthritis induced by mono-iodoacetate. J Orthop Res 35:1424-1430.

80. Caballero-Garrido E, Pena-Philippides JC, Galochkina Z, et al. 2017. Characterization of long-term gait deficits in mouse dMCAO, using the CatWalk system. Behavioural brain research 331:282-296.

81. Fulop GA, Ahire C, Csipo T, et al. 2019. Cerebral venous congestion promotes blood-brain barrier disruption and neuroinflammation, impairing cognitive function in mice. GeroScience 41:575-589.

82. Moritz MS, Tepp WH, Inzalaco HN, et al. 2019. Comparative functional analysis of mice after local injection with botulinum neurotoxin A1, A2, A6, and B1 by catwalk analysis. Toxicon 167:20-28.

83. Chen H, Du J, Zhang Y, et al. 2017. Establishing a reliable gait evaluation method for rodent studies. Journal of neuroscience methods 283:92-100.

84. Kappos EA, Sieber PK, Engels PE, et al. 2017. Validity and reliability of the CatWalk system as a static and dynamic gait analysis tool for the assessment of functional nerve recovery in small animal models. Brain and behavior 7:e00723.

85. Chiang CY, Sheu ML, Cheng FC, et al. 2014. Comprehensive analysis of neurobehavior associated with histomorphological alterations in a chronic constrictive nerve injury model through use of the CatWalk XT system. Journal of neurosurgery 120:250-262.

86. Forgione N, Chamankhah M, Fehlings MG. 2017. A Mouse Model of Bilateral Cervical Contusion-Compression Spinal Cord Injury. Journal of neurotrauma 34:1227-1239.

87. Abdo H. 2015. Gait Analysis and Therapeutic Application of Carbon Monoxide in a Rodent Model of Complex Regional Pain Syndrome Type-1. Western University Electronic Thesis and Dissertation Repository.

88. Sato T, Tanino H, Nishida Y, et al. 2017. Dynamic femoral head translations in dysplastic hips. Clinical biomechanics (Bristol, Avon) 46:40-45.

89. Yamaguchi S, Sasho T, Kato H, et al. 2009. Ankle and subtalar kinematics during dorsiflexion-plantarflexion activities. Foot & ankle international 30:361-366.

90. Tanino H, Ito H, Harman MK, et al. 2008. An in vivo model for intraoperative assessment of impingement and dislocation in total hip arthroplasty. J Arthroplasty 23:714-720.

91. Guillot M, Gravel P, Gauthier ML, et al. 2015. Coxofemoral joint kinematics using video fluoroscopic images of treadmill-walking cats: development of a technique to assess osteoarthritis-associated disability. Journal of feline medicine and surgery 17:134-143.

92. Tinga S, Kim SE, Banks SA, et al. 2018. Femorotibial kinematics in dogs with cranial cruciate ligament insufficiency: a three-dimensional in-vivo fluoroscopic analysis during walking. BMC veterinary research 14:85.

Chapter 2

2 Image-based Design and 3D-metal Printing of a Rat Hip Implant for use in a Clinically Representative Model of Joint Replacement

2.1 Introduction

The development of clinically representative animal models is critical for advancing translational orthopaedic research into areas related to joint replacement, such as osseointegration,[1-8] metal-on-cartilage wear,[9-11] and peri-prosthetic joint infection (PJI).[12-16] Preclinical studies that evaluate changes around a functional implant have been limited to large-animal[9; 10; 17] and companion-animal models,[18-20] which can accommodate commercially available joint-replacement components that mimic or replicate human implants. However, the costs of procurement and long-term housing limit the sample sizes used in large-animal studies. To mitigate these limitations, small-animal models, especially murine models, are used in the initial stages of research. Compared to large-animals these models are low-cost, offer higher throughput, and have several advantages such as small size, ease of handling, and compatibility with preclinical systems for imaging and gait analysis.

Typical orthopaedic studies in rats and mice utilize cortical pins,[2; 3; 6] intramedullary rods,[5; 7] and screws[8] installed into the bone to investigate changes at the bone-implant interface. Nonetheless, these implants are non-functional and do not articulate within a weight-bearing joint. A murine model that utilizes a load-bearing

implant to effectively mimic the peri-prosthetic environment would be an ideal preclinical platform for basic scientists conducting orthopaedic research aimed at improving implant longevity.[12-16; 21] This approach has been attempted previously: Carli *et al.* described a model of PJI in the mouse knee;[14] Jie *et al.* summarized several animal models of PJI in the knee,[13] and; Powers *et al.* described a rat model of cemented total hip replacement.[21] Nevertheless, due to the difficulty of designing implants that mimic human implants – but are murine-specific, and can be manufactured such in the sizes required for *in vivo* testing – murine models of functional joint replacement have not been widely adopted. Performing joint replacement surgery in murine models is also inherently challenging due to size constraints, underscoring the need for implants that are anatomically conformal to facilitate installation.

Recent advances in additive manufacturing (3D printing) allow for the creation of custom implants in medical-grade metal alloys,[14; 15] such as titanium, cobalt-chrome and stainless steel. This approach is ideal for developing and testing novel implants for small-animal models, as prototypes can be produced in small numbers, at modest costs, and tested iteratively to improve their design and functionality. The additive manufacturing process typically involves the development of a 3D model in computer-aided design (CAD) software in conformity with the anatomical parameters of the joint of interest. This template can also then be used to scale components to create a set of implants that covers the range of anatomical sizes in the animal population of interest, after which implants can be printed in an alloy of choice to match their application.

To create a highly conformal implant to match the anatomical requirements of the species of interest, anatomical measurements of the bony anatomy of a murine model

(such as the rat) should first be obtained; this can be optimally achieved by analyzing high-resolution micro-computed tomography (micro-CT) volumes. By combining this type of image-based analysis, CAD, and additive manufacturing, we propose that the creation of a functional hip implant for the rat is feasible. Thus, our objectives are to: (i) quantify high-resolution micro-CT volumes of the proximal rat hip to create a set of measurements that can be used to inform a parameterized CAD model of a rat hip implant; (ii) determine if rat femoral dimensions can be predicted by animal weight; iii) determine an appropriate range of implant sizes to accommodate rats of different weights and femoral sizes, and; (iv) manufacture 3D-printed implants in medical-grade alloys. We also describe the surgical installation of implants in a rat model of hip-hemiarthroplasty as a proof-of-concept, as well as iterative prototype revisions that were based on both *ex vivo* and *in vivo* surgical trials.

2.2 Materials and Methods

2.2.1 Proximal Femoral Quantification

Whole-body micro-CT volumes of (N=25) rats (male Sprague-Dawley, 390g – 605g) were selected at random from a database of 52 previously acquired live animal scans.[22] These scans were originally acquired on a commercially available cone-beam scanner (eXplore Locus Ultra, GE Medical, London, Ontario) at 154μm isotropic voxel resolution (120kVp, 20mA, 16s).[22] Volumes were analyzed in MicroView 2.2 (Parallax Innovations, Ilderton, Ontario), by a single user. Volumes were cropped manually to isolate each femur, yielding 25 left and 25 right femora for analysis. Due to the innate curvature of the rat femur, the proximal medullary cavity (nominally the superior 1/3 of

the bone) was cropped and aligned so that a linear long-axis through this region could be maintained. An isosurface of the bone was generated to aid the consistent reorientation of each femur (Fig. 2.1). Reorientation of volumes was done such that: (i) the coronal plane (anterior-posterior) bisected the center femoral head and the center of the proximal medullary cavity; (ii) the sagittal plane (medial-lateral) bisected the proximal medullary cavity along its centerline, and (iii) the transverse plane (superior-inferior) was perpendicular to the long-axis of the proximal medullary cavity (Fig. 2.2). Both extracortical and intramedullary measurements were obtained based on the assumption that the dimensions of four implant sections should be parameterized; (i) the head and neck, (ii) the proximal stem, (iii) the central stem, and (iv) the distal stem. The Inclination Angle, comparing Neck-Head Axis to the long-axis of the proximal medullary cavity, was also obtained.

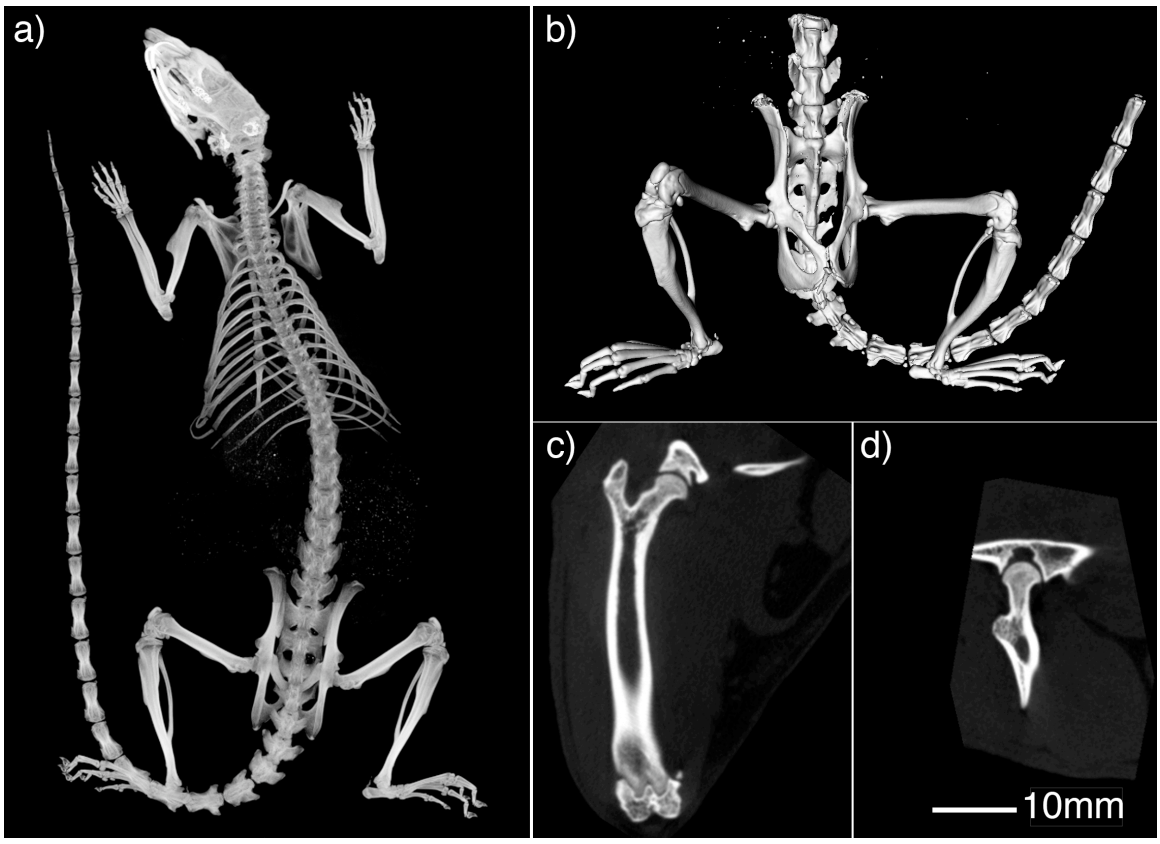

Figure 2.1: Micro-CT volume of a male Sprague-Dawley rat. a) Whole-body maximum intensity projection (MIP); b) isosurface of lower-limb skeletal anatomy that is useful for reorienting volumes for repeatable measurement; c) slice through the femur, and; d) slice through femoral head and neck.

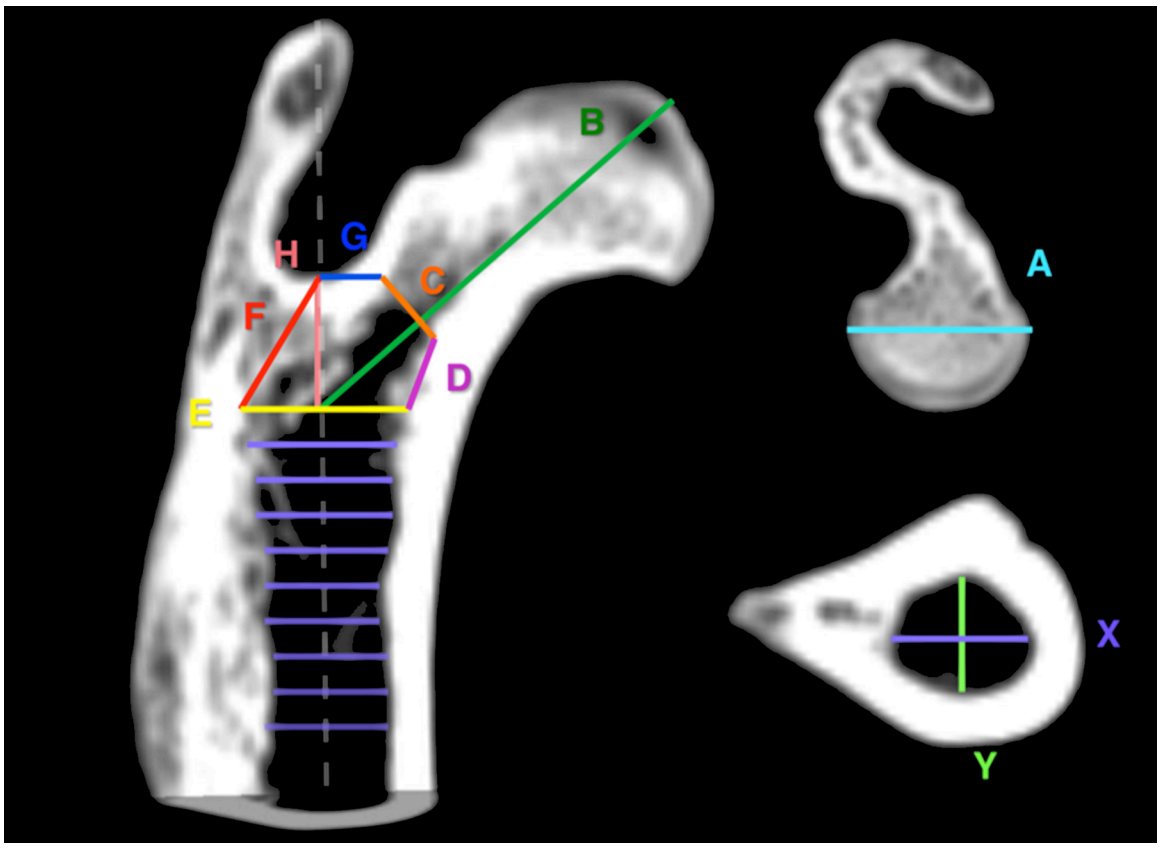

Figure 2.2: Micro-CT derived schematic of measurements obtained to quantify the rat proximal femoral anatomy collected in the coronal plane (left) and transverse planes (right). Measurements included (A) Femoral Head Diameter; (B) Neck-Head Axis Length; (C) Intramedullary Neck Width; (D) Medial Proximal Cortical Measurement; (E) Slice 1 M-L Diameter; (F) Lateral Proximal Cortical Measurement; (H) Proximal Stem Height, and; (G) Superior Proximal Cortical Measurement. Intramedullary diameter measurements were also obtained in the (X) Medial-Lateral and, (Y) Anterior-Posterior directions in the transverse plane at ten locations (Slices 1-10) separated distally by 770µm intervals. The Inclination Angle was also measured by comparing the angle between the Neck-Head Axis (B) and long-axis of the proximal medullary cavity (dashed line).

2.2.2 Statistical Analysis

Image volumes of N=25 rats were analyzed bilaterally to obtain anatomical measurements of the proximal femoral anatomy. Values obtained from left and right femora in the same animal were averaged; mean values were then analyzed. A D'Agostino & Pearson omnibus test was conducted to assess the normality of key measurement data; all key measurements passed normality ($p>0.05$). Linear regression analysis was performed to determine if key measurements of the proximal rat femur increased significantly with rat weight ($p<0.05$), which would inform if rats were indeed skeletally mature, or if their skeletons continued to grow with increasing weight (Fig. 2.3). Pearson r correlations of key implant measurements were also conducted to determine which measurements were significantly correlated ($p<0.05$), and subsequently if volumetric scaling of implant dimensions was appropriate for the creation of larger and smaller implants that could accommodate a range of rat femur sizes (Fig. 2.4).

2.2.3 Implant Design and Manufacturing

Generation 1 implants were modeled in computer-aided design (CAD) software (Solidworks, Dassault Systemes, Vélizy-Villacoublay, France). A monoblock hemiarthroplasty design was chosen due to the high complication rate of installing an acetabular cup, as noted in a previous study.[21] Several key assumptions were made for implant design features: (i) a sphere approximated the femoral head; (ii) the neck of the implant was minimal in diameter to reduce the risk of femoral acetabular impingement; (iii) the stem began proximally with a slot profile and tapered to a cylinder; (iv) the proximal portion of the stem was adjusted in shape and size to facilitate a smooth

transition between Slice 1 and the neck of the implant; (v) the distal stem, beyond the minimum measured cortex diameter, was set to an arbitrary length (10mm) and tapered in diameter (to a 1.5mm circular profile) to facilitate installation. The mean values of several key measurements obtained from rat micro-CT volumes (Table 1) were used to guide the dimensions of an average-sized rat implant (Fig. 2.5).

To accommodate the range of rats measured, it was determined that a set consisting of multiple implants should be created; this was accomplished by utilizing a scaling feature, which allows for an overall volumetric change in the CAD model that preserves the overall shape of the implant. Two additional models, one scaled by 0.9 and the other by 1.1 times the volume of the mean measurement-derived model were created using this approach. The standard deviation of the femoral head diameter was used to determine the aforementioned scaling values used for the overall volume of the implant; this approach was chosen because implant fit within the acetabulum cannot be adjusted, unlike fit of the stem within the bone. The resulting implants had head sizes that could nominally cover 99% of the rat population measured (approximately $\pm 2.5\sigma$). A model of 0.85 times the mean volume was also created to serve as a guide component when preparing the femoral canal during surgery.

The resulting set of four implants (and several copies of each size) were manufactured using a commercially available selective laser melting (SLM) 3D printer (AM-125, Renishaw plc, New Mills Wotton-under-Edge, UK). 316L stainless-steel metal powder (40μm average grain size) was used for Generation 1 implants. After printing, each implant was deburred and hand-polished to a matte finish with various grits of sandpaper (Fig. 2.6). Stems were left with inherent surface texture to assist fixation in

bone. Prior to surgery, implants were washed for 20 minutes in an ultrasonic bath of detergent before being rinsed with water, dried, and then sterilized via autoclave.

Generation 2 implants were designed using the same parameterized CAD template as Generation 1 implants (described above). Several features were added to Generation 2 implants in an effort to assist surgical installation and allow for potential bone growth into the stem of the implant: (i) a collar was added both as a visual reference (to prevent over-insertion of implants during surgery) and to improve primary stability of the components; (ii) a subtle medial curvature of the distal stem, with an accompanying decrease in length by 0.75mm, was implemented to mitigate impingement on the lateral medullary cortex during installation; (iii) a hexagonal porosity (nominally 0.5mm in diameter), as well as a slot feature were added to enhance surface area and improve the potential for bone integration into the stem, (iv) the neck diameter was increased by 0.2mm to add strength, and (v) material was removed from the distal head to make it easier to polish the head and neck with dental hand-tools (Fig. 2.7).

The scaling parameters used to create larger and smaller implant sizes were also adjusted for Generation 2 implants. Each key measurement in the parameterized CAD model implant was adjusted to be 0.75 and then 1.5 times its standard deviation, yielding two larger-sized implant models, and two smaller-sized implant models. This was done with the intent of creating a more conformal implant stem, compared to Generation 1 implants. The resulting set of five implants were made to accommodate approximately 85% of the rat population measured; we anticipated this would improve conformity in rats hips with femoral dimensions closer to the measured means, compared to Generation 1 implants.

Generation 2 implants were also manufactured using a commercially available SLM 3D printer (AM-400, Renishaw plc, New Mills Wotton-under-Edge, UK). Several copies of each implant size were printed in both titanium (Ti6Al4V) and cobalt-chrome (ASTM F75 Co-Cr) alloys from metal power (40μm average grain size). After manufacture, implants were heat-treated before removal from the build-plate and deburred. The head of each implant was then polished to a mirror-like finish with a rotary dental hand-tool and a series of polishing stones and rubber wheels (Fig. 2.8). Prior to surgery, implants were cleaned and sterilized in the same fashion as Generation 1 components (described above).

2.2.4 Animals

Cadaveric specimens were initially used for surgical training and to test the fit of implants into the femoral canal. Surgeries in live animals were then performed to determine whether or not animals could tolerate the procedure and ambulate on their affected limbs post-operatively, following approval by the institutional Animal Care Committee (Animal User Protocol 2013-027, Western University, London, Ontario, Canada). Four retired breeder rats (male, Sprague-Dawley, 500-900g) were acquired via donation for use in *in vivo* surgical trials. Animals were housed in a conventional vivarium with 12-hour light/dark cycle and provided *ad libitum* standard rodent chow and water. Animal weights were recorded prior to surgery (baseline) and at post-operative timepoints (Table 2.2).

2.2.5 Surgical Approach

Surgeries were performed in two cohorts – the first cohort of two rats received a Generation 1 implant (316L stainless steel), and the second cohort of two rats received a Generation 2 implant (F75 Co-Cr). The surgical findings from the Generation 1 rat surgeries informed design modifications for the Generation 2 implants. In total, four rat hip hemiarthroplasty procedures were attempted. Each procedure used a cranio-lateral approach to install implants into the right femur. Anesthesia was induced within a chamber using 4% isofluorane and maintained via nose cone at 1.5%. Antibiotics (Baytril, 10 mg/kg) and analgesics (Metacam, 1 mg/kg, Buprenorphine, 0.07 mg/kg SC) were administered subcutaneously. External heat support and anesthetic depth monitoring were maintained throughout the procedure. The animal was placed on lateral recumbency; the hair was clipped and the skin was aseptically prepared. A curvilinear incision was made atop the cranial aspect of the greater trochanter. The superficial gluteal muscle and the tensor fascia lata were incised to expose the middle and deep gluteal muscles, which were then retracted to expose the anterior joint capsule. A scalpel was used to incise the joint capsule, exposing the head of the femur. The femur was externally rotated to permit severing of the round ligament, followed by dislocation of the femoral head from the acetabulum. Ostectomy of the femoral head and neck was performed using a 90° dental drill with round burr. A series of dental files were used to hand ream the medullary cavity before the implant was potted into the bone using an impactor tool and a small hammer. Once positioned within the femur, forceps were used to grasp the implant to ensure that it was stable before the joint was relocated (Fig. 2.9). Routine closure of the surgical site was performed using 5-0 Monocryl sutures in a simple continuous

pattern to close the muscle and subcutaneous layers. The skin was closed with a subcuticular pattern using the same suture material and tissue glue.

2.2.6 Post-operative Protocol

Following recovery from anesthesia, animals were placed alone in cages with clean bedding. Therapy included antibiotics (Baytril, 10 mg/kg SC daily for 7 days) and drugs for pain management (Metacam, 1 mg/kg, daily for 7 days, Buprenorphine, 0.07 mg/kg SC daily for 3 days). Radiographs were obtained at post-operative day 1 and week 3 to confirm positioning of implant within the hip of the rat (120kVp, 20mA) and to assess implant position qualitatively. Animals were then kept under daily observation in their cages for one post-operative week, after which they were used as pilot animals for a concurrent gait analysis protocol, also approved by the institutional Animal Care Committee (Animal User Protocol 2013-027, Western University, London, Ontario, Canada) (Appendix A).

2.3 Results

The proximal femoral anatomy of N=25 rats was successfully quantified, and key measurements used to parameterize CAD models were summarized (Table 2.1). Linear regression of key measurements revealed a significant non-zero slope ($p<0.05$) when comparing animal weight (g) with both Femoral Head Diameter (mm) and Neck-Head Axis Length (mm); none of the remaining key measurements showed a non-zero slope when compared to rat weight (Fig. 2.3). Five significant correlations between key measurements were identified ($p<0.05$): (i) Femoral Head Diameter & Neck Head Axis

Length; (ii) Slice 1 M-L Diameter & Slice 5 M-L Diameter; (iii) Slice 1 M-L Diameter & Slice 5 A-P Diameter; (iv) Slice 1 A-P Diameter & Slice 5 M-L Diameter, and; (v) Slice 5 M-L Diameter & Slice 5 A-P Diameter (Fig. 2.4).

3D design and fabrication of parameterized custom rat hip implant sets was achieved for both generations of implants (Fig. 2.5 – 2.8). Additional features (collar, tool interface, distal curvature) were added to Generation 2 implants based on surgical findings in an effort to improve the ability for implants to be potted during installation. (Fig. 2.7, 2.8) Improvements to post-processing of implants were also made through the used of dental hand-tools to create a mirror-like finish on the heads of Generation 2 implants (Fig. 2.8).

Our surgical approach was sufficient to facilitate the press-fit installation (Fig. 2.9) of our prototype implants into 3 of 4 male Sprague-Dawley rats, preserving the greater trochanter. One animal was sacrificed via Euthanyl injection after an anterior femoral cortex fracture occurred whilst the proximal medullary cavity was being prepared by drilling. Remaining rats recovered uneventfully and were observed ambulating on both hind limbs immediately post-operatively. Animal weights were maintained within an expectable range of <15% body weight loss (Table 2.2). Radiographs revealed the stem of each implant was seated within the proximal medullary cavity of the femur, and the head of the implant remained located within the acetabulum at post-operative day 1, indicating successful installations (Fig. 2.10). However, implant subsidence can be observed for Generation 1 rats at week 3, leading to a subluxed hip in Rat 2; subsidence is not observed at this timepoint in the Generation 2 animal (Fig. 2.10).

Table 2.1: Key measurements obtained from high-resolution micro-computed tomography volumes of N=25 rats (male, Sprague-Dawley, 390-605g), measured bilaterally, which were used to guide the 3D design of rat-specific hip implants.

Measurement	Mean (± Standard Deviation)	95% Confidence Interval
Weight (g)	497.6 (± 5.0)	477.4, 518.8
Femoral Head Diameter (mm)	4.81 (± 0.20)	4.75, 4.87
Inclination Angle (degrees)	130.4 (± 1.5)	130, 131
Neck-Head Axis Length (mm)	8.61 (± 0.40)	8.5, 8.72
Slice 1 M-L Diameter (mm)	2.97 (± 0.28)	2.89, 3.05
Slice 1 A-P Diameter (mm)	2.13 (± 0.26)	2.06, 2.20
Slice 5 M-L Diameter (mm)	1.97 (± 0.19)	1.92, 2.02
Slice 5 A-P Diameter (mm)	1.67 (± 0.15)	1.63, 1.71

Table 2.2: Baseline and post-operative weights for animals following hip hemiarthroplasty.

Animal	Baseline Weight (g)	Day 1 Post-op Weight (g)	Week 3 Post-op Weight (g)
Rat 1	900.0	902.7	926.1
Rat 2	500.0	495.3	540.7
Rat 3	751.6	743.8	726.4

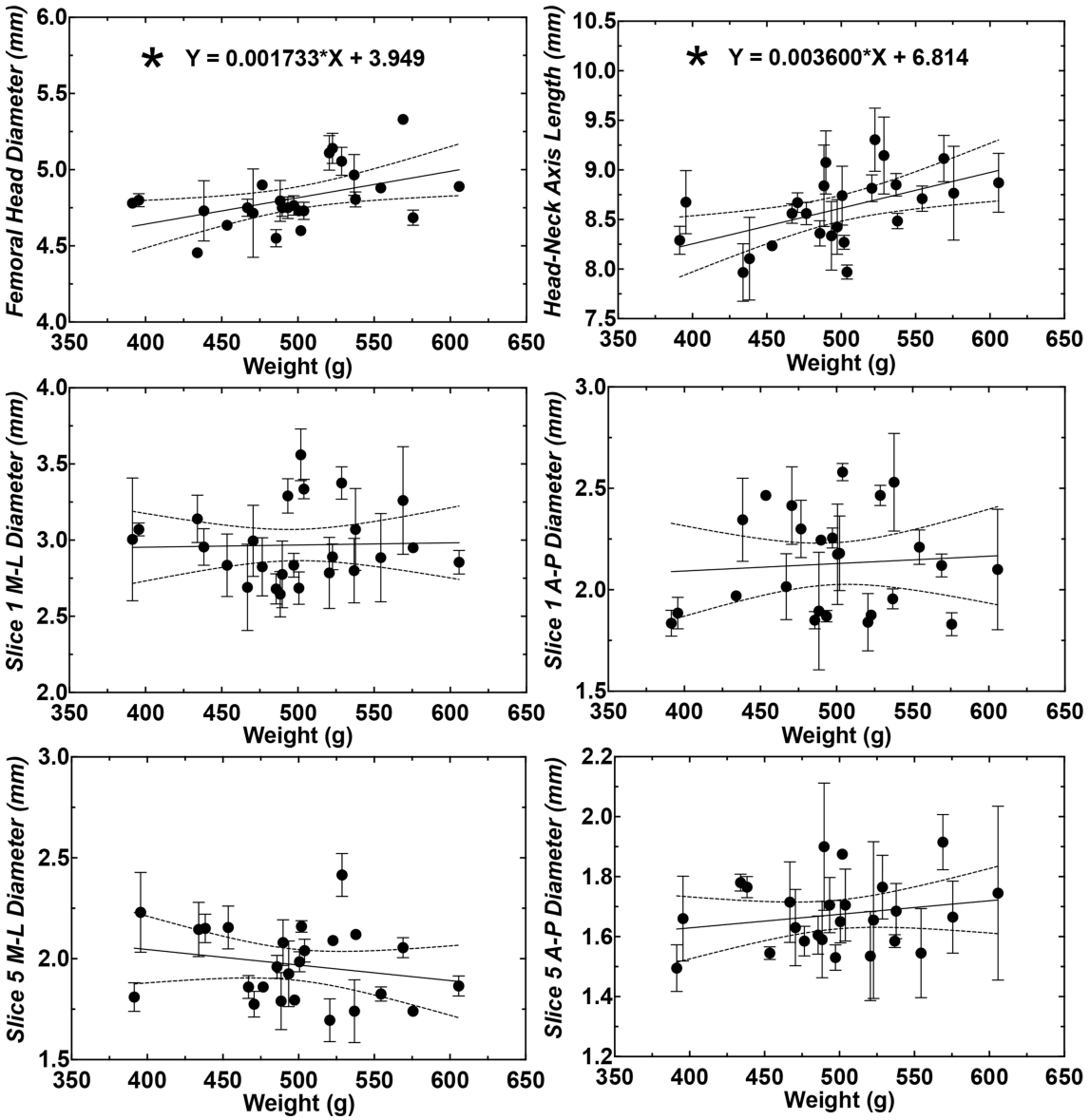

Figure 2.3: Linear regressions of key rat proximal femur measurements (mm) compared to animal weight (g), obtained from high-resolution micro-computed tomography volumes of N=25 rats (male, Sprague-Dawley, 390-605g), measured bilaterally. A significant non-zero slope, indicated by an asterisk, was found for Femoral Head Diameter and Weight, and Neck-Head Axis Length and Weight ($p<0.05$).

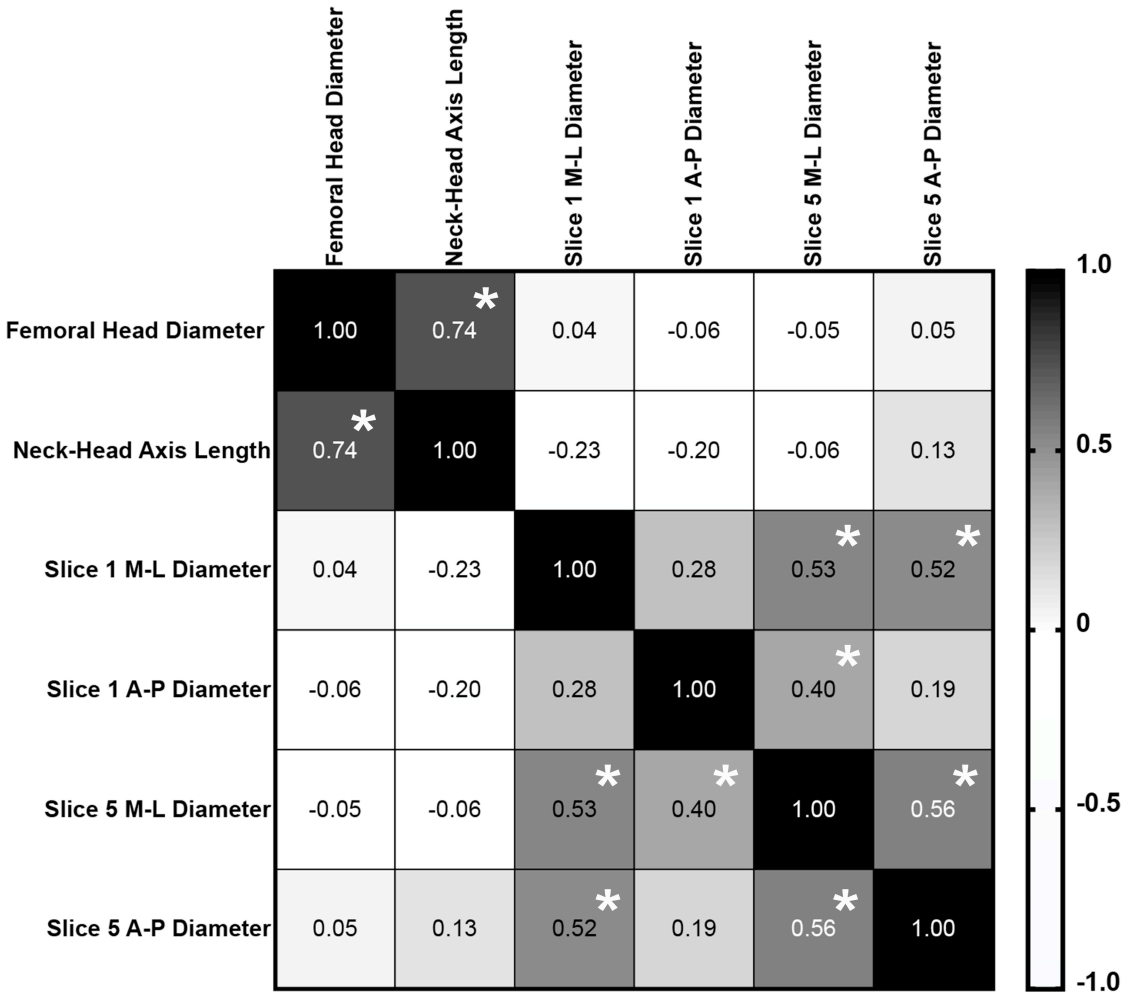

Figure 2.4: Pearson r correlation matrix of key implant measurements, obtained from high-resolution micro-computed tomography volumes of N=25 rats (male, Sprague-Dawley, 390-605g), measured bilaterally. A perfect positive correlation score between measurements is 1.0 and a perfect negative correlation is -1.0. An asterisk indicates a significant correlation ($p<0.05$) between different key measurements.

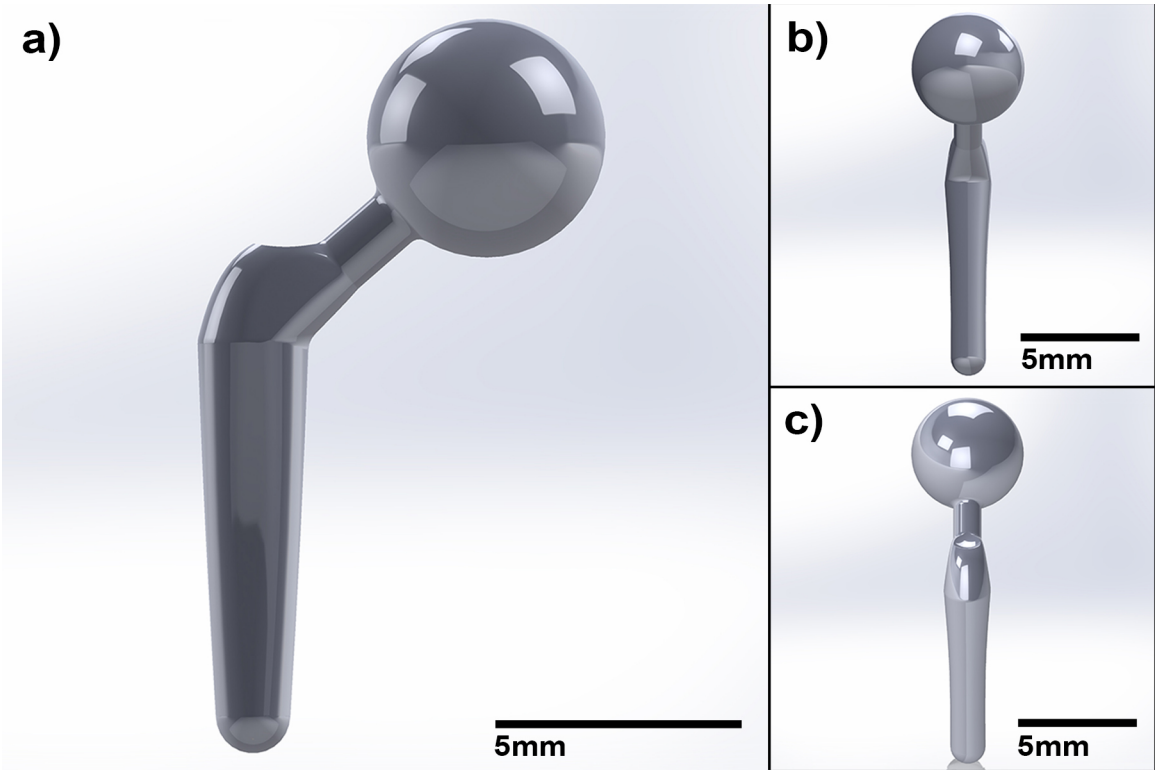

Figure 2.5: Computer-aided design model of a monoblock Generation 1 rat hip implant. a) Frontal b) Medial-Lateral, and c) Oblique lateral-medial views are displayed. The mean-sized implant displayed was parameterized from image-based bilateral measurements of the proximal femora of N=25 rats (male, Sprague-Dawley, 390-605g).

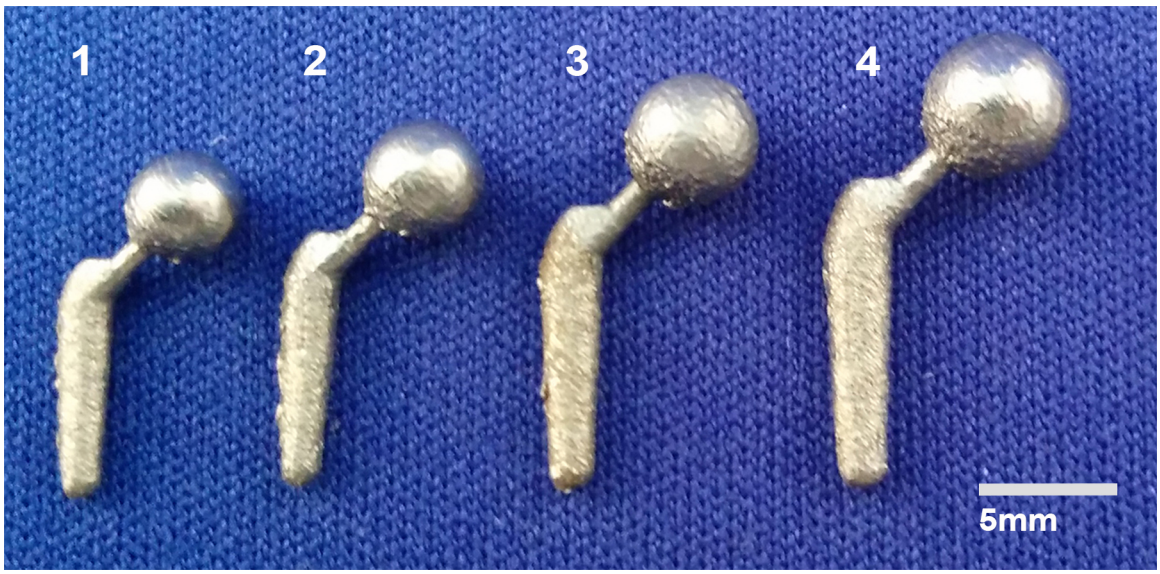

Figure 2.6: Generation 1 rat-specific 3D-printed implants. Three sizes (2-4) were created to accommodate a range of skeletally mature rats, and one size (1) was created slightly smaller as a surgical tool to help with filing of the proximal medullary to accommodate an implant. Implants shown were 3D-printed in 316L stainless steel. Heads were polished by hand to a matte finish with progressively finer grits of sandpaper; this technique, which did not yield a mirror-like finish, was modified for generation 2 implants.

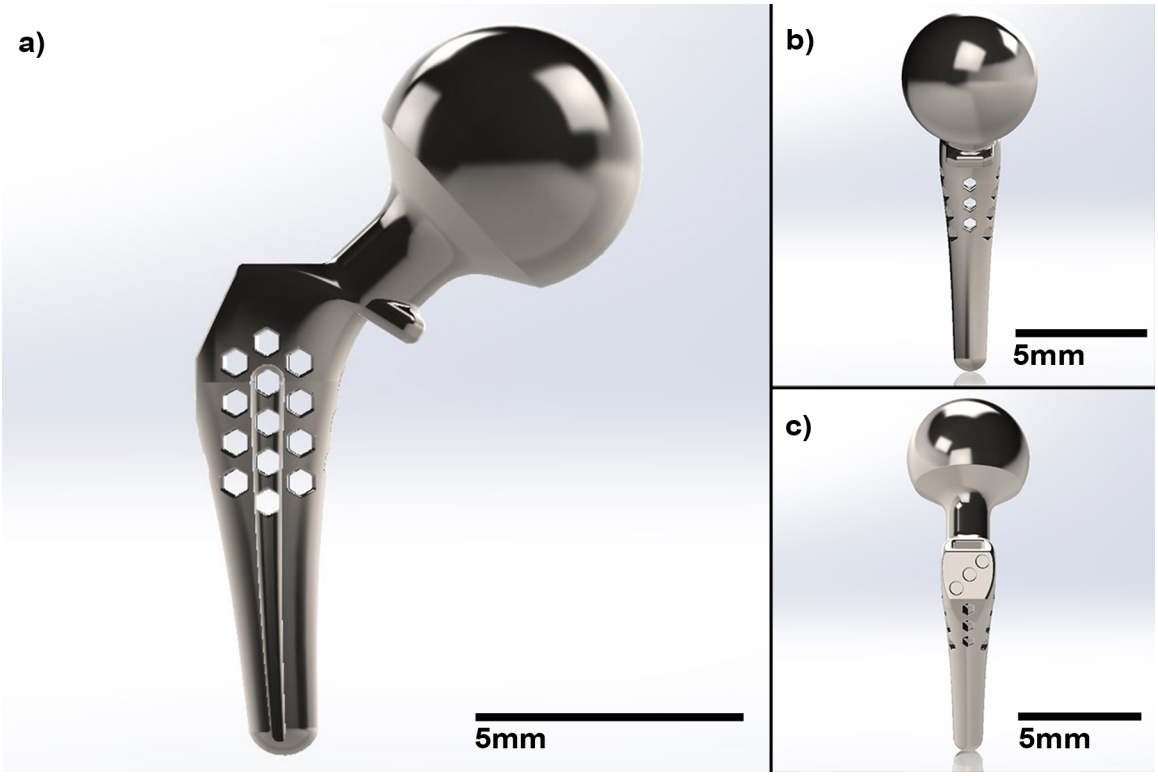

Figure 2.7: Computer-aided design model of a monoblock Generation 2 rat hip implant. a) Frontal b) Medial-Lateral, and c) Oblique lateral-medial views are displayed. The mean-sized implant displayed was parameterized from image-based bilateral measurements of the proximal femora of N=25 rats (male, Sprague-Dawley, 390-605g). Parameterized dimensions were kept consistent with the Generation 1 implants, except for the Femoral Head Diameter, which was increased by 0.02mm to account for some material removal during polishing. Additional features (collar, tool interface, distal curvature) were added to improve the ability for implants to be potted during installation. A hexagonal porosity (0.5mm in diameter) and a slot feature were also incorporated into the stem to increase surface area in an effort better promote bone integration.

Figure 2.8: Generation 2 rat-specific 3D-printed implants. Five sizes (1-5) were created to accommodate a range of skeletally mature rats (male, Sprague-Dawley, 390-605g). Implants shown were 3D-printed in Ti6Al4V titanium with heads polished to a mirror-like finish with a dental tool and progressively finer grits of polishing stones and rubber wheels.

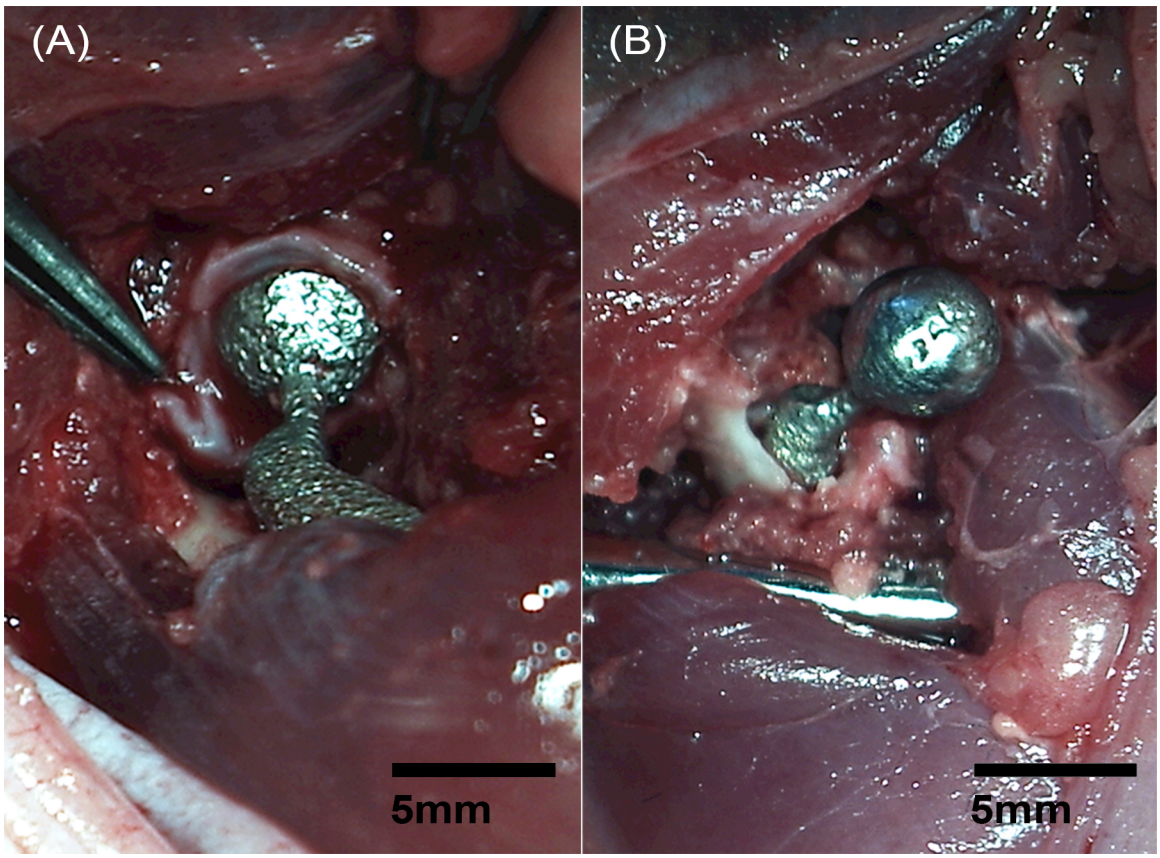

Figure 2.9: Intraoperative view of a Generation 1 custom rat hip monoblock implant *in situ*. (A) Implants were selected by the surgeon intraoperatively based on primarily on fit within the acetabulum. (B) Implants were then press-fit into the proximal femur following preparation with a dental drill and files.

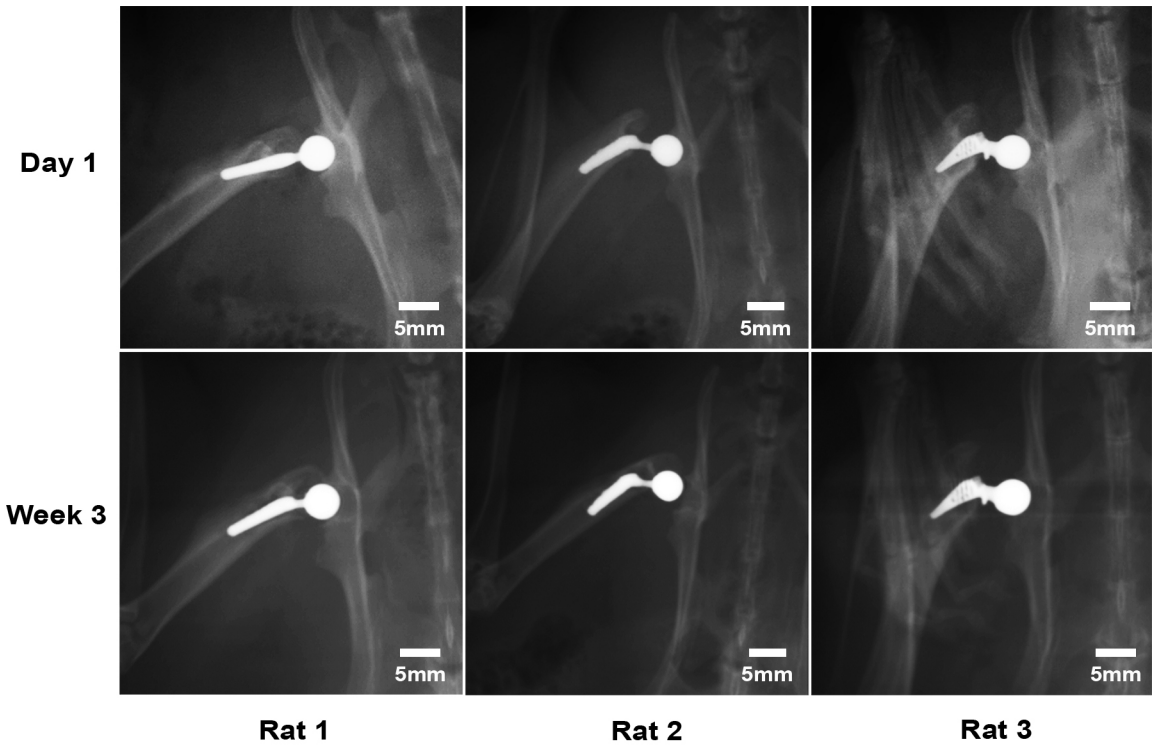

Figure 2.10: Dorsal-ventral radiographs of the right hind-limb of rats (male, Sprague-Dawley 500-900g) in a prone position, each with a monoblock hip implant *in situ* at post-operative day 1 and week 3. Animals were ambulatory at each timepoint. Rat 1 and 2 received a Generation 1 316L SS component (Size 3, Size 2). Some implant subsidence was observed at post-operative week 3 in Rats 1 and 2, but not in Rat 3, which had an ASTM F75 Co-Cr Generation 2 implant (size 3). Rat 2 also appears to have a partially subluxed hip at week 3.

2.4 Discussion

We describe the first efforts to quantify dimensions of the rat proximal femur for the purpose of designing a rat-specific hip implant, for use in a rat model of functional joint replacement. We also describe the design and manufacture of rat-specific 3D-metal-printed implants in surgical-grade metal alloys, as well as the first hip-hemiarthroplasty

procedures to install these implants into live rats, preserving the greater trochanter and permitting ambulation on the affective limb post-operatively.

Quantification of the proximal femoral anatomy in the rat using micro-CT based measurements was sufficient for determining key measurements that could be used to create a parameterized 3D computer-aided design (CAD) model of a monoblock rat femoral hip implant. These measurements were limited to male Sprague-Dawley rats (390-605g); it is unclear if similar rat species, or animals of different weights outside of the range included would be properly served by the implants we have developed. However, this approach could easily be expanded to include rats from a broader range of sizes, species and female rats. An image-based design approach could also be used to create a custom implant for each animal, but this may not be advisable as this process would be time-consuming in a larger cohort of animals. Instead, the increase in implant options between Generation 1 and Generation 2 implant sets was done so that implants could be more conformal to the individual rat hip, without the need to create a specific implant for each animal.

Linear regression of key proximal femoral measurements revealed a significant increase ($p<0.05$) in femoral head diameter and neck-head axis length with rat weight (Fig. 3). This suggests that some continued bone growth may be occurring, as rats grow larger in weight, even in rats thought to be skeletally mature. Since animals would age throughout a potential longitudinal study, it may be prudent to select larger or older animals in future investigations, in order to mitigate the risk implants loosing congruency within the acetabulum. Linear regression of the remaining key measurements showed a non-zero slope when compared to rat weight (Fig. 3), suggesting that an appropriate stem

size for each rat cannot be predicted by animal weight. Instead, preoperative imaging might be appropriate in the future to determine the correct fitting implant size for each animal prior to surgery.

Pearson r correlations of key implant measurements revealed five significant correlations between implant features (Fig. 4), suggesting that scaling implant designs to create multiple sizes was appropriate. However no significant correlations were found between Femoral Head Diameter and any of the intramedullary measurements, which suggested that independent scaling of the head and stem of the implant is more ideal. For this reason, key measurements were each scaled independently in Generation 2 implants compared to Generation 1 implants, which were scaled by overall volume.

Given the findings from both linear regression and Pearson r correlation analyses (Fig. 3,4), it could be argued that it would have been appropriate to scale only the Femoral Head Diameter when creating larger and smaller implants, leaving the stem size the same. However in practice, it was thought that having multiple stem sizes would be crucial to facilitate a proper press-fit installation of the implant into the femur even with the ability to shape the proximal medullary cavity. For this reason, and because we chose to use a monoblock design for our implants, it was determined that changes in stem size would follow changes in Femoral Head Diameter.

In the future, it may be beneficial to create heads that can be fit modularly with implant stems, to achieve an optimal implant fit in both the acetabulum and the proximal femur in each animal. This would also allow for combinations of metal alloys to be used, such as a cobalt-chrome head that is preferred for studying an articulating joint surface at

the metal-on-cartilage interface[10; 11], and a modifiable titanium stem that is preferred for osseointegration studies[1-5]. Engineering an appropriately scaled and consistent taper joint between the head and neck of a rat-sized implant would likely be difficult to achieve, but could be investigated as well.

The animals obtained for use in this proof-of-concept study were male breeders obtained through donation, which resulted in the procurement of animals that exceeded the weight range of rat weights analyzed for the development of our implant sets. However, since intramedullary dimensions in the rat hip did not significantly increase with rat weight (Fig. 3), it is reasonable to assume that the implant sizes we have created can be extrapolated to larger animals. Nevertheless, in the future, measurements of larger animals could be added to the set of analyzed image volumes to avoid extrapolation.

Further limitations of this pilot study include the absence of post-operative data to determine longitudinal function of implants. The objective of this study was to determine an appropriate design for a rat hip implant to facilitate surgical installation while preserving major features of the rat hip anatomy. Metrics of implant position were not obtained, but could collected in the future through the used of X-ray or micro-CT imaging. Histopathology would be beneficial for determining if bone is able to integrate with the surface of 3D printed implant stems, or into any other engineered surface aimed at promoting osseointegration. Collection of post-operative data, such as rat weight at various timepoints would be useful to illustrate the quality of post-operative recovery; gait analysis would be ideal to determine the quality of movement that is afforded to animals post-operatively. Nonetheless, the present *in vivo* experiments to install components were the first of their kind using a rat-specific 3D-metal printed hip implant,

and highlighted several areas for implant design and surgical refinements. First, from the initial pair of animals that received a Generation 1 implant, it was determined that a change in stem shape, particularly adding a slight curvature to the distal stem, may ease installation. The location of the greater trochanter (directly superior to the canal) makes it difficult to install a long, cylindrical implant without substantial filing to prevent impingement on the lateral cortex of the medullary cavity. Over-filing may have contributed to implant subsidence observed for generation 1 animals (Fig. 10) and provided the rationale for making changes to the stem in the Generation 2 implants.

Second, it was noted that reaming of the proximal medullary cavity by hand with dental files was time consuming, and likely did not ensure that the proximal medullary cavity was filed to exactly match the geometry of the implant. Canal preparation could potentially be improved by developing a set of broaches congruent with our set of implants, to allow for incremental widening of the rat medullary cavity. This technique could potentially improve the precision and repeatability of implant potting, compared to the use of dental hand files alone, but would also likely exacerbate the risk of cortical fracture revealed in this study. Moreover, the cranio-lateral approach we have described may not be feasible for effective broaching; the spine of the rats, and the surrounding muscle bulk, obstruct access to the medullary cavity, even with the limb in excessive adduction. Altering the approach to access the hip joint posteriorly might be advantageous; this would allow for adduction and internal rotation of the femur, which would improve visualization down the proximal medullary cavity within the surgical field. This orientation would permit better access for tools, and could reduce the risk of fracture during future procedures.

Lastly, it was determined that the addition of a collar on the base of the neck would be useful as a visual reference; it was difficult to visualize the appropriate depth the implant should be inserted to achieve appropriate fit. During a longitudinal study, a collar may also be useful to prevent the implant from subsiding down the medullary canal, even if ideal fixation is not achieved, or is lost due to the introduction of an infectious agent. Furthermore, while an uncemented, press-fit approach was demonstrated, the implants described would also be suitable for a cemented approach; this would be practical for studies investigating concepts such as metal-on-cartilage wear, or antibiotic eluting cements, and would eliminate the need for a highly conformal medullary cavity around the implant stem. Metal alloys used to create implants could be adjusted as needed, along with surface preparation techniques to enhance head or stem of each implant, depending on the desired application.

2.5 Conclusions

We have demonstrated the use of quantitative, high-resolution micro-CT volumes of the proximal rat hip to create parameterized implants that were 3D-printed in medical-grade metal alloys and installed in an *in vivo* rat model of hip hemiarthroplasty. Our findings support further development of this model for use as a low-cost translational test platform for preclinical orthopaedic research into areas such as osseointegration, metal-on-cartilage wear and peri-prosthetic joint infection. This initial work was critical in establishing that the rat hip hemiarthroplasty model is feasible. Because of the difficulties encountered in our aforementioned surgical approach, the next objectives of this project involved determining if implants could be installed repeatedly, if implants would remain

stable in the bone over 12 weeks. Thus, Chapter 3 describes our efforts to establish a reliable surgical procedure that facilitates reproducible installation of components into the rat hip, as well as a post-operative imaging protocol to longitudinally evaluate implant position *in situ.*

2.6 References

1. Al-Jandan B, Marei HF, Abuohashish H, et al. 2018. Effects of sunitinib targeted chemotherapy on the osseointegration of titanium implants. Biomed Pharmacother 100:433-440.

2. Li K, Wang C, Yan J, et al. 2018. Evaluation of the osteogenesis and osseointegration of titanium alloys coated with graphene: an in vivo study. Sci Rep 8:1843.

3. He T, Cao C, Xu Z, et al. 2017. A comparison of micro-CT and histomorphometry for evaluation of osseointegration of PEO-coated titanium implants in a rat model. Sci Rep 7:16270.

4. Ma T, Ge XY, Hao KY, et al. 2017. Simple 3,4-Dihydroxy-L-Phenylalanine Surface Modification Enhances Titanium Implant Osseointegration in Ovariectomized Rats. Sci Rep 7:17849.

5. AbuMoussa S, Ruppert DS, Lindsay C, et al. 2018. Local delivery of a zoledronate solution improves osseointegration of titanium implants in a rat distal femur model. J Orthop Res 36:3294-3298.

6. Lindtner RA, Castellani C, Tangl S, et al. 2013. Comparative biomechanical and radiological characterization of osseointegration of a biodegradable magnesium alloy pin and a copolymeric control for osteosynthesis. Journal of the mechanical behavior of biomedical materials 28:232-243.

7. Ruppert DS, Harrysson OLA, Marcellin-Little DJ, et al. 2017. Osseointegration of Coarse and Fine Textured Implants Manufactured by Electron Beam Melting and Direct Metal Laser Sintering. 3D Print Addit Manuf 4:91-97.

8. Huanhuan J, Pengjie H, Sheng X, et al. 2017. The effect of strontium-loaded rough titanium surface on early osseointegration. J Biomater Appl 32:561-569.

9. Field JR, Callary SA, Solomon LB, et al. 2016. Early acetabular cartilage wear following hemiarthroplasty: An ovine model. Vet Comp Orthop Traumatol 29:125-130.

10. Stotter C, Stojanovic B, Bauer C, et al. 2019. Effects of Loading Conditions on Articular Cartilage in a Metal-on-Cartilage Pairing. J Orthop Res 37:2531-2539.

11. Stojanovic B, Bauer C, Stotter C, et al. 2019. Tribocorrosion of a CoCrMo alloy sliding against articular cartilage and the impact of metal ion release on chondrocytes. Acta Biomater 94:597-609.

12. Bargon R, Bruenke J, Carli A, et al. 2019. General Assembly, Research Caveats: Proceedings of International Consensus on Orthopedic Infections. J Arthroplasty 34:S245-S253 e241.

13. Jie K, Deng P, Cao H, et al. 2019. Prosthesis design of animal models of periprosthetic joint infection following total knee arthroplasty: A systematic review. PLoS One 14:e0223402.

14. Carli AV, Ross FP, Bhimani SJ, et al. 2016. Developing a Clinically Representative Model of Periprosthetic Joint Infection. J Bone Joint Surg Am 98:1666-1676.

15. Carli AV, Bhimani S, Yang X, et al. 2017. Quantification of Peri-Implant Bacterial Load and in Vivo Biofilm Formation in an Innovative, Clinically Representative Mouse Model of Periprosthetic Joint Infection. J Bone Joint Surg Am 99:e25.

16. Taha M, Abdelbary H, Ross FP, et al. 2018. New Innovations in the Treatment of PJI and Biofilms-Clinical and Preclinical Topics. Current reviews in musculoskeletal medicine 11:380-388.

17. El-Warrak AO, Olmstead M, Schneider R, et al. 2004. An experimental animal model of aseptic loosening of hip prostheses in sheep to study early biochemical changes at the interface membrane. BMC musculoskeletal disorders 5:7.

18. DiVincenzo MJ, Frydman GH, Kowaleski MP, et al. 2017. Metallosis in a Dog as a Long-Term Complication Following Total Hip Arthroplasty. Vet Pathol 54:828-831.

19. Volstad NJ, Schaefer SL, Snyder LA, et al. 2016. Metallosis with pseudotumour formation: Long-term complication following cementless total hip replacement in a dog. Vet Comp Orthop Traumatol 29:283-289.

20. DeYoung DJ, Schiller RA. 1992. Radiographic criteria for evaluation of uncemented total hip replacement in dogs. Vet Surg 21:88-98.

21. Powers DL, Claassen B, Black J. 1995. The rat as an animal model for total hip replacement arthroplasty. J Invest Surg 8:349-362.

22. Granton PV, Norley CJ, Umoh J, et al. 2010. Rapid in vivo whole body composition of rats using cone beam muCT. J Appl Physiol (1985) 109:1162-1169.

Chapter 3

3 Longitudinal Micro-Computed Tomography of A Rat Model of Hip Hemiarthroplasty Using 3D-printed Titanium Implants

3.1 Introduction

The establishment of clinically representative animal models of human disease is critical for testing new concepts, before innovations can be applied to patients. In orthopaedics, models such as sheep,[1] pigs,[2] goats,[3] and dogs[4] are often selected to investigate joint replacements, in part because their skeletal size permits the installation of human-like components. However, as decscribed in previous chapters, there are challenges related to the use of large animals in preliminary studies, including the expense of procurement, the need for specialized housing and husbandry, and the limited availability across all research institutions to conduct these studies. By comparison, small-animal models like mice,[5-7] rabbits,[8] guinea pigs,[9] and rats[10-14] offer substantially lower experimental costs, higher throughput potential, and can be easily housed in most institutions. Such studies have typically utilized cortical pins,[11; 15] screws,[12] and intramedullary rods[13; 14] installed into the bone, but such models are limited compared to large animal studies. Specifically, traditional small-animal models do not replicate the peri-prosthetic environment, which ideally includes a functioning, load-bearing component that interacts against cartilage within a synovial joint space. A small-animal model that utilizes a functional implant could serve as a clinically representative platform

for research into areas such as osseointegration,[8; 11-14] metal-cartilage wear,[16; 17] and peri-prosthetic joint infection (PJI).[5; 7]

Previous work by Powers *et al.* proposed the rat as an ideal model for translational joint replacement studies, due to its use across a variety of medical research disciplines.[10] Their study tested a cemented rat total hip system, but had limitations that have prevented this rat model from being widely adopted, including: (i) removal of the greater trochanter during surgical installation, compromising post-operative functionality of the hip joint, (ii) difficulty in achieving fixation of the acetabular component due to the thin rat pelvis, and (iii) the non-conformal proximal femoral anatomy of the rat, which required bone cement to be used for fixation.[10] While the design, manufacture, and surgical implantation of implants in the rat hip model is inherently challenging, the advantages of its potential use in preliminary orthopedic research are numerous, and warrants further investigation.

To improve the efficacy of the rat hip model, several improvements could be made: (i) preservation of the greater trochanter to improve the stability of the hip and facilitate recovery; (ii) a hemi-arthroplasty approach to simplify the procedure and reduce the potential for complications, and; (iii) a highly conformal, functional, rat-specific implant that permits an uncemented approach to allow potential changes at the bone-implant interface to be investigated. The current study investigates the feasibility of implementation of a functional, uncemented rat hip implant.

Previous work by Carli *et al.* demonstrates that recent advances in additive manufacturing (3D metal printing), allow for the creation of miniature joint replacement

components in medical-grade metal alloys, and in the sizes required for use in a mouse-knee model of PJI.[5] This work leads to the possibility of using this manufacturing approach to develop a custom implant for the rat hip joint. The benefit of using the rat, which has larger joints than the mouse, is that features such as tool attachments and porosities, found on commercially available joint implants, could be incorporated into components, adding to their utility. In addition, micro-computed tomography (micro-CT) is an ideal imaging modality for evaluating rats[11; 18] and can permit longitudinal analysis of the skeleton, without the need to sacrifice animals at multiple time-points. Thus our objectives are to manufacture a rat-specific set of uncemented, functional femoral implants, to demonstrate the installation of such components, and show that implant position can be evaluated over time, using high-resolution cone-beam micro-CT.

3.2 Materials and Methods

3.2.1 Implant Manufacturing

Implants were designed in five different sizes, to accommodate rats of different weight and skeletal dimensions, as described in Chapter 2 (Fig. 3.1). Computer-aided design (CAD) software (Solidworks by Dassault Systemes, Vélizy-Villacoublay, France) was used to design the implants. Dimensions were selected based on proximal femoral measurements, obtained from previously acquired high-resolution micro-CT volumes of rats.[18] Additional features were included in an effort to facilitate effective installation and long-term fixation: (1) a collar to assist with primary fixation by deterring subsidence and over-seating of implants during press-fitting; and (2) a honey-comb-like porosity (500μm

diameter hexagonal holes) to help facilitate secondary fixation, ideally promoting osseointegration.

Figure 3.1: Custom rat hip implants created in medical-grade titanium alloy (Ti6Al4V) in a range of sizes to accommodate rats of various weights, shown beside a Canadian dime for scale. A hexagonal porosity was introduced into the stem design (0.5mm diameter) in an effort to facilitate osseointegration. A collar was included to help prevent over-pressing of components and aid in primary stability. An impactor tool was also printed to facilitate the press-fit of implants into the medullary cavity.

Implants were then printed in medical-grade titanium alloy (Ti6Al4V) on a commercially available 3D-metal printer (AM-400, Renishaw plc, New Mills Wotton-under-Edge, UK). The articulating heads of each implant were polished to a mirror-like finish using a dental hand-tool and a series of stones and rubber wheels. Once polished, implants were cleaned for 20 minutes in an ultrasonic bath of detergent before being rinsed with water, dried, and sterilized via autoclave prior to surgery. An impactor tool was inserted into the proximal stem of each implant to help facilitate press-fitting of

implants into the proximal femoral medullary cavity; this tool was also 3D-printed in titanium (Ti6Al4V) and cleaned in the same fashion (Fig. 3.1).

3.2.2 Animals

Animal studies were approved by the institutional Animal Care Committee (AUP 2017-156). Sprague-Dawley rats (N=6) were obtained for use in this study (Charles River Laboratories, Senneville, Canada) (Table 3.1). Animals were housed in a conventional vivarium with 12-hour light/dark cycle and provided *ad libitum* standard rodent chow and water. The hemiarthroplasty surgical procedures were performed aseptically and inside a sterile field. Anesthesia was induced within a chamber using 4% isofluorane and maintained via nose cone at 1.5%. External heat support and anesthetic depth monitoring were maintained throughout the procedure.

Table 3.1: Baseline metrics obtained one week prior to surgery of male Sprague-Dawley rats (N=6). Means are listed below, with measurement range bracketed.

Weight (g)	Inclination Angle (degrees)	Anteversion (degrees)	Length of Femur (mm)
627.4	130.4	13.0	44.01
(552.0, 761.9)	(128.5, 132.7)	(8.8, 15.6)	(41.21, 45.76)

3.2.3 Surgical Technique

A posterior approach was selected for accessing the hip joint. A 3-4 cm linear incision was made over the greater trochanter of the right femur. Subcutaneous tissue was

incised and retracted. The tensor fascia lata was located and an incision along the fascia was extended to the length of the skin incision. Muscle fibres of the gluteus maximus were split using blunt dissection, revealing deep muscles and the sciatic nerve. The hip was internally rotated to locate the group of short rotator muscles (piriformis, superior gemellus, obturator internus, inferior gemellus). The attachment of the short rotators was cut using microsurgical scissors and detached as close to the hip joint as possible and then reflected backward to protect the sciatic nerve. The joint capsule was incised using microsurgical scissors and the hip was dislocated using internal rotation after capsulotomy. The hip joint capsule incision was then extended in a dorsocaudal direction using scissors to provide better visualization of the acetabulum, which was cleaned of tissue.

A dental scaling tool was used to perform an osteotomy of the head and neck of the femur, above the superior aspect of the lesser trochanter, then used to remove bone from the base of the greater trochanter to access the medullary cavity and provide space for the implant to be introduced into the proximal femur. The impactor tool was then inserted into the shoulder of the implant to facilitate press-fit of the implant with a small hammer. Once positioned, the neck of the implant was then gripped by forceps and manipulated to ensure the implant was securely press-fit. The ball of the implant was then placed into the acetabulum to re-locate the joint. The joint capsule was then closed using a simple interrupted pattern with 5-0 Monocryl sutures. The muscle layers were loosely apposed to reduce dead space. The gluteus maximus, fascia lata and subcutaneous layers were closed using 5-0 Monocryl in a simple continuous pattern. The skin was closed with subcuticular 6-0 Monocryl and tissue glue.

3.2.4 Post-operative Protocol

Following recovery from anesthesia, animals were placed alone in cages with clean bedding. Therapy included antibiotics (Baytril, 10 mg/kg SC daily for 10 days) and drugs for pain management (Metacam,1 mg/kg, daily for 7 days, Buprenorphine, 0.07 mg/kg SC daily for 3 days).

3.2.5 Imaging

Micro-CT imaging was conducted on a commercially available cone-beam scanner (eXplore Locus Ultra, GE Medical, London, Ontario) with 154μm isotropic voxel resolution and a consistent scan protocol (120kVp, 20mA, 16s). Scans centered on the hip joint were conducted at 1 week prior to surgery (baseline), post-operative day 1 (week 0), and at post-operative weeks 1, 3, 6, 9 and 12 to evaluate the position of implants over time. A beam-hardening correction was implemented to reduce the impact of metal artifacts within each scan volume.[19] Rat micro-CT volumes were analyzed in MicroView 2.2 (Parallax Innovations, Ilderton, Ontario), by a single user. Volumes were cropped to isolate the affected femur, then reoriented to ensure accurate measurements: the coronal plane bisected the center of the affected limb's femoral head and the center of the proximal medullary cavity, while the sagittal plane was aligned to bisect the center of the proximal medullary cavity along its centerline (Fig. 3.2). The vertical distance between the superior tip of the greater trochanter and the junction of the neck and collar of the implant was used to determine if translation of the implant distally (subsidence) was occurring over time. Three angles were also measured to convey implant position: (1) the inclination angle between the axis through head and neck of the implant and the

long-axis of the proximal medullary cavity; (2) the anterior tilt angle of the stem of the implant, compared to the long-axis of the medullary cavity, in the sagittal plane with respect to the femur; (3) the anteversion angle of the head and neck of the implant compared to the medial-lateral axis through the femoral condyles, in the transverse plane with respect to the femur (Fig. 3.2). The length of the rat femur was also measured from the distal edge of the lateral femoral condyle in the coronal plane to the superior aspect of the greater trochanter of the femur. Measurements were repeated three times and averaged.

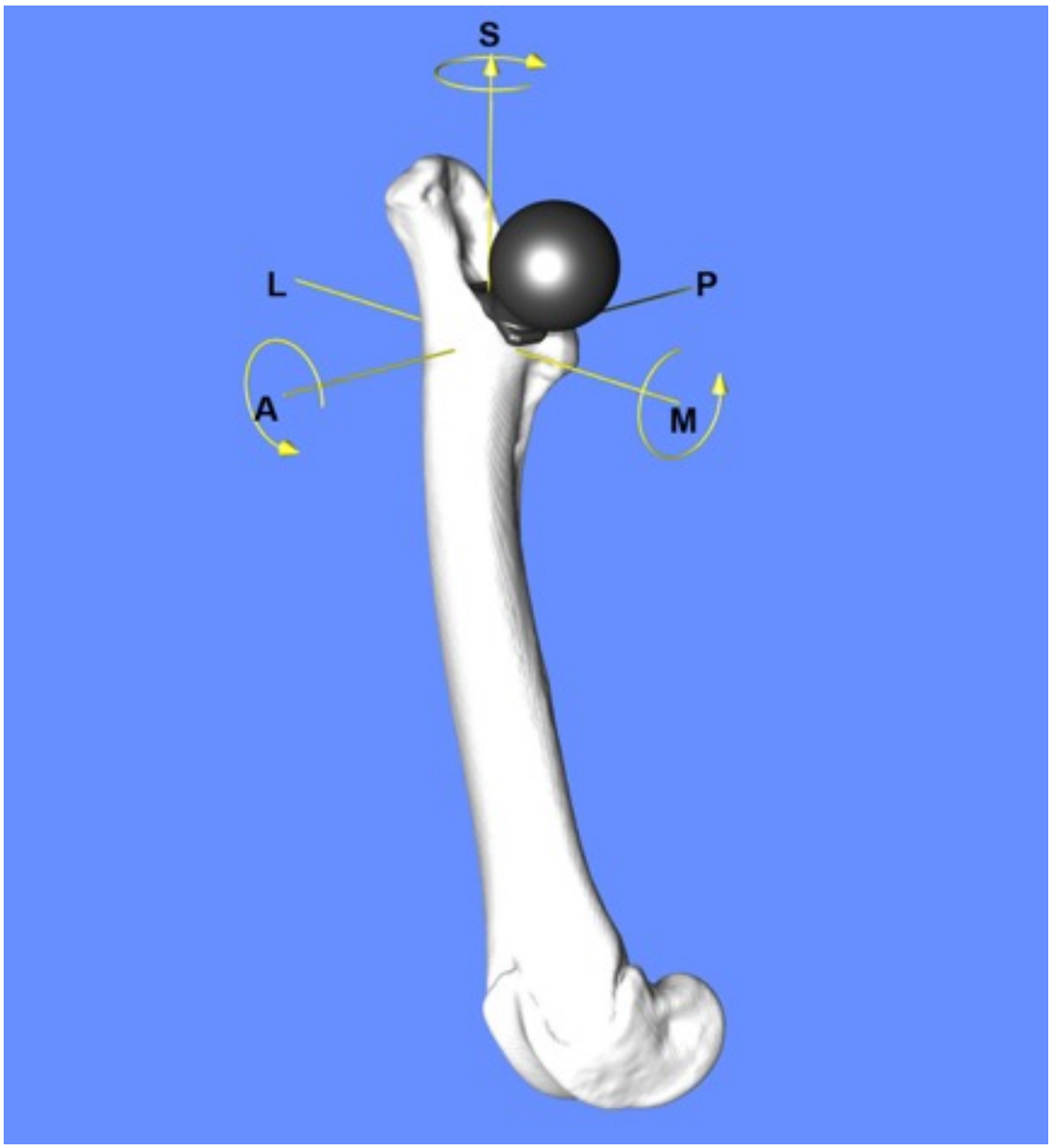

Figure 3.2: Co-ordinate system used to reorient each femur during micro-CT analysis. Angular measurements, made to reflect changes in implant position over time, were implemented by comparing implant position to the anterior-posterior (AP), medial-lateral (ML) and superior-inferior (SI) axes and their associated planes. Translation (subsidence) was measured along the SI axis. Arrows indicate direction of increasing values.

3.2.6 Statistics

Animals were followed longitudinally for six time-points and measurements (as described above) were obtained for five animals. Note that one animal was removed from the study at week 6 (described below), and thus these data could not be included in statistical analysis. Normality was assessed using the Kolmogorov-Smirnov test; all data were found to be consistent with a Gaussian distribution. Column statistics were analyzed (GraphPad Prism, San Diego, California) using repeated-measures ANOVA, with a Bonferroni multiple-comparison post-hoc test. Significance between data at all time-points was determined at the $p < 0.05$ level.

3.3 Results

Surgical installation of implants was successful in N=6 animals. The greater trochanter was preserved in all cases, and each animal was observed ambulating and rearing on their affected limb immediately post-operatively. One animal experienced a drop-foot gait initially, likely due to inadvertent sciatic nerve irritation, which resolved within the first post-operative week. This rat was later sacrificed after the 6-week post-operative time-point, due to initial concerns that subsidence occurred secondary to a joint infection; this concern was later ruled out by a veterinary pathologist. The remaining five rats all progressed to the 12-week post-operative time-point. *Post mortem* analysis revealed variable amounts of motion when implants were manipulated with forceps, with more gross movement detected in subsided implants. The stem of each implant appeared to be surrounded by fibrous tissue.

The micro-CT protocol described above was sufficient to measure translation of the titanium implants within the bone over time (Fig. 3.3). All implant stems were observed to be in direct contact with the endosteum 1 day and 1 week following implantation. A loss of close contact between the implant stem and endosteum could be observed at post-operative week 6 and later time-points (Fig. 3.3). Implant translation distally in the femur (subsidence) was observed for all animals. Hip dislocation following subsidence was observed in two of five animals at the 6-week post-operative time-point. Translation was significantly greater at post-operative weeks 6, 9 and 12 compared to week 0 ($p<0.05$) (Fig. 3.4). Instances of hip dislocation unrelated to subsidence were not observed.

The inclination angle had changed to become significantly more valgus at post-operative week 12 compared to week 0 ($p<0.05$) (Fig. 3.5). The anterior tilt angle fluctuated, but no significant difference was found between time-points ($p>0.05$) (Fig. 3.6). The anteversion angle also fluctuated, suggesting that implants were prone to rotation within the medullary canal, but again no significant difference was found between time-points ($p>0.05$) (Fig. 3.7). Three of five animals appeared to be growing throughout the study; as a result, femoral length increased significantly in this cohort between week 0 and post-operative weeks 9 and 12 ($p<0.05$) (Fig. 3.8).

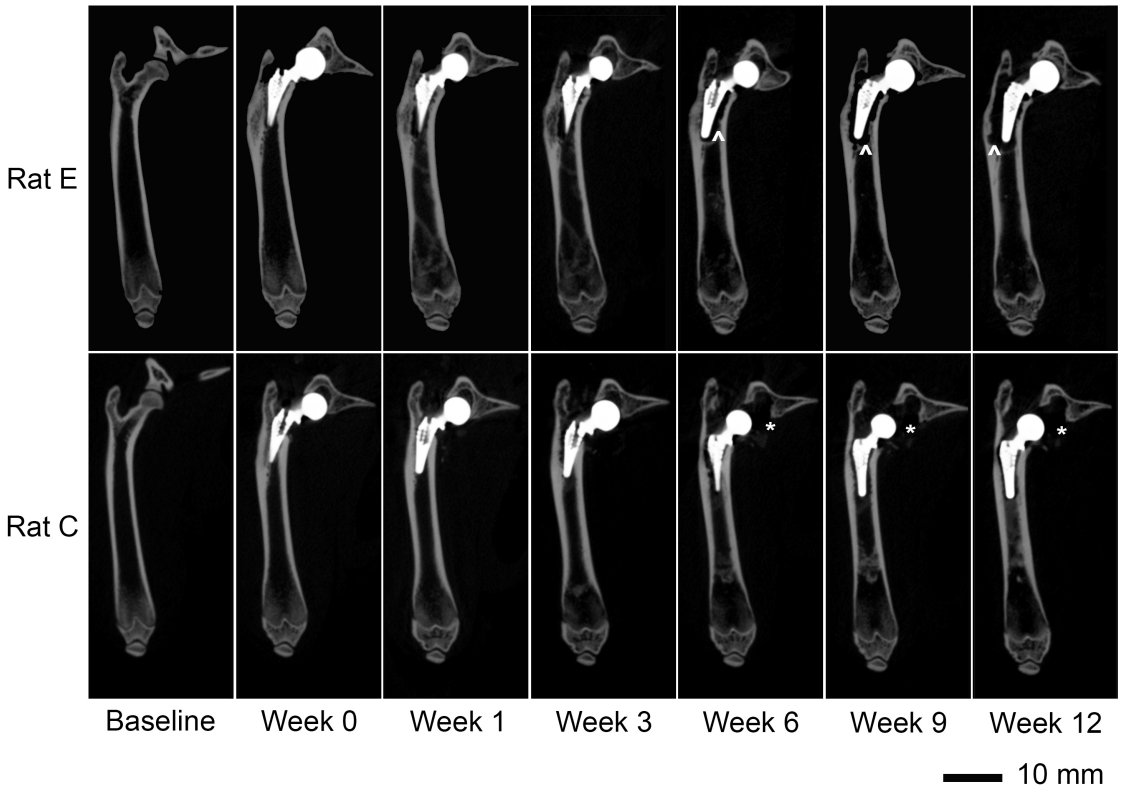

Figure 3.3: Progression of implant position at baseline, day 1 post-op (week 0), post-operative weeks 1, 3, 6, 9 and 12. Subsidence resulting in dislocation of the hip can be observed at week 6 for Rat C, indicated by asterisks, while the implant belonging to Rat E remains within the acetabulum at week 12. For Rat E, bone resorption around the implant, with probable replacement with fibrous tissue, can be seen beginning at week 6, indicated by carets.

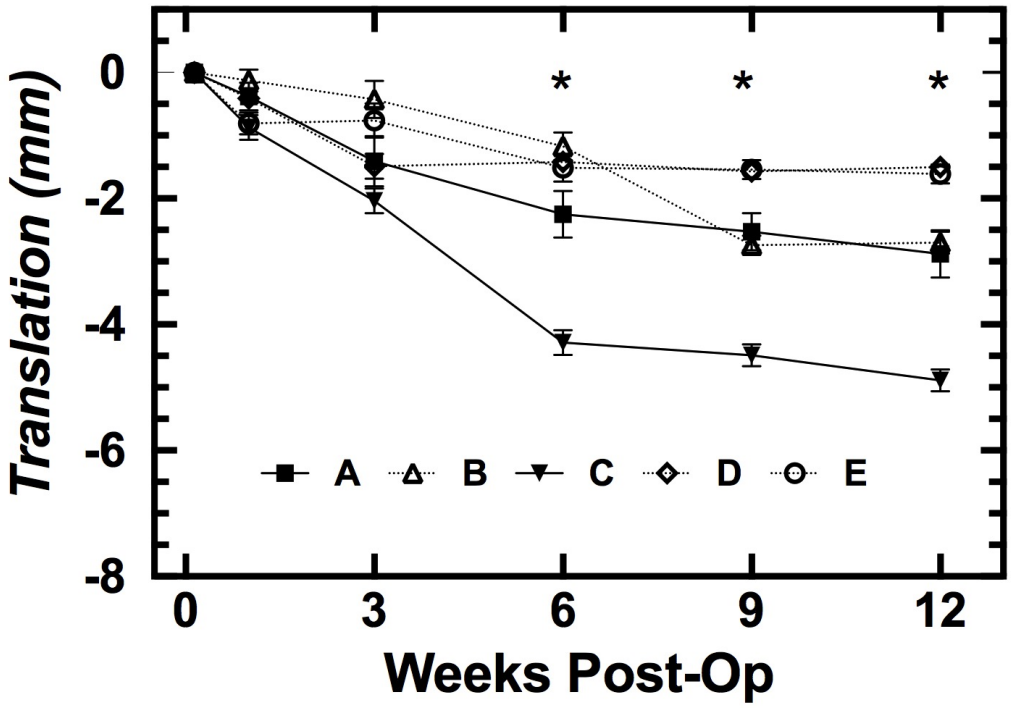

Figure 3.4: Translation (mm) of implants (subsidence) for Rat A-E at post-operative time points compared to initial post-operative position measured at post-op day 1 (week 0). Translation was evaluated based on changes in vertical displacement from the tip of the greater trochanter to the stem-neck junction of each implant. Negative translation indicates distal movement within the medullary canal, away from the greater trochanter along the superior-inferior axis. Translation was significantly different at weeks 6, 9 and 12 ($p<0.05$) compared with week 0 (denoted by an asterisk). Mean translation reached a maximum value of 2.7mm at week 12. Error bars represent the standard error of the mean.

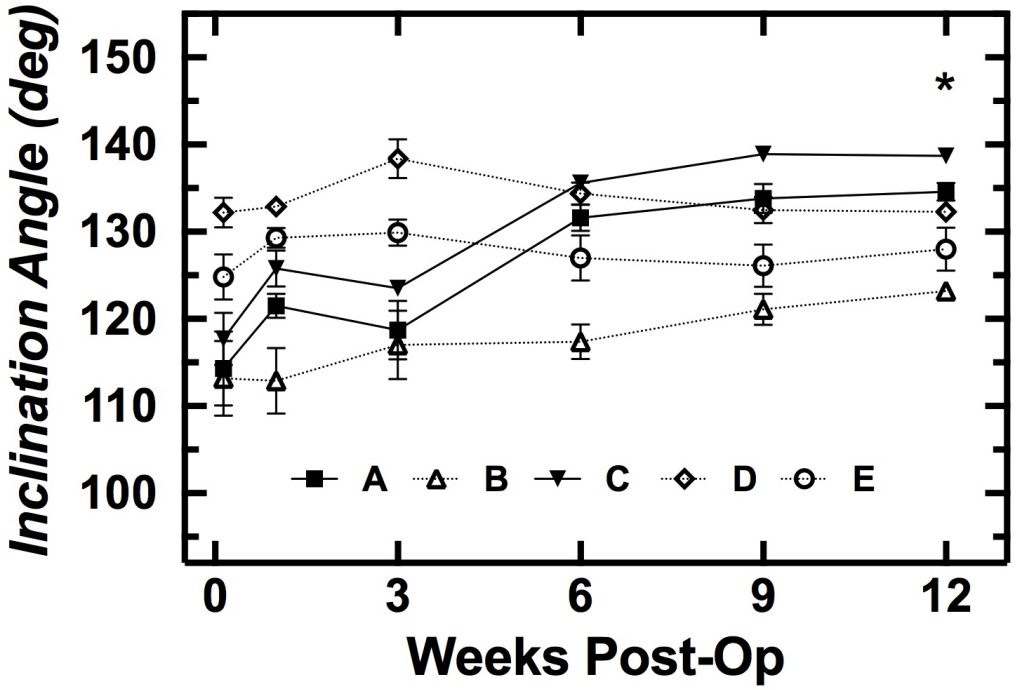

Figure 3.5: Inclination angle (degrees) measured for Rats A-E at Post-operative weeks 0, 1, 3, 6, 9 and 12. Inclination was measured as the angle between the head and neck of the implant and the superior-inferior axis of the proximal medullary cavity. Increasing angles correspond a more valgus alignment of the femur. Implants at week 12 had a significantly higher inclination angle compared to week 0 ($p<0.05$), denoted by an asterisk, with a mean increase of 10.92 degrees. Error bars represent the standard error of the mean.

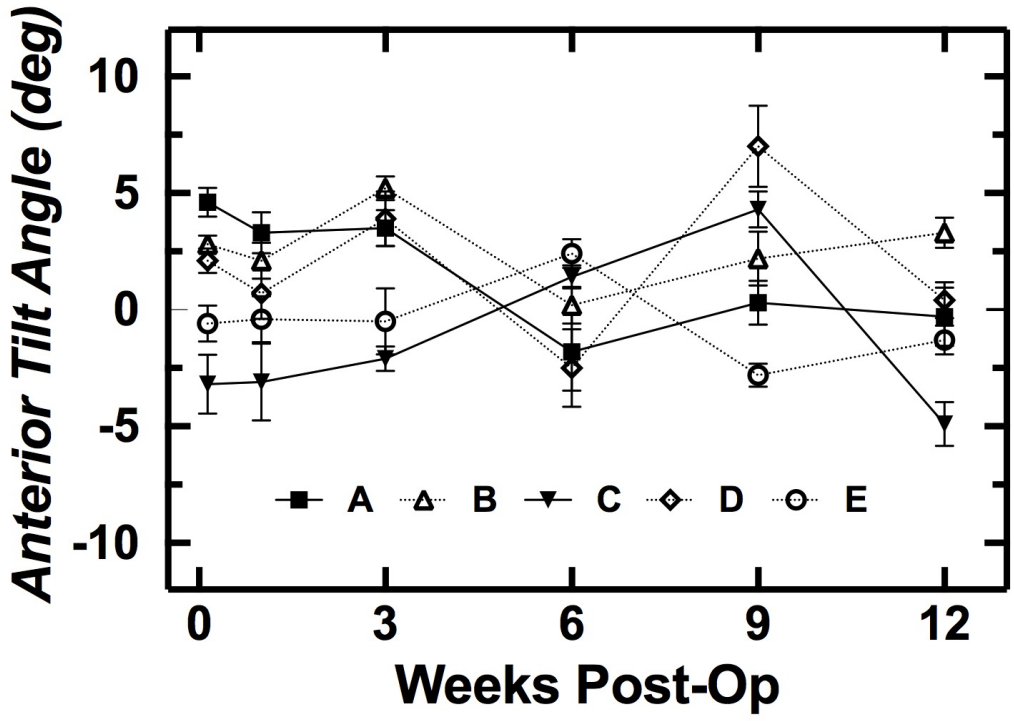

Figure 3.6: Anterior tilt angle of the stem of the implant (degrees), compared to the superior-inferior axis of the medullary cavity, measured at post-operative weeks 0, 1, 3, 6, 9 and 12. Positive tilt angles indicate a more anterior position of the proximal stem, compared to distal. No significant differences in alignment were found between week 0 and later time points ($p>0.05$). Error bars represent standard error of the mean.

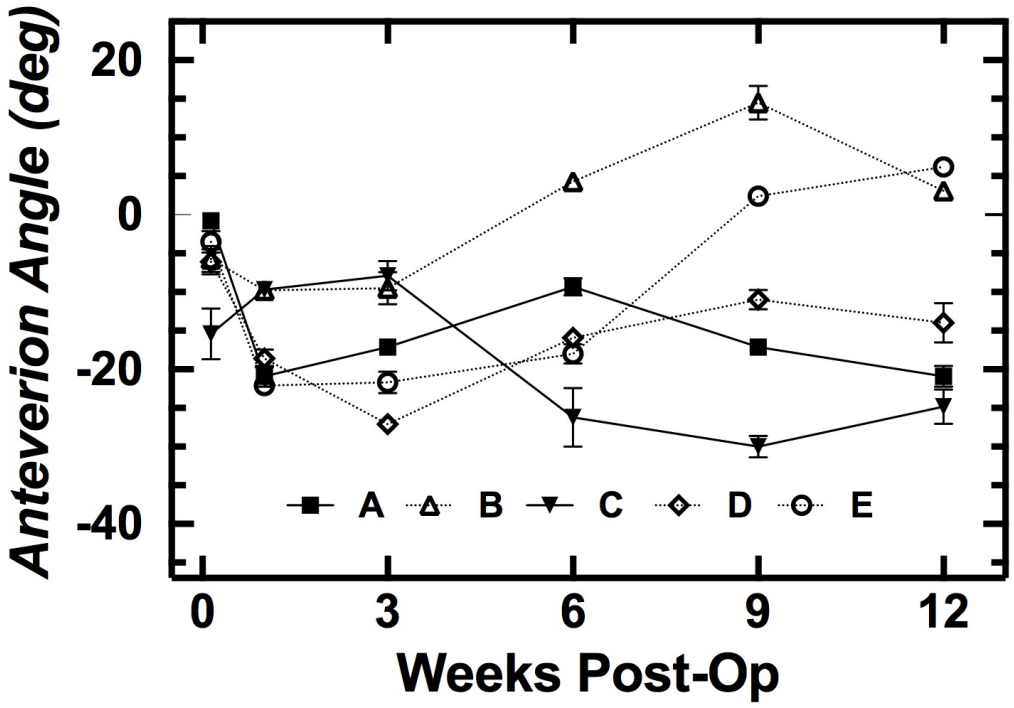

Figure 3.7: Anteversion angle of the head and neck of the implant (degrees) compared to the medial-lateral axis, which was parallel through the femoral condyles of the knee, measured at post-operative weeks 0, 1, 3, 6, 9 and 12. Negative anteversion infers a retroverted head position. No significant differences in anteversion angle were found between week 0 and the later post-operative time points ($p>0.05$). Error bars represent the standard error of the mean.

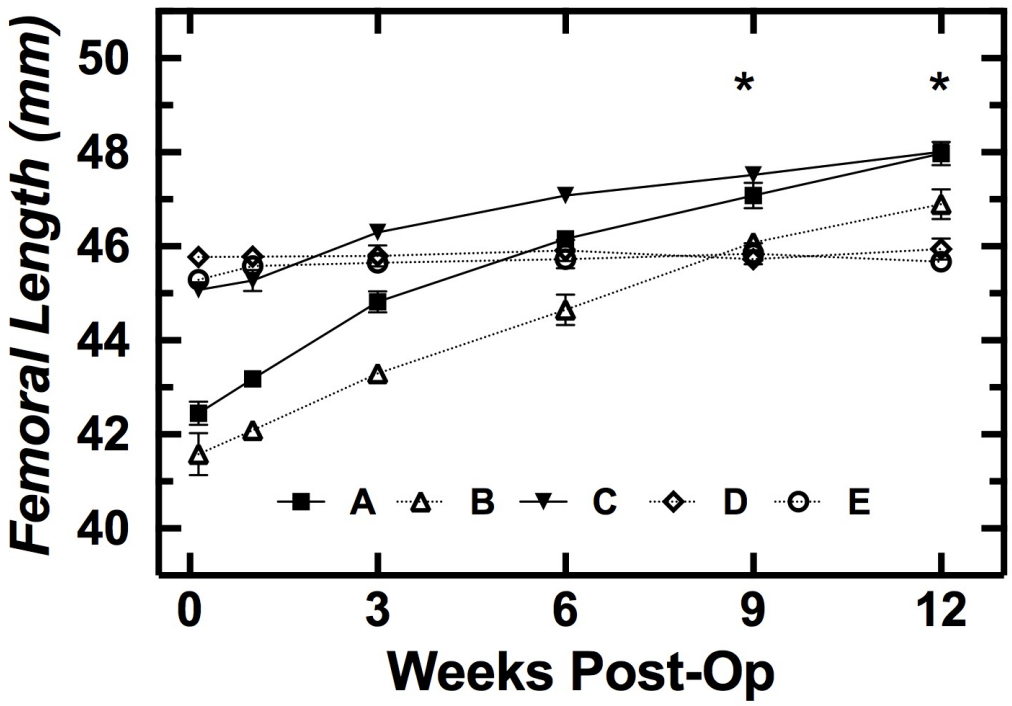

Figure 3.8: Length of the femur (mm) for Rats A-E, measured from the superior aspect of the greater trochanter to the distal edge of the lateral femoral condyle along the superior-inferior axis. Femoral length increased significantly ($p<0.05$) at post-operative weeks 9 and 12 compared to baseline, with an average increase in length of 2.42mm at week 9 and 2.86mm at week 12. Error bars indicate the standard error of the mean.

3.4 Discussion

This study has demonstrated the feasibility of both the fabrication and surgical implementation of a new model for hemiarthroplasty in the rat. Titanium alloy components of the required shape and dimensions were fabricated using additive manufacturing techniques, and the rat model was compatible with live-animal imaging using micro-CT to track the stability of the implant over time. Overall, animals were able

to tolerate the procedure and resumed normal cage behaviour within the first week, post-operatively. The implants installed were press-fit into the bone sufficiently to facilitate ambulation in each animal following recovery from anaesthesia. This work expands on previous efforts to establish a small-animal model that includes a functional joint replacement component.[5; 10]

The mouse knee model described by Carli *et al.* also utilized additive manufacturing to create implants in the sizes needed for small-animal testing, and demonstrates a clinically relevant model of peri-prosthetic joint infection (PJI).[5] The importance of furthering our understanding of PJI is clear, as it is one of the most catastrophic complications that can occur following an otherwise successful surgical procedure to install an implant.[5; 20] Our findings suggest that the rat hip hemiarthroplasty model could potentially serve as a complement to knee models of PJI,[21] and offer basic scientists another preclinical tool to help improve understanding of this devastating complication. In this case, fixation would become important, since infection is accompanied by osteolytic processes[5] that would likely accelerate subsidence.

The rat total-hip arthroplasty model described by Powers *et al.*[10] had several limitations that were addressed in this study. Specifically we were able to demonstrate the preservation of the greater trochanter during our surgical procedure, the introduction of an uncemented implant, and elimination of the acetabular component to limit potential for post-operative compilations. An uncemented rat hip implant also has potential to serve as model for osseointegration, and maintain comparability to both small animal studies that use non-functioning implant, and large animal studies in this area.

The removal of the acetabular component also has the added benefit of providing an option to investigate cartilage changes as a result of regular articulation with a metal implant. While articulating components in clinical implants are typically not fabricated from titanium alloy – largely due to concerns about wear – the use of a titanium head in this rat model may provide new information about the metal-cartilage interface. It is also worth noting that the same additive manufacturing process that was used here to produce titanium alloy components can be used to fabricate in Cobalt-Chrome (ASTM F75); this may be advantageous in studies that are focused on the cartilage interface, rather than osseointegration.

Overall, our surgical approach was feasible and allowed for effective access to the rat hip joint to install components, but had several limitations. First, irritation of the sciatic nerve, which is visible in the surgical field when performing a posterior approach, was likely responsible for the one instance of drop-foot gait observed post-operatively. Cases of subsidence were observed, mimicking a known clinical complication.[1; 4] Although subsidence resulting in hip dislocation was observed, such a complication should not prevent the use of this model in future studies, as optimal integration by unaltered implants could diminish the ability to evaluate novel stem coatings aimed at promoting osseointegration.

Second, when performing cementless hip arthroplasty, achievement of primary mechanical stability and secondary biological fixation is crucial to ensure that the implant does not subside. Since infection was not identified during post-mortems, several factors related to primary and secondary implant fixation may have contributed to subsidence in this cohort. Preparation of the inner cortex of the proximal medullary cavity by hand may

not have created a sufficiently congruent space to maximize the bone contact area around stems of the implants and prevent micro-motion. A broaching system may have some utility in resolving this issue by allowing for incremental widening of the medullary canal, provided that broaching is accomplished without fracturing the observably thin cortex in the rat femur.

Third, the additive manufacturing process produced an inherent surface texturing of the implant, which was removed from the articulating surface, but left intact on the stem in an effort to promote osseointegration. The addition of an engineered porosity through the implant stem, also intended to promote osseointegration, may not have been sufficient in promoting biological fixation of bone, which was not observed in this study. The application of a known osteoconductive substance such as hydroxy-apatite may be useful in future studies to better facilitate biological fixation through osseointegration.[3] Furthermore, the increasing femoral length observed in three of five animals (Fig. 8) may be indicative of overall bone growth. This could suggest that the implant selected at the time of surgery may not be of sufficient size at a later time-point to retain its congruent press-fit in the medullary cavity. Animal procurement in future studies should perhaps consider older animals that have reached skeletal maturity, and avoid selection based on rat weight alone.

Finally, loss of an observable bone-implant interface was revealed at later time-points during this study, with bone likely being replaced with fibrous tissue, which was found surrounding each implant during *post-mortem* analysis (Fig. 3). Future efforts could include more robust measurements to quantify the bone-implant interface as a measure of osseointegration, with complementary histology. Gait analysis to understand

the post-operative kinematics of the rat following hip hemiarthroplasty would also be beneficial to determine how well gait is restored, compared to baseline or its contralateral limb.

3.5 Conclusions

Our findings support further development of the rat hip hemiarthroplasty model as a preclinical platform, which could be expanded for studies investigating osseointegration, metal-cartilage wear and peri-prosthetic joint infection around a functional implant. While we were unable to achieve consistent bone fixation, the surgical approach to install implants consistently was validated, as well as the use of micro-CT imaging to track implant position post-operatively and detect clinically representative complications. As mentioned above, one research question that should be investigated is to what extent animals are able to ambulate on their affected limbs post-operatively. The establishment of a post-operative gait analysis protocol, along with functional dynamic imaging of an implant as it articulates within the rat hip is explored in Chapter 4.

3.6 References

1. Jakobsen T, Kold S, Baas J, et al. 2015. Sheep Hip Arthroplasty Model of Failed Implant Osseointegration. The open orthopaedics journal 9:525-529.

2. Hunt S, Stone C, Seal S. 2011. Timing of femoral prosthesis insertion during cemented arthroplasty: cement curing and static mechanical strength in an in vivo model. Can J Surg 54:33-38.

3. Harboe K, Gjerdet NR, Sudmann E, et al. 2014. Assessment of retention force and bone apposition in two differently coated femoral stems after 6 months of loading in a goat model. Journal of orthopaedic surgery and research 9:69.

4. Liska WD, Doyle ND. 2015. Use of an Electron Beam Melting Manufactured Titanium Collared Cementless Femoral Stem to Resist Subsidence After Canine Total Hip Replacement. Vet Surg 44:883-894.

5. Carli AV, Ross FP, Bhimani SJ, et al. 2016. Developing a Clinically Representative Model of Periprosthetic Joint Infection. J Bone Joint Surg Am 98:1666-1676.

6. Li Z, Kuhn G, Schirmer M, et al. 2017. Impaired bone formation in ovariectomized mice reduces implant integration as indicated by longitudinal in vivo micro-computed tomography. PLoS One 12:e0184835.

7. Hegde V, Dworsky EM, Stavrakis AI, et al. 2017. Single-Dose, Preoperative Vitamin-D Supplementation Decreases Infection in a Mouse Model of Periprosthetic Joint Infection. The Journal of bone and joint surgery American volume 99:1737-1744.

8. Al-Jandan B, Marei HF, Abuohashish H, et al. 2018. Effects of sunitinib targeted chemotherapy on the osseointegration of titanium implants. Biomed Pharmacother 100:433-440.

9. De Smet E, Jaecques SV, Wevers M, et al. 2013. Constant strain rate and peri-implant bone modeling: an in vivo longitudinal micro-CT analysis. Clin Implant Dent Relat Res 15:358-366.

10. Powers DL, Claassen B, Black J. 1995. The rat as an animal model for total hip replacement arthroplasty. J Invest Surg 8:349-362.

11. He T, Cao C, Xu Z, et al. 2017. A comparison of micro-CT and histomorphometry for evaluation of osseointegration of PEO-coated titanium implants in a rat model. Sci Rep 7:16270.

12. Huanhuan J, Pengjie H, Sheng X, et al. 2017. The effect of strontium-loaded rough titanium surface on early osseointegration. J Biomater Appl 32:561-569.

13. AbuMoussa S, Ruppert DS, Lindsay C, et al. 2018. Local delivery of a zoledronate solution improves osseointegration of titanium implants in a rat distal femur model. J Orthop Res 36:3294-3298.

14. Ruppert DS, Harrysson OLA, Marcellin-Little DJ, et al. 2017. Osseointegration of Coarse and Fine Textured Implants Manufactured by Electron Beam Melting and Direct Metal Laser Sintering. 3D Print Addit Manuf 4:91-97.

15. Li K, Wang C, Yan J, et al. 2018. Evaluation of the osteogenesis and osseointegration of titanium alloys coated with graphene: an in vivo study. Sci Rep 8:1843.

16. Heiner AD, Smith AD, Goetz JE, et al. 2013. Cartilage-on-cartilage versus metal-on-cartilage impact characteristics and responses. Journal of orthopaedic research : official publication of the Orthopaedic Research Society 31:887-893.

17. Oungoulian SR, Durney KM, Jones BK, et al. 2015. Wear and damage of articular cartilage with friction against orthopedic implant materials. Journal of biomechanics 48:1957-1964.

18. Granton PV, Norley CJ, Umoh J, et al. 2010. Rapid in vivo whole body composition of rats using cone beam muCT. Journal of applied physiology (Bethesda, Md : 1985) 109:1162-1169.

19. Edey DR, Pollmann SI, Lorusso D, et al. 2019. Extending the dynamic range of biomedical micro-computed tomography for application to geomaterials. Journal of X-ray science and technology 27:919-934.

20. Schwarz EM, Parvizi J, Gehrke T, et al. 2019. 2018 International Consensus Meeting on Musculoskeletal Infection: Research Priorities from the General Assembly Questions. J Orthop Res 37:997-1006.

21. Jie K, Deng P, Cao H, et al. 2019. Prosthesis design of animal models of periprosthetic joint infection following total knee arthroplasty: A systematic review. PLoS One 14:e0223402.

Chapter 4

4 Post-operative Gait Analysis in a Rat Model of Hip Hemiarthroplasty

4.1 Introduction

Joint replacement surgeries are performed to replace damaged bone and cartilage and restore functional mobility in patients. As described in Chapter 1; while the vast majority of procedures are successful, implants do not always last a lifetime and may be replaced for reasons such as aseptic loosening[1-3] or infection.[4-7] Revision surgeries to replace failed components are more costly and have higher complication rates compared to primary joint replacement surgeries, placing an added burden on both patients and healthcare systems. Consequently, preclinical orthopaedic research continues to be dedicated towards improving the longevity of joint replacement implants. Traditionally, large-animal models have used as preclinical test platforms to answer research questions related to implant function and longevity. Large-animal models including pigs[8], sheep[9; 10], dogs[11; 12], and horses[13] are often selected because their joint sizes are of similar dimensions to humans, which permits human-sized implants to be installed, using tools and procedures that mimic human surgeries. Small-animal models on the other hand, such as mice[14-16], rats[17-19] and rabbits[20] have historically been reserved for earlier stages of preclinical research, where basic scientists have tested innovations related to implant longevity, including osseointegration, metal cartilage wear and infection. Small-animal studies are much less costly to conduct compared to large-animal trials, however small-

animal models typically do not receive functional implants that mimic human components. Instead non-functional hardware in the form of metal rods[17; 21], screws[22] and pins[19; 23] are often used, as they are much easier to install into smaller bones.

Recently, efforts have been made to incorporate functional implants into murine models, specifically rats[24] and mice[6; 14], to allow basic scientists to perform cost-efficient studies involving functional implants in small-animal models that are also clinically representative of human joint replacement surgeries. While the design and surgical installation of small-animal specific implants is now possible, it is unclear to what extent functional recovery of ambulation on the affected limb is achieved. Ideally, approaches should permit the eventual recovery of the ipsilateral (affected) limb to the point where it could not be distinguished from its contralateral (unaffected) limb during normal ambulation. It follows that quantifying the post-operative gait of small-animals who have undergone joint replacement surgery would be an important next step in demonstrating a clinical representative functional implant model.

In order to assess functional gait recovery, a variety of small-animal specific hardware options exist. In particular, an optical gait analysis system, known as the CatWalk XT (Noldus, Leesburg, Virginia) has been used for a variety of studies in rats[25-28] and mice[29] for both neurologic[26; 29] and orthopaedic[27; 28] applications. Briefly, the CatWalk XT system is a runway with a glass floor that has fluorescent light passing through it. As the animal contacts the floor, the light that normally is internally reflected within the floor, reflects downward. A camera captures each paw print as the animal transverses the walkway, and a series of gait metrics are computed. Miyamoto et al[25] recently utilized the CatWalk XT a study in rats with hip osteoarthritis, revealing

significant differences in several gait metrics when comparing affected versus unaffected limbs. It follows that the CatWalk XT system would likely be ideal to use for quantifying the gait of small-animals, specifically rats, following joint replacement surgery.

One potential disadvantage to using the CatWalk XT to assess gait, particularly as it pertains the joint replacement, is that such a system, which relies on optics, does not facilitate direct observations of the joint of interest during locomotion. The ability to observe an implant function during cyclic loading is important to ensure that the component is serving its intended purpose (bearing weight and articulating within the joint). Using another gait analysis approach in tandem with the CatWalk XT, such as X-ray fluoroscopic video analysis, which is routinely performed in both humans and animals, would be beneficial; this would provide two sets of complementary data that could be analyzed concurrently to give an accurate representation of small-animal gait following joint replacement surgery.

To permit the acquisition of fluoroscopic data it is beneficial to create a treadmill system; this allows the X-ray source and detector to remain stationary while images are collected of the joint of interest during repeated gait cycles, minimizing image blur. A variety of small-animal treadmill systems exist, however commercially available systems are rarely designed specifically for fluoroscopic assessment, meaning that they are not build with radiolucent materials to permit unimpeded visualization of the subject in multiple fields-of-view. Guillot et al[30] recently demonstrated a radiolucent treadmill system in cats, as well as the use of a high-pass filter to enhance the edges of structures (bone in particular) within each frame so that anatomical features could be observed more clearly in the resulting videos and still-frame radiographs. While a typical fluoroscopic

setup would include a dedicated X-ray source capable of capturing successive radiographs at a given frequency, cone-beam micro-computed tomography scanners can also be used to acquire fluoroscopic x-ray videos if the gantry is kept stationary during acquisition. Furthermore, such systems can be programed so that the gantry can be parked at specific view angles (i.e. 0 degrees, and 90 degrees) to facilitate video collection in multiple anatomical planes (i.e. dorsal-ventral, and medial-lateral) without the need to manually reposition the X-ray source and detector. Such features would be ideal for the rapid collection of fluoroscopic data in multiple subjects during a study, and would permit the visualization of an implant during multiple gait cycles at different viewing angles. Thus, we describe a rat-specific radiolucent treadmill (Ratwalk) that is build to be compatible with a commercially available micro-CT scanner (serving the X-ray source). We also describe the post-operative gait assessment of rats that have undergone a hip hemi-arthroplasty procedure, using both the CatWalk XT and Ratwalk systems at several timepoints. We hypothesize that following hip hemiarthroplasty, animals will favour their contralateral hindlimb at earlier timepoints, but will not favour either hindlimb by 12 post-operative weeks, indicating that the hip hemiarthroplasty procedure produced a clinically representative model of functional joint replacement.

4.2 Materials and Methods

4.2.1 Animals

All surgical trials and post-operative gait and imaging protocols were approved by the institutional Animal Use Committee (AUP 2017-156, Western University, London, Ontario, Canada) (Appendix A). N=5 male Sprague-Dawley rats from a concurrent

surgical study (described in the previous chapter) were analyzed for this study. Rats were originally obtained from a commercial vendor (Charles River Laboratories, Senneville, Quebec, Canada). Animals were housed in a conventional vivarium with 12-hour light/dark cycle and provided standard rodent chow and water *ad libitum.*

4.2.2 Surgical Procedure

Each rat underwent a hip hemiarthroplasty surgery to install a titanium (Ti6Al4V) hip implant into the right femur; the surgical procedure was characterized in the previous chapter. Briefly, procedures were performed aseptically within a sterile field. Peri-operative medication included antibiotics (Baytril, 10 mg/kg SC) and drugs for pain management (Metacam, 1 mg/kg, and; Buprenorphine, 0.07 mg/kg SC). Anesthesia was induced within a chamber using 4% isofluorane and maintained via nose cone at 1.5%. External heat support and anesthetic depth monitoring were maintained throughout the procedure. A posterior approach was used to access the hip joint through a 3-4cm curvilinear incision over the greater trochanter. The attachment of the deep external rotators and the posterior joint capsule were excised using microsurgery scissors. The femur was then dislocated from the acetabulum to expose the femoral head. A dental scaling tool, in combination with dental files and custom rat-hip broaches were used to prepare the proximal femur to receive an implant, which was potted using an uncemented, press-fit technique. The implant was then relocated into the acetabulum. The joint capsule was then closed using a simple interrupted pattern with 5-0 Monocryl sutures. Muscle layers were then loosely apposed to reduce dead space. The gluteus maximus, fascia lata and subcutaneous layers were closed using 5-0 Monocryl in a simple

continuous pattern. The skin was closed with subcuticular 6-0 Monocryl sutures and tissue glue. Following recovery from surgery, animals were placed alone in cages with clean bedding. Post-operative therapy included antibiotics (Baytril, 10 mg/kg SC daily for 10 days) and drugs for pain management (Metacam, 1 mg/kg, daily for 10 days, and; Buprenorphine, 0.07 mg/kg SC daily for 7 days).

4.2.3 Radiolucent Treadmill (Ratwalk) Construction

The Ratwalk treadmill was constructed using an acrylic enclosure mounted on carbon fibre support beams and secured using screws (Fig. 4.1). The enclosure contained a hinged door on its top surface to allow an animal to be placed within the enclosure. Perforations were made within each end of the enclosure to serve as air holes. Rotating plastic rollers were fixed between the carbon fibre supports at a distance and separated by a plastic floor; this created the running laneway. A commercially available vinyl rat treadmill belt (Harvard Apparatus, St. Laurent, Quebec, Canada) was placed over the rollers and the floor and served as the running surface. Removable plastic trays were built under the runway in order to catch and facilitate the removal of excrement from the device. Metal rods were installed on one side of the track so that excrement could fall under the track, but not the animals. The carbon fibre supports were fixed to an aluminum mounting block, which was custom build to fit into the housing that normally supports carbon fibre specimen beds in a commercially available micro-CT scanner (eXplore Locus Ultra, GE Medical, London, Ontario, Canada). This allowed the movement of treadmill into and out of the scanner, to be controlled in the same way the scanner bed would normally operate; this gave the operator the ability to remotely adjust the position

of the Ratwalk within the field-of-view of the scanner's X-ray source and detector. A stepper motor was used to power the device and was mounted, along with a control unit, on top of the aluminum block (Fig. 4.2). The stepper motor was connected to the plastic rollers using a toothed belt and two gears, one at the roller and one at the stepper motor. The control unit had two cable systems; the first allowed the device to be connected to a power source (set to 30volts) and, the second allowed the treadmill to be connected to a laptop outside of the scan room (to operate the treadmill without radiation exposure). Commands sent from the laptop controlled the speed and direction (forward or reverse) of the treadmill.

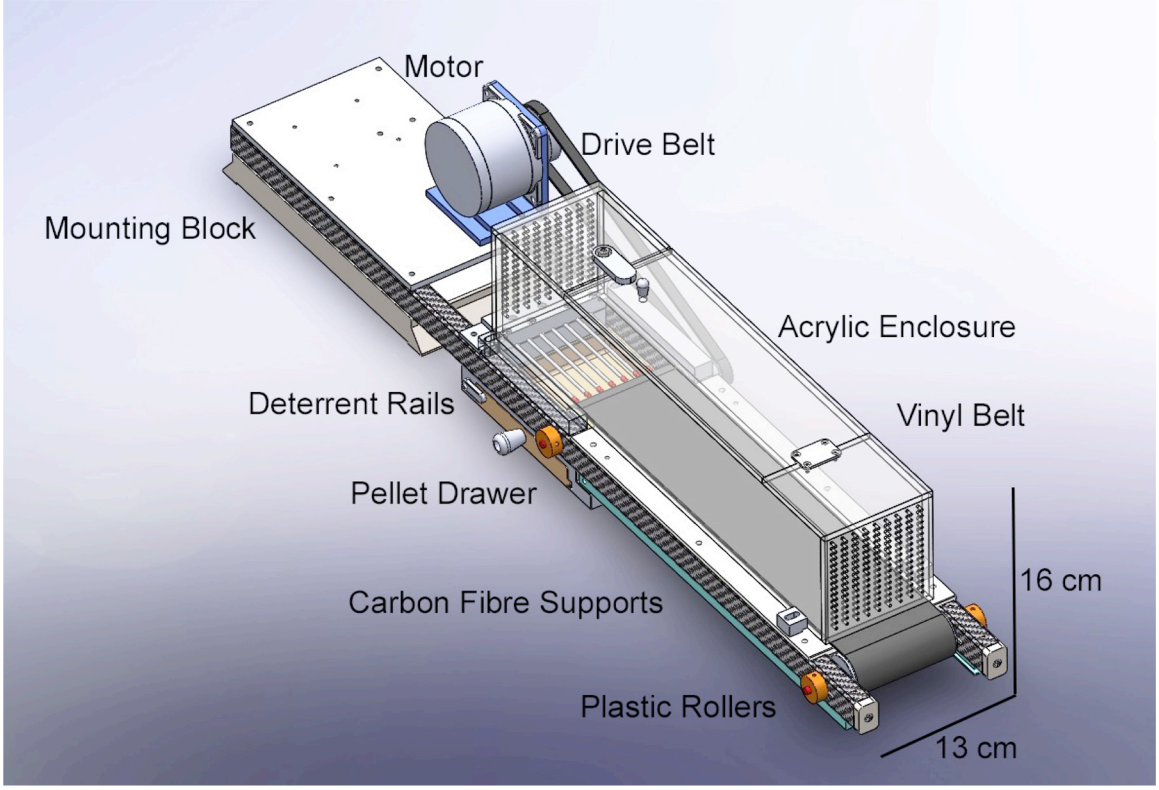

Figure 4.1: Computer-aided design schematic of the Ratwalk radiolucent treadmill, highlighting pertinent design features. The control unit and power supply are not pictured, but were included in the final design, along with a 3D-printed plastic block to restrict space over the deterrent rails.

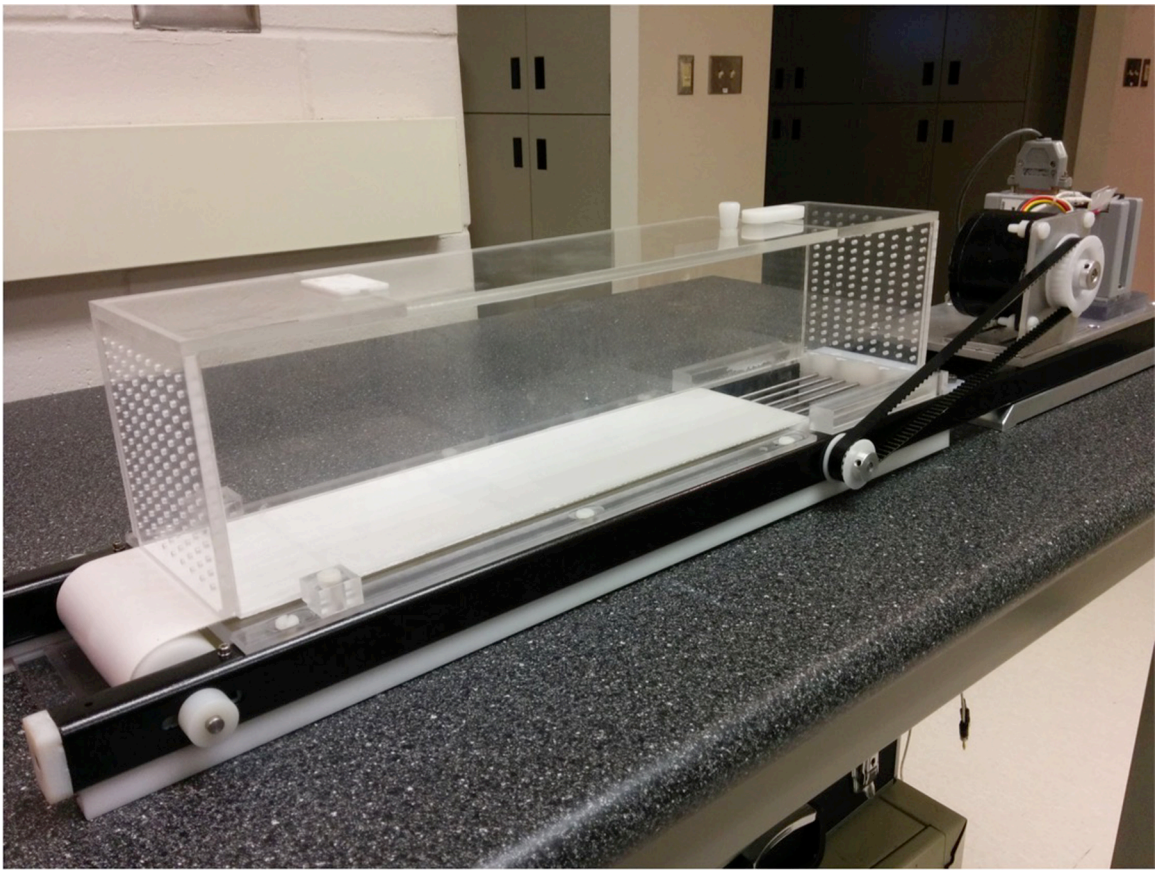

Figure 4.2: The "Ratwalk" Radiolucent Treadmill post construction. The control unit with cable attachment can be seen behind the stepper motor (right).

4.2.4 X-ray Fluoroscopic Imaging

To ensure animal safety, prior to animal trials, a research veterinarian and a hardware technician both inspected the device for potential hazards. After the device was determined to be safe for animal testing, the veterinarian and technician were also present to oversee the runs of an initial test-group of male Sprague-Dawley rats (Fig. 4.3). Once it was determined that the Ratwalk was safe for repeated use, the device was incorporated into the post-operative protocol for rats following hip hemiarthroplasty surgery.

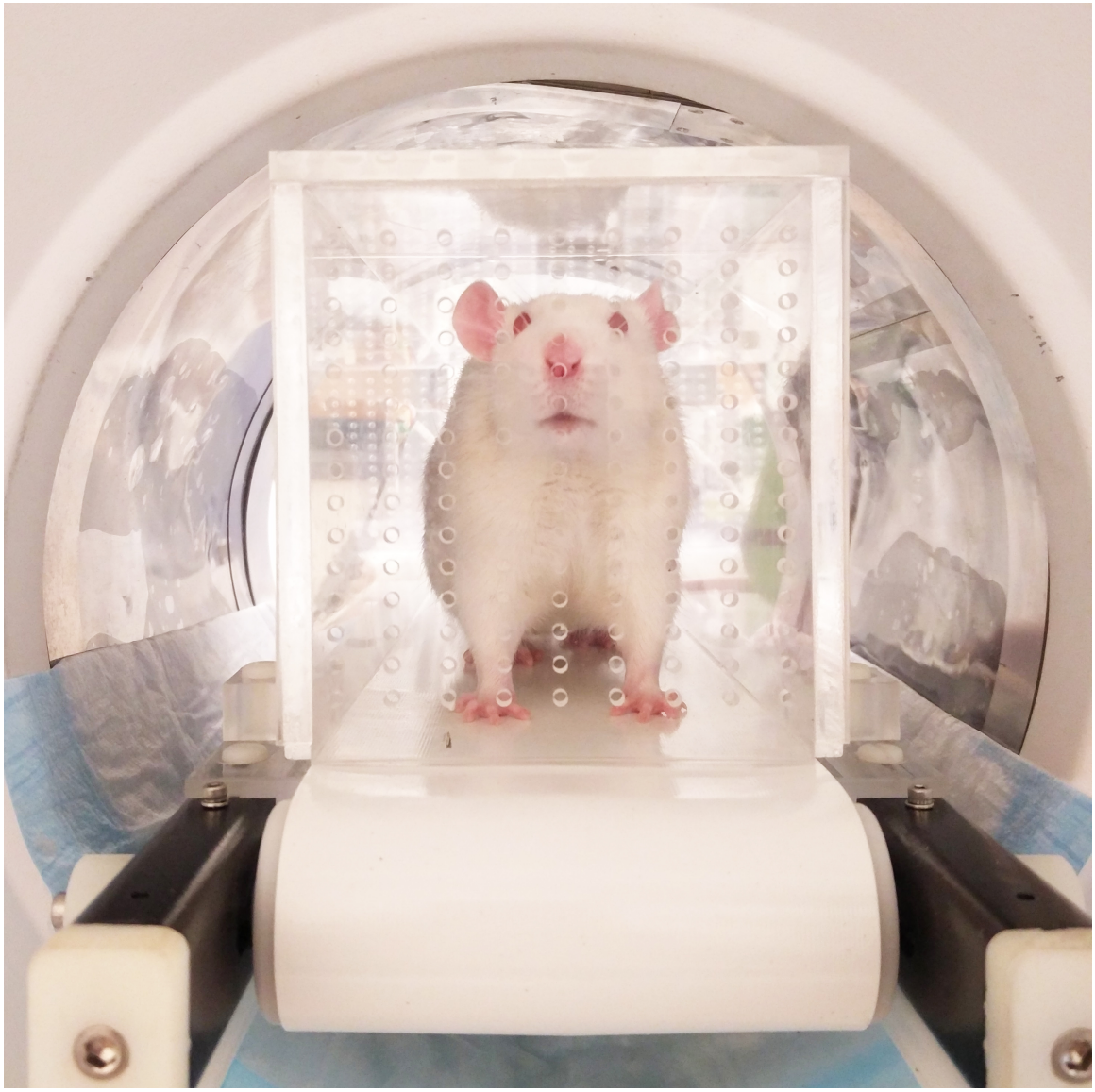

Figure 4.3: A male Sprague-Dawley rat within the custom radiolucent treadmill (Ratwalk) enclosure, which is integrated for use within a GE Locus Ultra cone beam micro-CT scanner (GE Medical, London, Ontario Canada).

Animals were trained to run on the Ratwalk prior to testing. Initially, animals were placed within the treadmill and permitted to explore the enclosure for several minutes. The treadmill was then turned on at slow speeds (<10cm/sec) so that the animal could practice walking on the moving floor. Once the animal was comfortable walking in

the appropriate direction and location on the belt, speeds were slowly increased to a moderate pace (26cm/sec) and rats were allowed to run freely for several seconds. Breaks were taken at regular intervals, which involved an incremental deceleration of the treadmill before the belt was stopped. The same protocol was followed to ensure animal comfort and safety during post-operative trials, which were conducted at post-operative weeks 3, 6, 9 and 12. X-ray fluoroscopic imaging was obtained three run speeds, 12cm/sec, then at 19cm/sec and finally 26cm/sec, in both dorsal-ventral and medial-lateral directions. Animals were monitored throughout trials for signs of discomfort or difficulty in maintaining runs speeds, where if observed, the treadmill speed was immediately decreased, and gradually lowered to zero so that the animal could be inspected and allowed to recover.

The imaging protocol used for fluoroscopy was completed on a Locus Ultra cone beam micro-CT scanner (GE Medical, London, Ontario, Canada). The protocol consisted of 1000 x-ray frames (120kVp, 20mA) over 16s for each imaging trial (62.5Hz); images were acquired with the gantry held stationary in either AP or Lateral orientations. X-ray dose for the imaging protocol with these settings was measured with a radiation meter to be 81mGy; the estimated dose over the course of the study fell well below the 5Gy threshold that has been shown to be safe for murine subjects.[31] Following image acquisition, radiographs were converted into JPEG stacks and transferred into ImageJ (U. S. National Institutes of Health, Bethesda, Maryland, USA) for post-processing. Window and Level were maintained at 8400 and 2800 respectively. A high-pass filter (for edge enhancement) was used to improve the visualization of bone boundaries within each

image (Figure 4.4). The resulting image stacks were then analyzed to qualitatively assess implant position over several gait cycles.

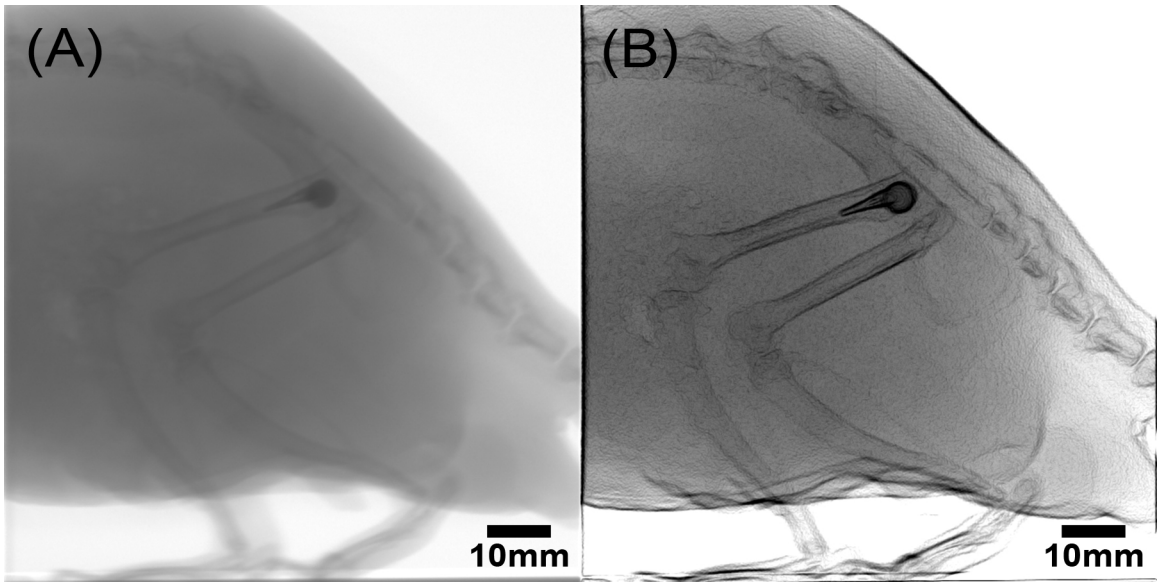

Figure 4.4: X-ray fluoroscopy still-frames of a male Sprague-Dawley rat walking on the Ratwalk radiolucent treadmill, with a titanium hip implant *in situ.* (A) is an unaltered image and, (B) is an image that has been processed using a high-pass filter (edge detection) to improve visualization of the hindlimb anatomy.

4.2.5 CatWalk XT Gait Assessment

Animals were trained to walk across the CatWalk XT system (Noldus, Leesburg, Virginia) prior to testing, incentivized by treats (cereal, peanut butter). Runs were collected pre-operatively and at post-operative weeks 3, 6, 9 and 12. Three runs were collected at each timepoint; these consisted of the first three compliant runs, or pseudo-

compliant runs each animal was able to achieve. A compliant run was counted if the animal was able to transverse the glass floor (pass across the camera field of view) in less than 5 seconds. In some cases animals did not meet this speed requirement over successive tests; in these instances the three fastest runs were used for analysis, provided that the animal transversed the field-of-view with an uninterrupted gait pattern. Data was collected and processed using the CatWalk XT software version 10.6 (Noldus, Leesburg, Virginia). Pawprints were initially classified using the Automatic Footprint Classification feature (Fig. 4.5). A single user then reviewed each run and determined if pawprints had been correctly classified. Where there were incorrect or incomplete classifications, this task was performed manually. Run data was tabulated in Catwalk XT software before being exported for analysis.

Figure 4.5: Image of a male Sprague-Dawley rat with a titanium hip implant as it transverses the walkway of the CatWalk XT system. Pawprints have been classified within the device software (version 10.6) to allow gait metrics to be computed (Noldus, Leesburg, Virginia).

4.2.6 Data and Statistical Analysis

Quantitative gait analysis was conducted longitudinally over 5 timepoints (Pre-op, post-op weeks 3, 6, 9, 12) using the CatWalk XT system (Noldus, Leesburg, Virginia). CatWalk XT runs were completed at each timepoint; qualitatively assessed Ratwalk runs

were only completed at post-operative timepoints and were not used for statistical analysis. CatWalk XT run data was imported into Prism 8 (GraphPad, San Diego, California) for statistical analysis. The run metrics analyzed were Standing time(s), Duty Cycle (Stand/(stand+swing)x100%), Swing Speed (cm/s), Print Area (cm^2), Maximum Contact Area (cm^2) and Maximum Intensity (pixels) (Table 4.1); these metrics were shown to be significantly different between a hip with osteoarthritis and the unaffected side, in a previous study by Miyamoto et al.[25] Our assumption was that suboptimal hip performance of the affected following the hemiarthroplasty surgery would also result in significant differences, compared to the contralateral side, for the aforementioned metrics. The Miyamoto approach was also followed in that ratios comparing contralateral and ipsilateral hindlimbs were calculated for the aforementioned output metrics prior to analysis; this approach accounts for weight variability between animals and timepoints. Normality was assessed using a Kolmogorov-Smirnov test; data from the pre-operative (baseline) timepoint for the print area variable did not pass normality therefore column statistics for print-area were analyzed using repeated measures one-way ANOVA, with a Friedman *post hoc* test. All other data followed a Gaussian distribution; column statistics were analyzed using repeated measures one-way ANOVA and Bonferroni's multiple comparisons *post hoc* test. Significance between data at all timepoints was determined at the $p<0.05$ level.

Table 4.1: CatWalk XT output gait metrics analyzed for rat hip hemiarthroplasty cohort.

CatWalk XT Metrics Analyzed	Description
Standing Time (s)	Time in seconds that each paw is in contact with the glass plate and weight-bearing during a given run.
Duty Cycle (%)	Percentage of time a given limb is weight-bearing during a given run.
Swing Speed (cm/s)	Speed that a given limb travels between steps, in centimeters per second.
Print Area (cm^2)	Area of a given paw identified to be in contact with the glass floor during a run, in centimeters squared.
Maximum Contact Area (cm^2)	Total floor area covered by a paw print at the moment when it is at its peak contact with the floor, in centimeters squared.
Maximum Intensity (pixels)	Maximum light intensity value measured during paw contact with the floor, in unitless pixel values.

4.3 Results

As described in Chapter 3, installation of titanium hip hemiarthroplasty implants into the right femur was successful in the N=5 animals analyzed in this study, without any intraoperative complications. The greater trochanter was preserved in all cases.

Animals were observed ambulating on their affected limbs immediately following recovery from general anaesthesia as well as at all timepoints throughout the study.

CatWalk XT assessment was completed for all animals at each timepoint. The duty cycle percentage ratio of the ipsilateral to contralateral hindlimb at post-operative week 6 was significantly different from baseline ($P<.05$) (Figure 4.6). Significant differences were not observed for any other metrics between timepoints. Individual metrics were also plotted to display the distribution of data across the study cohort (Figure 4.7).

X-ray fluoroscopic assessment was completed for all animals at each timepoint. Three of five rats performed compliant runs at all three belt speeds (12cm/s, 19cm/s and 26cm/s) at each post-operative timepoint; two of five animals did not comply with the 26cm/s setting. The Ratwalk treadmill maintained functionality throughout the duration of the study. Analysis of the collected X-ray fluoroscopy image sequences revealed dislocated ipsilateral hips (Figure 4.8), caused by implant subsidence, in two animals (Rats A and C) beginning at the 6-week post-operative timepoint and subsequently at post-operative weeks 9 and 12. No complications were observed for the other 3 animals.

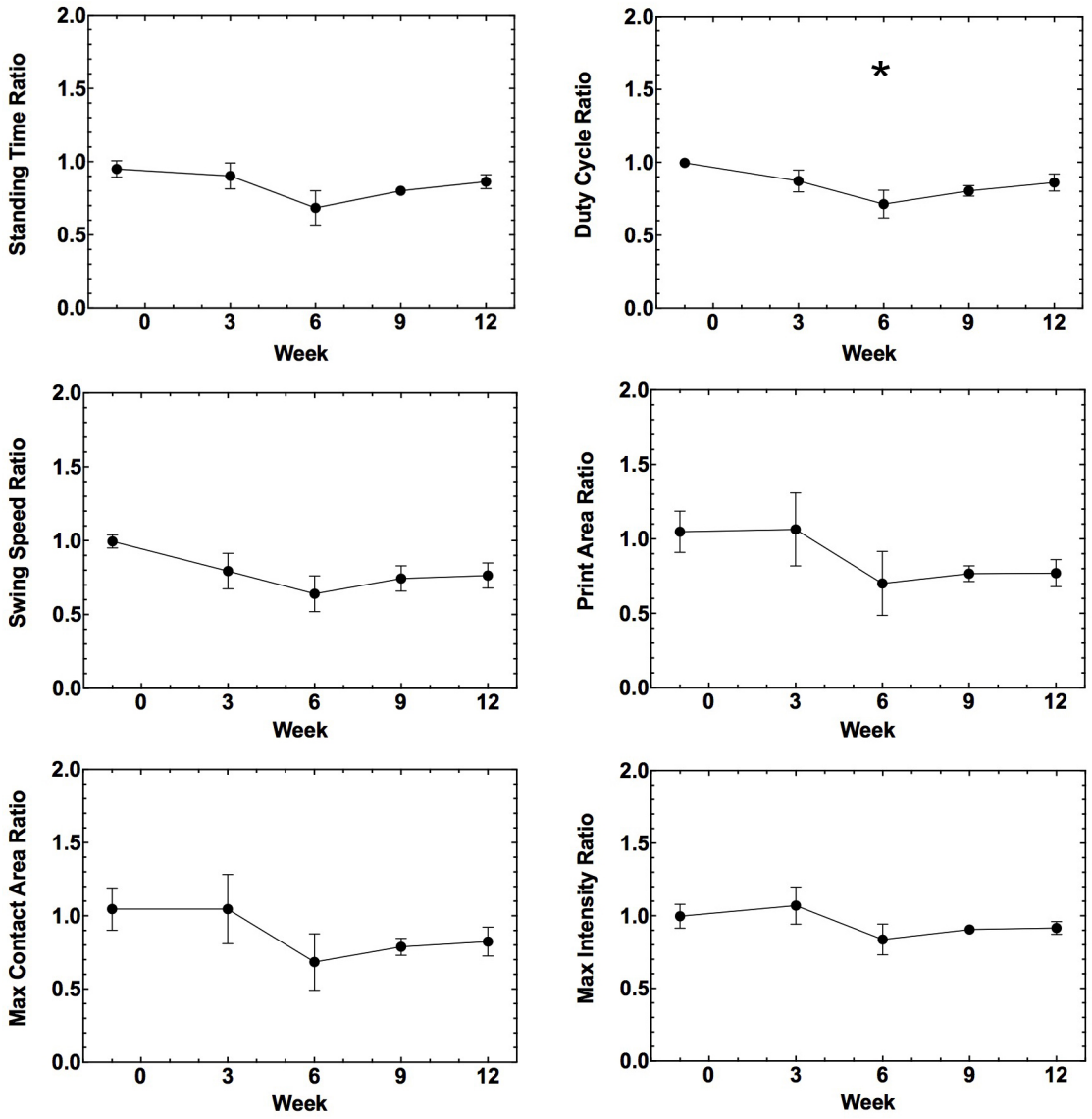

Figure 4.6: Group mean gait metrics collected on the CatWalk XT system for N=5 male Sprague-Dawley rats prior to and following hip hemiarthroplasty. Data displayed are ratios of the ipsilateral (affected) limb results divided by the contralateral (unaffected) limb. A significant reduction in Duty Cycle was observed at post-operative week 6 compared to baseline (P<.05), denoted by an asterisk. Error bars represent standard error of the mean at each timepoint.

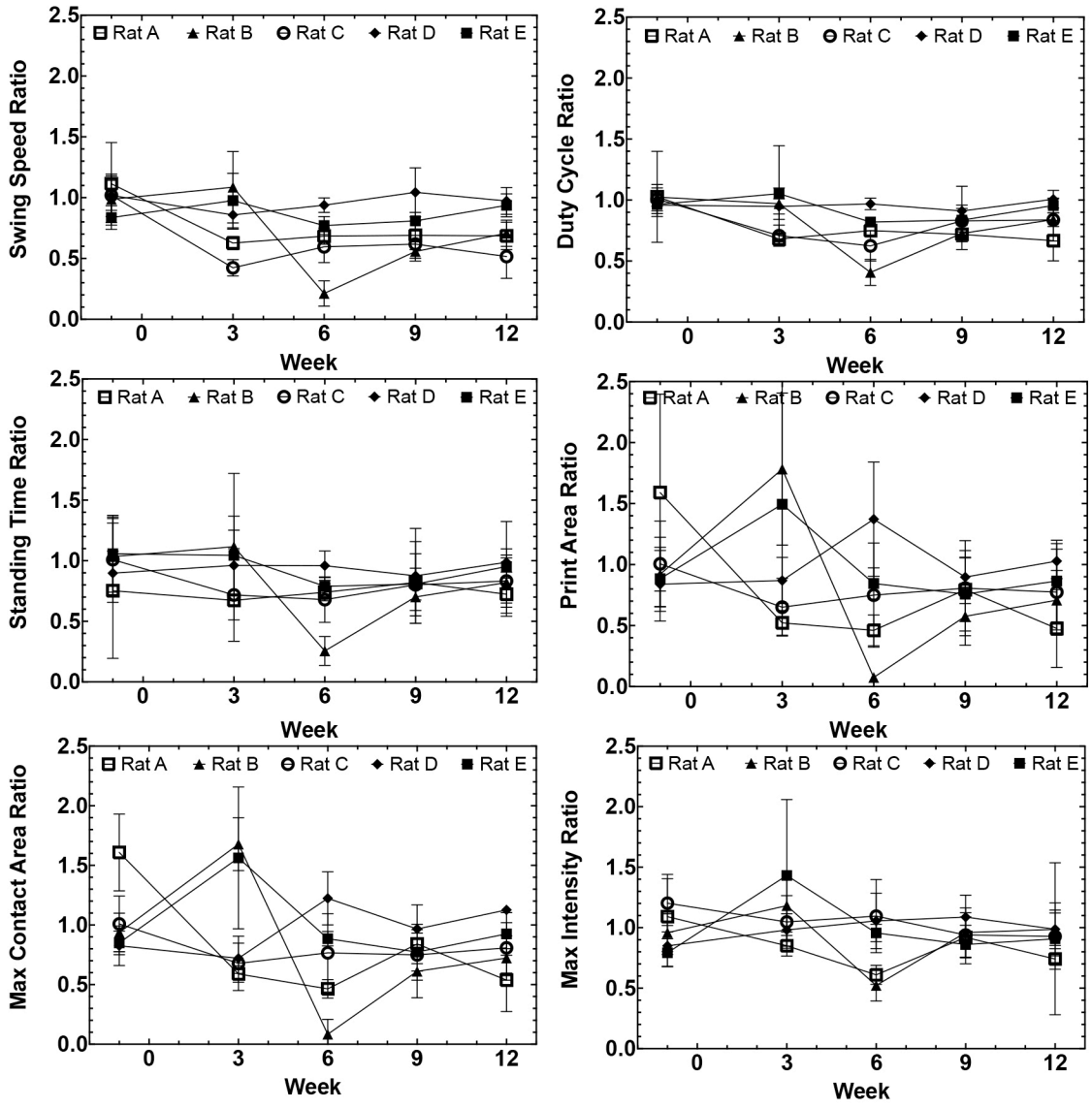

Figure 4.7: Gait metrics collected on the CatWalk XT system for N=5 male Sprague-Dawley rats prior to and following hip hemiarthroplasty; individual scores are shown to highlight the distribution of results. Data displayed are ratios of the ipsilateral (affected) limb results divided by the contralateral (unaffected) limb. A significant reduction in Duty Cycle was observed at post-operative week 6 compared to baseline (P<.05), denoted by an asterisk. Error bars represent standard error of the mean.

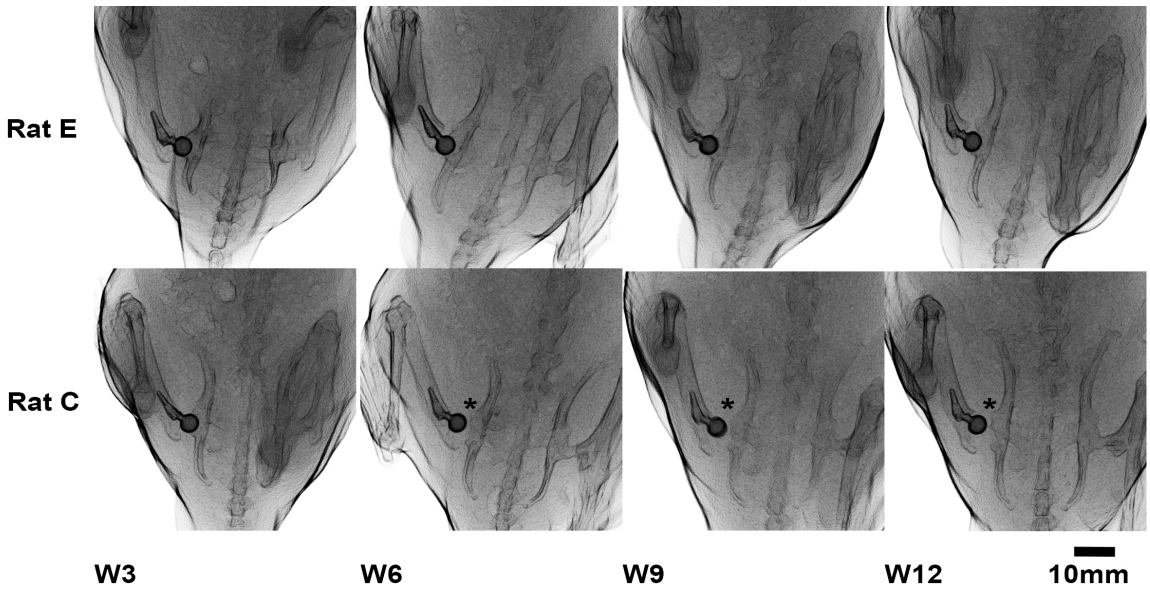

Figure 4.8: X-ray fluoroscopy anterior-posterior images of male Sprague-Dawley rats at heel strike, collected on the Ratwalk radiolucent treadmill. An edge-enhancement filter has been applied to all images. Rows compare a rat with a functional implant at all post-operative timepoints (Rat E), with an animal with an observable complication (Rat C); a dislocated hip and subsided implant can be observed beginning at post-operative week 6, persisting at post-operative weeks 9 and 12, indicated by asterisks.

4.4 Discussion

We describe the first efforts to assess the post-operative gait of rats following hip hemiarthroplasty surgery using the CatWalk XT system and a novel radiolucent treadmill (Ratwalk). Our results indicate that ambulation on the ipsilateral limb is recovered within the first three post-operative weeks following hip hemiarthroplasty; these data support that implants installed via this approach can be considered functional post-operatively. However, a significant difference in duty cycle percentage at post-operative week 6 was

observed (Figure 4.6, 4.7), which suggests that this group of animals did begin to favour their ipsilateral limbs at the week 6 post-operative timepoint. It is likely that gait was affected by the cases of implant subsidence and subsequent hip dislocation (Figure 4.8) observed in two of the five animals at post-operative week 6.

One animal that had a subsided implant (Rat C) was non-compliant at both the 3 and 6 week post-operative timepoints at moderate treadmill speeds; the animal also did not meet the 5 second threshold for compliant runs on the CatWalk XT at post-operative week 6. This animal likely had apprehension or discomfort to ambulation at moderate speeds on a recently failed component. However, this animal performed at all treadmill speeds at post-operative weeks 9 and 12, which could suggest that muscle compensation around a failed implant occurred gradually over several weeks. One animal that was observed to have a functional implant at all timepoints also failed to perform compliant treadmill runs at 26cm/s at post-operative weeks 3 and 12. It is unclear why this animal did not tolerate the higher speeds, but this could suggest either some underlying discomfort around the hip joint, or apprehension to run at higher speeds. Moreover, one animal (Rat B) appeared to favour the ipsilateral limb preferentially at week 3, followed by the contralateral limb at week 6 (Fig. 4.7). It is unclear why this was the case, but it could be that pain or discomfort could have been a contributing factor. Thus, while animals exhibited normal cage behaviour throughout the study, in the future rat pain scores could be collected at regular timepoints to determine if there is underlying hip pain contributing to poor performance during gait assessments.[32]

Although there was an observed drop in ipsilateral limb function at post-operative week 6, ipsilateral limb function compared to baseline recovered to be not significantly

different from baseline at post-operative weeks 9 and 12. These findings suggest that some compensatory changes may have occurred around the hip joint prior the post-operative week 9 timepoint that allowed animals to ambulate on the ipsilateral limb despite not having a functional implant. Ambulation on a non-functional hip is perhaps to be expected after a period of recovery. In quadrupeds, muscle compensations alone can often be sufficient to restoring gait even if the joint is non-functional; femoral head and neck resections are performed in dogs to relieve chronic coxofemoral joint pain and necrosis[33]. Femoral head and neck ostectomies are commonly performed in pets, particularly dogs[34] and cats.[35] Such procedures forgo the installation of a femoral prosthesis; quadrupeds are routinely able to ambulate on their affected limb without a functional hip joint.[33] Similar compensations likely occurred in the two animals with implant subsidence, which could explain why gait metrics for this cohort improved somewhat after post-operative week 6 and did not significantly differ from baseline at post-operative weeks 9 and 12.

While post-operative gait assessment was achieved on the CatWalk XT system, a drawback of this method of gait analysis is the inability to interrogate the function of the hip joint during motion. In this trial it would have been difficult to observe a non-functional hip implant without the use of X-ray fluoroscopy, or another imaging modality, and only using optical gait measurements alone. Moreover while static techniques, such as static X-ray and micro-CT imaging can highlight post-operative joint complications such as subsidence and dislocation, they do not offer any information regarding implant position during various stages of the gait cycle; a component prone to subluxation for instance may appear to be located within the hip joint during static

imaging. Other potential complications, such as implant toggling within the proximal femur could be explanatory in determining why certain implants are prone to subsidence, as excessive micro-motion can prevent effective osseointegration of bone into the implant stem.[36]

Implant motion, particularly toggling of the stem within the proximal medulla was suspected for some subjects but could not be definitively observed. Incorporating a quantitative approach to image analysis, particularly 2D to 3D image registration[37], could facilitate kinematic measurements of implant motion in future investigations; this was however beyond the scope of our current study. Such an approach would be especially promising to investigate on a system like the Ratwalk, which integrates with a micro-CT system. This way the same scanner could be used to collect volumetric 3D data along with 2D fluoroscopic image sequences, which would likely simplify any prospective 2D-3D co-registration process. A limitation of this study was that no pre-operative treadmill runs were collected for this cohort. This was done intentionally to reduce the amount of X-ray dose the animals were subjected to, and because assessment was to be limited to qualitative observations regarding implant position. In the future, pre-operative trials should be collected, particularly if quantitative metrics are to be collected similar to the CatWalk XT protocol.

Another limitation of the current Ratwalk setup is the limited field-of-view (FOV) afforded by the micro-CT cone beam detector (14cmx10cm); the axial FOV (10cm) in particular only partially captures the rat's anatomy during image acquisition. This led to several failed trials, particularly in training and earlier tests, where the animal's hindlimb would either partially or fully be outside of the FOV. Selecting where to position the

treadmill relative to the detector, based on observations of where the animal typically ran on the belt, was crucial for centering the hindlimb within the FOV. Creating a mechanism to automatically centre the hindlimb within the FOV, such as incorporating a self-pacing feature to adjust the belt speed to compensate for changes in run speed, could improve the probability of acquiring successive gait cycles within the image sequence.

Rats also had a tendency to position their hindlimbs on the rails to avoid running, especially at increased belt speeds. A custom 3D-printed plastic block was particular useful in restricting the space within the enclosure behind the tread over the rails, and helped to address the aforementioned issues. Several animals also preferred to turn in the wrong direction before and after runs were attempted. There was no clear explanation for this behaviour, but it meant that delays occurred between trials as animals had to be facing the right direction before the treadmill speed would be increased. This issue was somewhat mitigated by keeping the tread moving at a low speed during breaks between trials, instead of stopping the belt completely. This ensured rats kept walking in the correct direction, thereby reducing the number of turn-arounds that occurred in later trials. In the future, time during initial training (perhaps the use of auditory queues or positive reinforcement with edible treats) should be dedicated to addressing this turn-around behaviour on the Ratwalk.

4.5 Conclusions

We describe the post-operative gait assessment of rats following the installation of titanium implants via hip hemiarthroplasty. Our findings support that implants can be considered functional, and served to restore rat gait within the first three post-operative

weeks. We were able to detect a significant reduction in duty cycle % in this cohort at post-operative week 6 using data collected on the CatWalk XT system, followed by a recovery in gait at post-operative weeks 9 and 12. The Ratwalk radiolucent treadmill system facilitated the collection of X-ray fluoroscopic gait data of the rat hindlimb, which was used to identify post-operative complications that were initially detected in CatWalk XT trials, but not at later timepoints. Future studies in this area should consider the use of fluoroscopic imaging in tandem with CatWalk XT trials to best evaluate implant function in the rat hindlimb post-operatively.

4.6 References

1. Warth LC, Grant TW, Naveen NB, et al. 2020. Inadequate Metadiaphyseal Fill of a Modern Taper-Wedge Stem Increases Subsidence and Risk of Aseptic Loosening: Technique and Distal Canal Fill Matter! J Arthroplasty.

2. Floerkemeier T, Budde S, Lewinski GV, et al. 2020. Greater early migration of a short-stem total hip arthroplasty is not associated with an increased risk of osseointegration failure: 5th-year results from a prospective RSA study with 39 patients, a follow-up study. Acta orthopaedica:1-6.

3. Park CW, Lim SJ, Kim JH, et al. 2020. Hip resurfacing arthroplasty for osteonecrosis of the femoral head: Implant-specific outcomes and risk factors for failure. Journal of orthopaedic translation 21:41-48.

4. Clauss M, Hunkeler C, Manzoni I, et al. 2020. Debridement, Antibiotics and Implant Retention for Hip Periprosthetic Joint Infection: Analysis of Implant Survival after Cure of Infection. Journal of bone and joint infection 5:35-42.

5. Taha M, Abdelbary H, Ross FP, et al. 2018. New Innovations in the Treatment of PJI and Biofilms-Clinical and Preclinical Topics. Current reviews in musculoskeletal medicine 11:380-388.

6. Carli AV, Ross FP, Bhimani SJ, et al. 2016. Developing a Clinically Representative Model of Periprosthetic Joint Infection. J Bone Joint Surg Am 98:1666-1676.

7. Bargon R, Bruenke J, Carli A, et al. 2019. General Assembly, Research Caveats: Proceedings of International Consensus on Orthopedic Infections. J Arthroplasty 34:S245-S253 e241.

8. Hunt S, Stone C, Seal S. 2011. Timing of femoral prosthesis insertion during cemented arthroplasty: cement curing and static mechanical strength in an in vivo model. Can J Surg 54:33-38.

9. Jakobsen T, Kold S, Baas J, et al. 2015. Sheep Hip Arthroplasty Model of Failed Implant Osseointegration. The open orthopaedics journal 9:525-529.

10. Field JR, Callary SA, Solomon LB, et al. 2016. Early acetabular cartilage wear following hemiarthroplasty: An ovine model. Vet Comp Orthop Traumatol 29:125-130.

11. Liska WD, Doyle ND. 2015. Use of an Electron Beam Melting Manufactured Titanium Collared Cementless Femoral Stem to Resist Subsidence After Canine Total Hip Replacement. Vet Surg 44:883-894.

12. DeYoung DJ, Schiller RA. 1992. Radiographic criteria for evaluation of uncemented total hip replacement in dogs. Vet Surg 21:88-98.

13. Husby KA, Reed SK, Wilson DA, et al. 2016. Evaluation of a Permanent Synthetic Osteochondral Implant in the Equine Medial Femoral Condyle. Vet Surg 45:364-373.

14. Carli AV, Bhimani S, Yang X, et al. 2017. Quantification of Peri-Implant Bacterial Load and in Vivo Biofilm Formation in an Innovative, Clinically Representative Mouse Model of Periprosthetic Joint Infection. J Bone Joint Surg Am 99:e25.

15. Li Z, Kuhn G, Schirmer M, et al. 2017. Impaired bone formation in ovariectomized mice reduces implant integration as indicated by longitudinal in vivo micro-computed tomography. PLoS One 12:e0184835.

16. Yang SY, Yu H, Gong W, et al. 2007. Murine model of prosthesis failure for the long-term study of aseptic loosening. J Orthop Res 25:603-611.

17. AbuMoussa S, Ruppert DS, Lindsay C, et al. 2018. Local delivery of a zoledronate solution improves osseointegration of titanium implants in a rat distal femur model. J Orthop Res 36:3294-3298.

18. Ma T, Ge XY, Hao KY, et al. 2017. Simple 3,4-Dihydroxy-L-Phenylalanine Surface Modification Enhances Titanium Implant Osseointegration in Ovariectomized Rats. Sci Rep 7:17849.

19. He T, Cao C, Xu Z, et al. 2017. A comparison of micro-CT and histomorphometry for evaluation of osseointegration of PEO-coated titanium implants in a rat model. Sci Rep 7:16270.

20. Al-Jandan B, Marei HF, Abuohashish H, et al. 2018. Effects of sunitinib targeted chemotherapy on the osseointegration of titanium implants. Biomed Pharmacother 100:433-440.

21. Ruppert DS, Harrysson OLA, Marcellin-Little DJ, et al. 2017. Osseointegration of Coarse and Fine Textured Implants Manufactured by Electron Beam Melting and Direct Metal Laser Sintering. 3D Print Addit Manuf 4:91-97.

22. Huanhuan J, Pengjie H, Sheng X, et al. 2017. The effect of strontium-loaded rough titanium surface on early osseointegration. J Biomater Appl 32:561-569.

23. Li K, Wang C, Yan J, et al. 2018. Evaluation of the osteogenesis and osseointegration of titanium alloys coated with graphene: an in vivo study. Sci Rep 8:1843.

24. Paish ADM, Nikolov HN, Welch ID, et al. 2020. Image-based design and 3D-metal printing of a rat hip implant for use in a clinically representative model of joint replacement. J Orthop Res.

25. Miyamoto S, Nakamura J, Ohtori S, et al. 2017. Pain-related behavior and the characteristics of dorsal-root ganglia in a rat model of hip osteoarthritis induced by mono-iodoacetate. J Orthop Res 35:1424-1430.

26. Herold S, Kumar P, Jung K, et al. 2016. CatWalk gait analysis in a rat model of multiple sclerosis. BMC Neurosci 17:78.

27. Kameda T, Kaneuchi Y, Sekiguchi M, et al. 2017. Measurement of mechanical withdrawal thresholds and gait analysis using the CatWalk method in a nucleus pulposus-applied rodent model. Journal of experimental orthopaedics 4:31.

28. Miyagi M, Ishikawa T, Kamoda H, et al. 2013. Assessment of pain behavior in a rat model of intervertebral disc injury using the CatWalk gait analysis system. Spine 38:1459-1465.

29. Fulop GA, Ahire C, Csipo T, et al. 2019. Cerebral venous congestion promotes blood-brain barrier disruption and neuroinflammation, impairing cognitive function in mice. GeroScience 41:575-589.

30. Guillot M, Gravel P, Gauthier ML, et al. 2015. Coxofemoral joint kinematics using video fluoroscopic images of treadmill-walking cats: development of a technique to assess osteoarthritis-associated disability. Journal of feline medicine and surgery 17:134-143.

31. Detombe SA, Dunmore-Buyze J, Petrov IE, et al. 2013. X-ray dose delivered during a longitudinal micro-CT study has no adverse effect on cardiac and pulmonary tissue in C57BL/6 mice. Acta radiologica (Stockholm, Sweden : 1987) 54:435-441.

32. Hahm SC, Song E, Jeon H, et al. 2019. Transcutaneous Electrical Nerve Stimulation Reduces Knee Osteoarthritic Pain by Inhibiting Spinal Glial Cells in Rats. Physical therapy 99:1211-1223.

33. Harper TAM. 2017. Femoral Head and Neck Excision. The Veterinary clinics of North America Small animal practice 47:885-897.

34. Ireifej S, Marino D, Loughin C. 2012. Nano total hip replacement in 12 dogs. Vet Surg 41:130-135.

35. Schnabl-Feichter E, Tichy A, Bockstahler B. 2020. Evaluation of a pressure plate for detection of hind limb lameness in cats. PLoS One 15:e0231904.

36. Malfroy Camine V, Rüdiger HA, Pioletti DP, et al. 2018. Effect of a collar on subsidence and local micromotion of cementless femoral stems: in vitro comparative study based on micro-computerised tomography. Int Orthop 42:49-57.

37. Tinga S, Kim SE, Banks SA, et al. 2018. Femorotibial kinematics in dogs with cranial cruciate ligament insufficiency: a three-dimensional in-vivo fluoroscopic analysis during walking. BMC veterinary research 14:85.

Chapter 5

5 Conclusions and Future Directions

5.1 Summary of Presented Works

Joint replacement surgery continues to be highly prevalent in Canadian society, with around 130,000 procedures performed annually for hip and knee cases alone.[1] The most predominant reason for joint replacement surgery is degenerative osteoarthritis; for hip replacement surgery, femoral neck fracture also accounts for around 15% of primary replacement procedures.[1] While the success rate of primarily hip and knee procedures is high (~97%),[1] given the large numbers of joint replacement surgeries performed, even low complication rates implants can affect thousands of patients annually. When implants fail, they need to be replaced during revision surgeries, which are more costly, and have higher perioperative complication rates compared to primary arthroplasty procedures.[2] Such procedures are to avoided whenever possible. Consequently, research efforts to address the causes of implant failure, most notably instability caused by a failures of the bone-implant interface and infection,[1; 3] continue to be active.

Before innovations can be applied in the clinic, testing is required in animal models. In this dissertation, we describe the first clinically representative rat model of hip hemiarthroplasty that utilizes a functional implant created via 3D-metal printing in surgical grade metal alloys.[4] Such a model is beneficial to basic scientists and clinicians conducting research to resolve issues related to implant failure, because it allows the use

of a cyclically loaded implant that articulates within the joint space, to be used in a low-cost, high-throughput animal species. As we have previously detailed, clinically representative implant studies have been traditionally restricted to large-animal[5-7] and companion-animal species[8-10], as their size permits the installation of human-like components. Small-animal models, particularly rats and mice, which have the advantage of being widely used across the basic sciences, had previously relied on non-loaded intramedullary metal rods,[11; 12] screws,[13] and pins[14-16] to study changes at the bone-implant interface. The inherent disadvantage of non-functional devices is that they are not representative of clinical implants, nor do they require the same invasive surgical procedures that are needed to install functional joint replacement prostheses. We have described a novel approach to implant design and surgical installation, that allows us to incorporate a functional implant, into a low-cost small animal model, that can be used in preclinical orthopaedic research to conduct studies into areas that affect implant longevity, in particular osseointegration,[11; 17-19] metal-on-cartilage wear,[6] and periprosthetic joint infection.[20-23] We also described the creation of a radiolucent rat treadmill that is compatible with a commercially available micro-CT scanner that can be used to acquire X-ray fluoroscopic image sequences of rats as they ambulate on their conformal hip implants.

In Chapter 2, the aim was to obtain micro-computed tomography derived measurements of the rat proximal femur, to create parameterized rat hip implants that could be surgically installed in a clinically representative small animal model of joint replacement. The proximal femoral anatomy of N=25 rats (male, Sprague-Dawley, 390-605g) was quantified. Key measurements were used to parameterize computer-aided

design models of monoblock rat femoral implants. Linear regression analysis was used to determine if rat hip dimensions could be predicted from animal weight. A correlation analysis was used to determine how implants could be scaled to create a range of sizes. Additive manufacturing (3D printing) was used to create implants in medical-grade metal alloys. Linear regressions comparing rat weight to Femoral Head Diameter and Neck-Head Axis Length revealed a significant non-zero slope ($p<0.05$). Pearson's correlation analysis revealed five significant correlations between key measurements in the rat femur ($p<0.05$). Implants were installed into both cadaveric and live animals; iterative design modifications were made to prototypes based on these surgical findings. Animals were able to tolerate installation of implants, and were observed ambulating on their affected limbs post-operatively. Our results indicate that we were able to develop a preclinical rat hip hemiarthroplasty model using image-based and iterative design techniques to create 3D-metal printed implants in medical-grade metal alloys. Our findings support further development of this model for use as a low-cost translational test platform for preclinical orthopaedic research into areas such as osseointegration, metal-on-cartilage wear and peri-prosthetic joint infection.

In Chapter 3 we described a study in which the purpose was to develop and optimize a functional 3D-printed hip implant system and surgical approach for the rat that will allow for repeatable installation, in vivo testing, and imaging follow-up, in a preclinical model of hip hemiarthroplasty. Custom-designed unipolar rat femoral implants were created in five sizes and 3D-printed in titanium alloy. The cementless components were press-fit into the medullary canal of skeletally mature male rats (N=6), using a posterior approach to access the hip joint. Animals were evaluated post-

operatively (day 1) and at six time-points following surgery with in vivo micro-computed tomography to assess implant stability. Animals were sacrificed after 12 weeks and post-mortem analysis was conducted to assess fixation of each implant. Surgery was successful in all animals, and micro-CT imaging revealed stable implant positioning at 1 day and 1 week, post-operatively. Return to gait was observed in all cases, and rats remained ambulatory throughout the study. No incidences of implant failure were observed through the 3-week time-point. Micro-CT did, however, reveal implant subsidence in three of six animals at the 6-week time-point, resulting in hip subluxation. Post-mortem analysis revealed variable amounts of micro-motion when implants were manipulated with forceps, with more gross movement detected in subsided implants. We were able to report the first clinically representative rat hip hemi-arthroplasty surgeries using custom 3D-printed titanium alloy implants. Clinically relevant complications were observed (subsidence) that mimic complications of larger joint models. These findings support the use of this model as a preclinical platform that could be expanded for studies of osseointegration, metal-cartilage interactions, and joint infection around a functional implant.

Chapter 4 describes how clinically representative small-animal models of joint replacement have been developed as low-cost test platforms to test orthopaedic innovations aimed at reducing post-operative complications that lead to revision surgeries. Such models require implants that are functional and are able restore gait post-operatively in order to be considered clinically representative. The aim of this study was to assess the post-operative gait rats following the installation of Ti6AlV titanium alloy hip implants. N=5 male Sprague-Dawley rats from a concurrent study (described in

Chapter 3) underwent hip hemiarthroplasty surgery to install components via a posterior approach. Gait was assessed using a CatWalk XT system preoperatively, as well as at 3, 6, 9 and 12 weeks post-operatively. Data was analyzed via repeated measures one-way ANOVA; significance was determined at $P < .05$ level. A custom radiolucent rat treadmill was also developed to permit fluoroscopic assessment of post-operative hindlimb function at post-operative weeks 3, 6, 9 and 12. The ratio of affected limb to unaffected limb was not significantly different from baseline at post-operative week 3 compared to baseline for all metrics analyzed. A significant difference in duty cycle % at post-operative week 6 compared to baseline was revealed. Two cases of implant subsidence were observed following X-ray fluoroscopy analysis at post-operative week 6, likely contributing to the decline in gait at this timepoint. No significant differences in gait were observed compared to baseline at post-operative weeks 9 and 12. These results indicate that rat hip implants are able to restore ambulation in rats following hip hemiarthroplasty, but may lose functionality at later timepoints due to complications such as subsidence. Our findings also support that rat implants installed via hip hemiarthroplasty can be considered clinically representative; on the basis that functional cyclic loading was restored in rats post-operatively.

5.2 Future Directions

The accumulation of results presented within chapters 2-4 of this thesis demonstrate our ability to (1) design rat-specific femoral hip implants in a range of sizes that can accommodate rats of various weights; (2) manufacture rat implants in several medical-grade metal allows, including post-processing techniques that allow for a

polished finish on the heads of implants; (3) install implants surgically via both anterior and posterior approaches to demonstrate the world's first rat model of hip hemiarthroplasty; (4) evaluate implant position within the hip longitudinally using micro-CT image analysis; (5) evaluate the post-operative gait of rats following hip hemi-arthroplasty using both a gold-standard approach (CatWalk XT system) and a novel radiolucent treadmill, developed specifically for evaluating implant position in the hip during cyclic loading. We were able to show that implants could be designed, installed and assessed post-operatively for rats, laying the groundwork for future studies using this clinically representative model of hip hemiarthroplasty.

5.2.1 Osseointegration

Osseointegration is the apposition of bone onto the surface of an implant, and is critical to ensure secondary fixation and the long-term survival of cementless hip prostheses.[24] Post-operatively, growth factors are released from activated blood cells within the medulla at the bone-implant interface, which initiate a series of biological events that lead to bone formation around the stem of the implant.[24; 25] A tissue matrix, consisting of predominantly fibrin, is then created and acts as a scaffold to support osteoblasts (boneforming cells).[24; 25] This scaffold eventually becomes entirely filled with bone when osseointegration occurs properly, however if this process fails, a fibrous connection will instead form, which is not strong enough to prevent implant loosening over time.[24; 25] Several factors can contribute to a fibrous interface, including implant material, surface design, poor bone quality, surgical technique, loading conditions and insufficient bone turnover.[26] Extrapolating from histopathological *post mortem* analysis

performed on a Generation 1 rat, there is evidence that implants may have only facilitated a fibrous connection (Figures 5.1 and 5.2), indicating that one or more of these aforementioned areas would need to be addressed. Since implants were made in medical-grade alloys, and Sprague-Dawley rats have been used in many osseointegration studies,[11] the two areas that should be address to improve the osseointegration potential surface design and surgical technique.

The surface design we selected in Generation 1 implants (Chapter 2) consisted on an inherent surface texturing that results from the 3D printing process. This was done intentionally in an effort to promote osseointegration; we hypothesized this would be enhanced by a stem that was rough with larger surface area compared to a polished stem. Generation 2 implant stems (Chapters 2-4) also were left rough, with an engineered 500μm porosity added to further promote osseointegration; the optimal pore size to promote osseointegration onto titanium implants is between 150 and 600μm.[27] However, despite adding an engineered stem porosity, our components did not appear to facilitate effective osseointegration; this however may not be an outright limitation, since it would be difficult to evaluate new surface preparations aimed at promoting osseointegration in untreated control implants innately had this effect. Nevertheless in future studies, it would be useful to test our implants when prepared with conventional surface designs such as plasma-sprayed titanium and hydroxyapatite coating[28; 29] to determine if the overall geometry and installation of components is conducive to promote osseointegration.

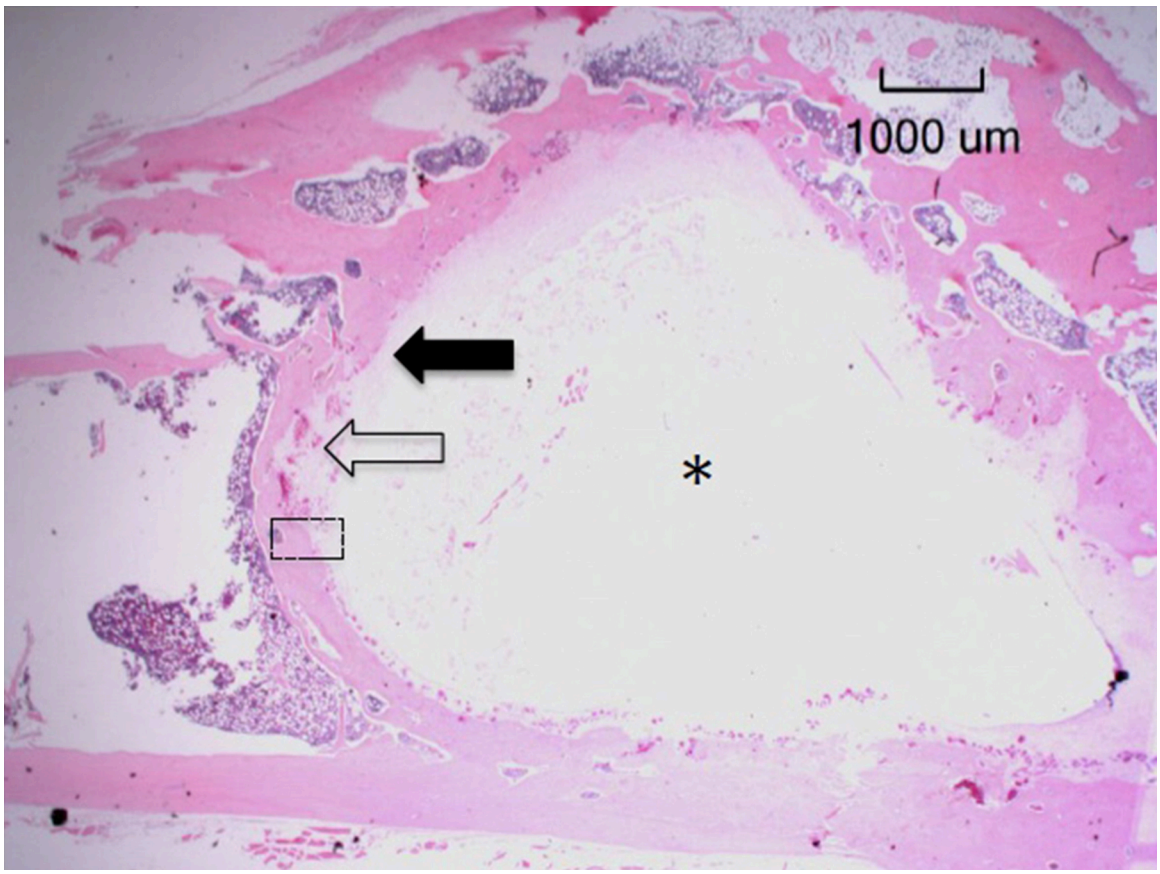

Figure 5.1: Histopathology section of a proximal femur (distal end towards left, articular surface towards right) of a male Sprague-Dawley rat at 11 post-operative months following installation of a Generation 1 316L stainless steel implant. The implant was removed prior to sectioning. A medullary cavity (asterisk) is lined by fibrous connective tissue (solid arrow) that contains numerous vessels (open arrow). Hatched box outlines area magnified in Figure 5.2.

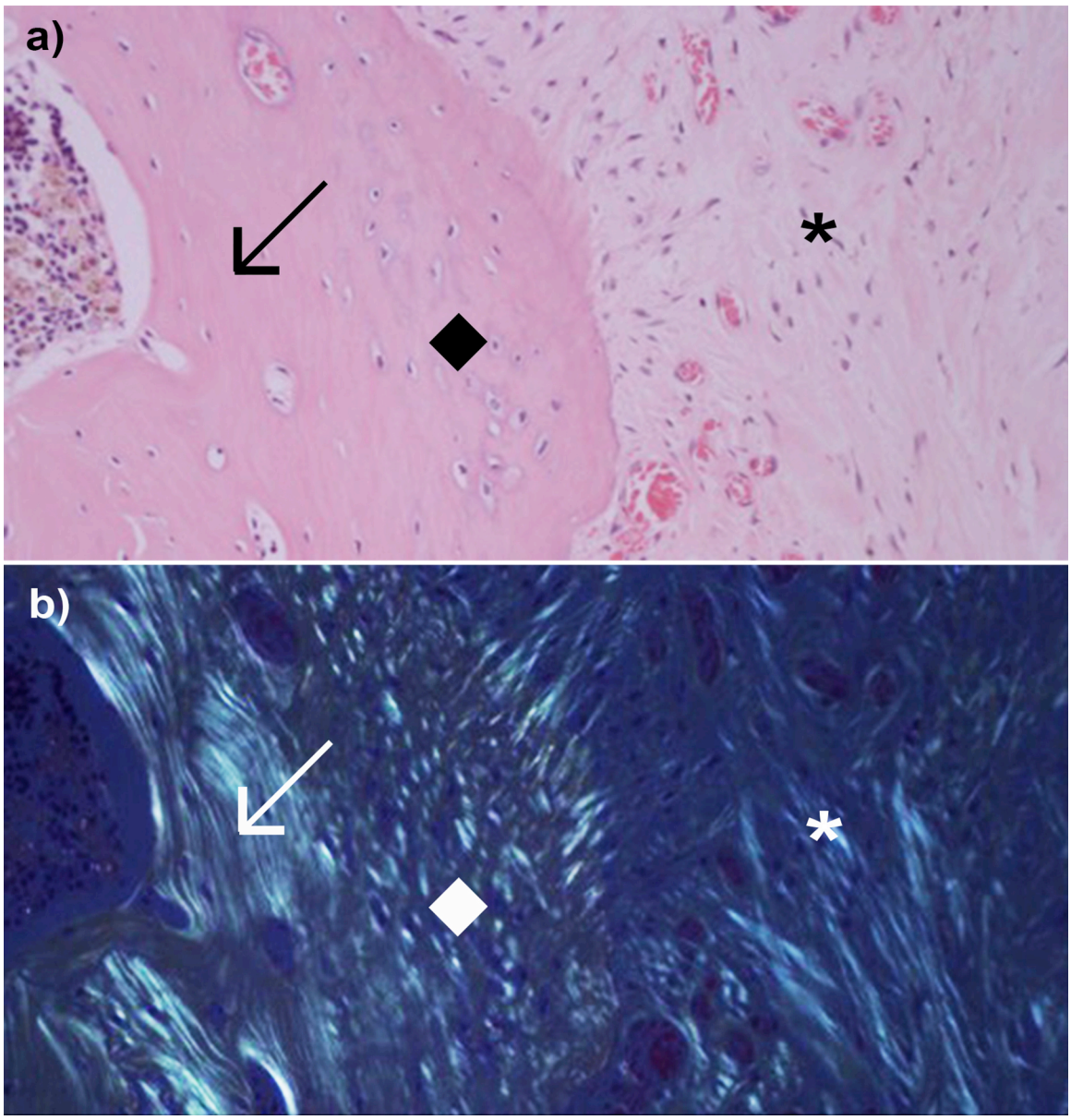

Figure 5.2: a) Hematoxylin and eosin stain of bone cavity bordered compared with b) polarized light of the same area. Sample is from a male Sprague-Dawley rat at 11 post-operative months following installation of a Generation 1 316L stainless steel implant. An asterisk indicates the fibrous connective tissue that at times has fibrocartilage characteristics. Refractile fibers help contrast woven bone architecture (arrow) relative to lamellar bone (diamond).

Surgical technique may also have contributed to the fibrous interface and unstable implants we observed in Chapters 2-4. In human and large-animal hip arthroplasty procedures, the intramedullary cavity is prepared using a broaching system, which facilitates incremental widening of the canal to receive an implant.[30] Broaching compacts the intramedullary bone and helps to ensure that the implant can be potted effectively, with maximum bone apposition against the stem. This approach was explored in the rat model using custom-developed broaches (Figure 5.3), however it was extremely difficult to tap broaches into the intramedullary space, with enough force to widen the canal, without causing a catastrophic fracture. To avoid fracture (which was also quite common when using a rotary drill), we instead used an ultrasonic dental scalar to prepare the proximal medullary cavity to receive an implant. The scalar afforded a fair amount of forgiveness from a surgical standpoint and was effective in creating a space where implants could be potted. However, it is possible that the scalar removed intramedullary bone that would normally be compacted around implants during broaching, thereby reducing the amount of bone that was in apposition to the implant stem and decreasing primary implant stability. In the future, instead of using a pointed tip on the end of the scalar, a custom broach or rasp could be designed to integrate with this device. This way, the broach or rasp could be oscillated to compress and shape intramedullary bone, without the need for tapping with a hammer, which risks fracture. Such a refinement in surgical technique would likely improve the chances of achieving effective osseointegration and reduce the instances of implant subsidence in the rat hip hemiarthroplasty model.

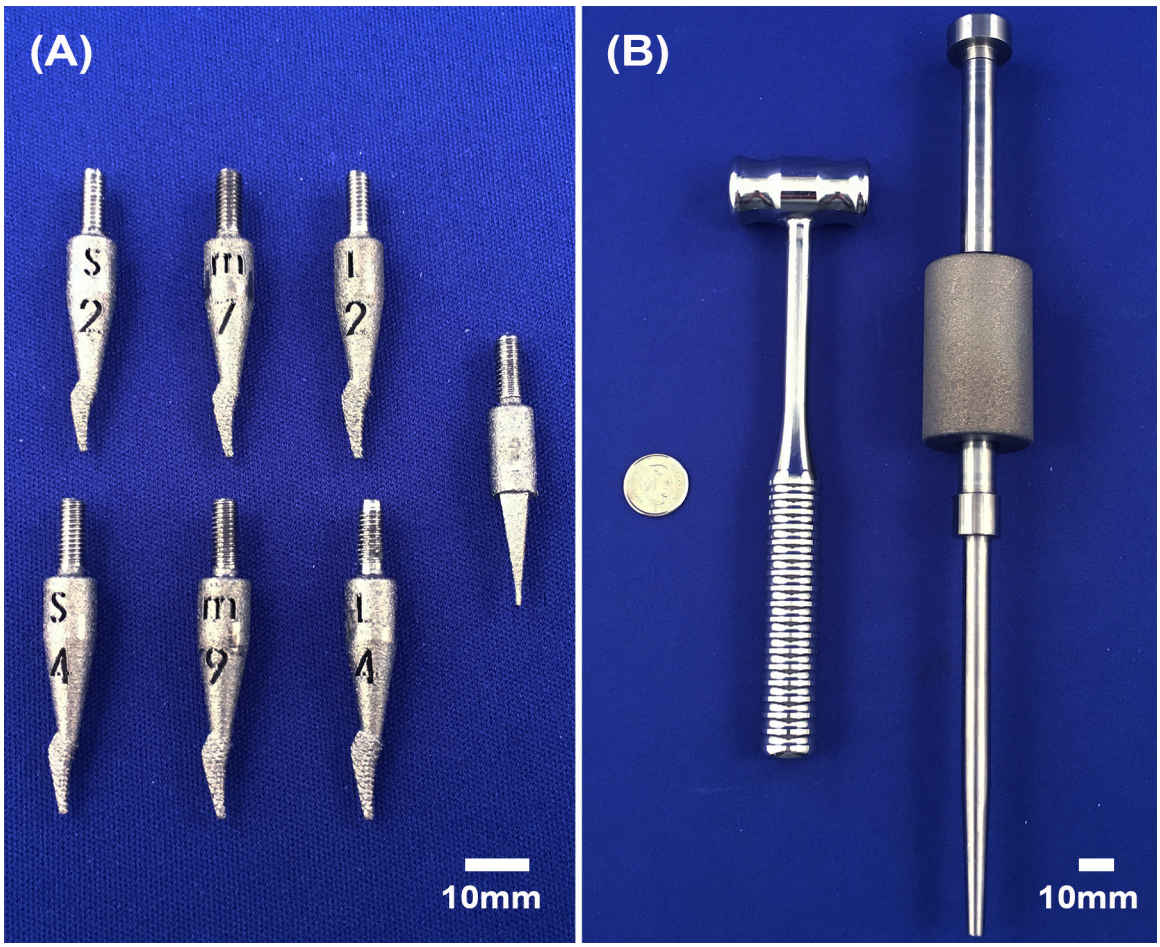

Figure 5.3: (A) Custom broach set and impactor tool 3D printed in F75 cobalt-chrome, created for incremental widening of the proximal medullary to facilitate effective press-fit of Generation 2 implants. (B) A commercially available stainless-steel dental hammer beside a custom slide hammer tool (aluminum shaft and titanium cylinder) and a Canadian dime for scale. Custom broaches and the impactor tool screw into the tip of the slide hammer, allowing for tool tapping and pullout.

5.2.2 Periprosthetic Joint Infection

Periprosthetic joint infection (PJI) is a devastating complication of total joint replacement, which occurs in 1% of patients who undergo total joint arthroplasty of the hip and knee.[22; 31] Although this percentage is small compared to some other surgical procedures, the high volume of joint replacement procedures performed annually means that PJI complications from orthopaedic surgeries are the most common source of surgery-contracted infections amount hospital inpatients in the industrialized world.[1; 22; 32] The pathogenesis of PJI involves the colonization of bacteria on the surface of the implant, followed by the creation of a protective layer called a biofilm (polysaccharide glycocalyx), which has a protective effect against the host's immune system, antibiotic therapy and even mechanical debridement.[22; 33] Several therapeutic options exist for resolving PJI including, combination antibiotic therapies, nanoparticles with bactericidal effects, phage therapy, and immunotherapy using monoclonal antibodies to name a few.[22] In most cases, treatment also involves revision surgery to remove the implant from the infected joint, via either a 1-stage revision, where a new implant is installed at the time of surgery, or; a 2-stage revision, where a temporary spacer (usually bone cement) is installed to maintain the joint space, followed by a second surgery to install a new component after the course of treatment in completed.[34] In either scenario, there is a high morbidity associated with revision surgery for PJI.[22; 34]

Recently, there has been a strong consensus amongst orthopaedic surgeons that better understanding the causes of PJI is needed, and therefore should be a major focus of research efforts in the coming years.[23] Consequently, the development of clinically

representative models of PJI has become an active area of research, particularly in the murine knee.[20; 21; 23; 35; 36] Such models use implants that interact with the synovium, since clinically representative infection involves the whole joint space microbiome.[23] Our rat hip model is therefore an ideal candidate for use in studying PJI, as it too utilizes an implant that articulates within the synovium. Also, no such model exists for the murine hip, making our model the ideal candidate for use as a clinically representative PJI model of hip arthroplasty.

In order to use our model in PJI studies, it will be first important to achieve osseointegration into our uncemented implants. Infection can often have a destabilizing effect of implant fixation,[37] therefore creating a component that is stable within the model at baseline will be important to help preserve the functionality of implants within the joint space during longitudinal studies. Approaches to help promote effective osseointegration are mentioned previously (above). Next, a common PJI bacterial pathogen, such as Staphylococcus aureus,[34; 37] could be cultured on our implants to investigate biofilm formation, followed by installation into live rats to investigate PJI progression longitudinally. Provided that there is adequate pain management to satisfy animal ethics, this approach would allow both systemic and localized treatments to be explored in the rat. Post-operative analysis should include both histopathology and imaging at multiple timepoints to characterize disease and/or treatment progression.

5.2.3 Metal-on-cartilage Wear

Metal-on-cartilage wear is perhaps an under-studied research area compared to osseointegration and infection, because the rates of hip hemi-arthroplasty surgery, which

only replaces one side of a joint, are much lower compared to total joint arthroplasty, where all articulating surfaces of the joint are replaced.[1] This is unsurprising because the most common reason for joint replacement surgery is degenerative osteoarthritis, where a patient's cartilage has degraded to the point that is chronically painful and must be removed completely.[1] However, in an effort to preserve bone-stock (in the event that a revision procedure is required), hip hemiarthroplasty is performed in patients who have healthy cartilage, particularly those who have suffered a femoral neck fracture, resulting in avascular necrosis of the femoral head.[1; 2; 5; 38]

In the short-term (2 year follow-up), the installation of a unipolar hip hemiarthroplasty implant has been shown to cause minimal acetabular cartilage wear,[39] but after long-term use, there is often concern that enough wear will accumulate to require resurfacing of the acetabulum with a femoral head prosthesis.[38] Femoral head hemiarthroplasty implants meant to articulate with healthy cartilage (unipolar) have highly polished articular surfaces and are usually made in cobalt-chrome alloys (Fig. 5.4); this has remained relatively unchanged since the first installations in 1939.[40] Surface topography modifications, such a dimple pattern like on a golf ball, could be explored to see if the added surface area allows for more synovial fluid to surround the articulating surface, which could potentially have a lubricating effect within the metal-on-cartilage joint. Moreover, the addition of coatings over the cobalt-chrome surface, using perhaps smoother or more pliable materials could be explored to see if they promote reduction in acetabular cartilage wear over time.

While we have demonstrated cementless components (since the majority of hip implants are uncemented), a cemented approach that uses either orthopaedic or dental

bone cement could easily be performed using our implants. In femoral head hemiarthroplasty cases, cemented implants have been shown to cause fewer complications compared to uncemented implants.[41] Using an approach that results in a lower complication rate from stem failure would be logical to pursue, especially when investigating articulating surface modifications, which should be agnostic to fixation technique. To modify our existing implant stems for optimal use in a cemented procedure, stems should be buffed to a smooth finish. This would have two benefits; first, this process would create an improved bonding surface for bone cement compared to a rough surface, and second; this would reduce the profile of the stems slightly, allowing space that the bone cement would fill between the implant and the bone. A cemented approach would better ensure that implants would be stable within the femur in the short-term,[41] meaning that cartilage wear would primarily be affected by the surface finish of the implant heads, avoiding damage that could occur as the result of an unstable implant. In the future, a cemented approach in live animals should be explored using polished generation 2 cobalt-chrome implants, with histopathology at several post-operative timepoints to determine the effect on rat hip cartilage wear longitudinally. An exercise regimen may also be useful in such a study, to ensure that articulation of the implant within the acetabulum is maximized.

Figure 5.4: An Austin Moore unipolar femoral hip hemiarthroplasty prosthesis beside an array of unipolar rat hip hemiarthroplasty implants in various medical grade alloys, and a Canadian dime for scale. Numerous implant iterations were created and tested before arrival on our final implant design.

5.2.4 2D-to-3D Image Registration

2D-3D image registration is a widely used technique for analyzing hip joint kinematics in both humans[42; 43] and animals.[44] Briefly, this process involves superimposing a 3D anatomical model, particularly bone, on a series of 2D images; these models are then moved in a virtual 3D space to precisely mimic their corresponding features in the original image sequence.[42] Open-source software exists (JointTrack) to facilitate both 2D-to-3D image registration and the quantification of joint kinematics.[45; 46] It would be ideal to explore this approach to gait analysis, particularly in our analysis of

fluoroscopic image sequences collected on the Ratwalk radiolucent treadmill system we describe in Chapter 4. Although 2D-to-3D registration can be automated, manual measurement and optimization by an experienced user is often required to ensure high-quality kinematic data is acquired.[42] The ability to use 3D bone models that are derived from micro-CT scans (Chapter 3) should be explored to determine if this could expedite the co-registration processes. Creating a workflow to allow the Ratwalk system to output quantitative kinematic measurements of post-operative gait performance would be ideal, providing objective data in addition to the qualitative observations of implant performance during cyclic loading that it already affords. If done correctly, 2D-to-3D registration could mean that post-operative gait analysis on the CatWalk XT may not be necessary in future studies involving the rat hip hemiarthroplasty model. Measurements that are specific to hip instability, such as femoral translation, could also be quantified via 2D-to-3D registration, providing objective measurements of implant function that the CatWalk XT cannot facilitate. Thus, using the Ratwalk for quantitative kinematic analysis should be explored in future works as this would simplify post-operative gait analysis, reduce pre-operative training time, and reduce the number of post-operative trials that would need to be conducted, compared to using both systems in parallel.

5.3 Final Remarks

In conclusion, this thesis has described the development of a clinically representative rat model of hip hemiarthroplasty, using image-based design to produce functional rat-specific 3D-printed implants in medical-grade alloys that can be installed into live animals. While clinically representative complications were observed

(subsidence), animals were able to facilitate the recovery of gait on the affected limb post-operatively. Our findings support further development of this model for use in studies of osseointegration, peri-prosthetic joint infection and metal-on-cartilage wear. Furthermore, we have described the design and implementation of a novel radiolucent treadmill that can be used in future studies to monitor the gait of rats post-operatively. These innovations offer basic scientists a translational test platform for conducting preclinical orthopaedic research aimed at improving the longevity of implants following joint replacement surgery.

5.4 References

1. 2019. Canadian Joint Replacement Registry Annual Report: Hip and Knee Replacements in Canada, 2017-2018. Ottawa, ON: Canadian Institute for Health Information.

2. Ryan SP, DiLallo M, Attarian DE, et al. 2018. Conversion vs Primary Total Hip Arthroplasty: Increased Cost of Care and Perioperative Complications. J Arthroplasty 33:2405-2411.

3. Gwam CU, Mistry JB, Mohamed NS, et al. 2017. Current Epidemiology of Revision Total Hip Arthroplasty in the United States: National Inpatient Sample 2009 to 2013. J Arthroplasty 32:2088-2092.

4. Paish ADM, Nikolov HN, Welch ID, et al. 2020. Image-based design and 3D-metal printing of a rat hip implant for use in a clinically representative model of joint replacement. J Orthop Res.

5. Field JR, Callary SA, Solomon LB, et al. 2016. Early acetabular cartilage wear following hemiarthroplasty: An ovine model. Vet Comp Orthop Traumatol 29:125-130.

6. Stotter C, Stojanovic B, Bauer C, et al. 2019. Effects of Loading Conditions on Articular Cartilage in a Metal-on-Cartilage Pairing. J Orthop Res 37:2531-2539.

7. El-Warrak AO, Olmstead M, Schneider R, et al. 2004. An experimental animal model of aseptic loosening of hip prostheses in sheep to study early biochemical changes at the interface membrane. BMC musculoskeletal disorders 5:7.

8. DiVincenzo MJ, Frydman GH, Kowaleski MP, et al. 2017. Metallosis in a Dog as a Long-Term Complication Following Total Hip Arthroplasty. Vet Pathol 54:828-831.

9. Volstad NJ, Schaefer SL, Snyder LA, et al. 2016. Metallosis with pseudotumour formation: Long-term complication following cementless total hip replacement in a dog. Vet Comp Orthop Traumatol 29:283-289.

10. DeYoung DJ, Schiller RA. 1992. Radiographic criteria for evaluation of uncemented total hip replacement in dogs. Vet Surg 21:88-98.

11. AbuMoussa S, Ruppert DS, Lindsay C, et al. 2018. Local delivery of a zoledronate solution improves osseointegration of titanium implants in a rat distal femur model. J Orthop Res 36:3294-3298.

12. Ruppert DS, Harrysson OLA, Marcellin-Little DJ, et al. 2017. Osseointegration of Coarse and Fine Textured Implants Manufactured by Electron Beam Melting and Direct Metal Laser Sintering. 3D Print Addit Manuf 4:91-97.

13. Huanhuan J, Pengjie H, Sheng X, et al. 2017. The effect of strontium-loaded rough titanium surface on early osseointegration. J Biomater Appl 32:561-569.

14. Li K, Wang C, Yan J, et al. 2018. Evaluation of the osteogenesis and osseointegration of titanium alloys coated with graphene: an in vivo study. Sci Rep 8:1843.

15. He T, Cao C, Xu Z, et al. 2017. A comparison of micro-CT and histomorphometry for evaluation of osseointegration of PEO-coated titanium implants in a rat model. Sci Rep 7:16270.

16. Lindtner RA, Castellani C, Tangl S, et al. 2013. Comparative biomechanical and radiological characterization of osseointegration of a biodegradable magnesium alloy pin and a copolymeric control for osteosynthesis. Journal of the mechanical behavior of biomedical materials 28:232-243.

17. Al-Jandan B, Marei HF, Abuohashish H, et al. 2018. Effects of sunitinib targeted chemotherapy on the osseointegration of titanium implants. Biomed Pharmacother 100:433-440.

18. Chen L, Komasa S, Hashimoto Y, et al. 2018. In Vitro and In Vivo Osteogenic Activity of Titanium Implants Coated by Pulsed Laser Deposition with a Thin Film of Fluoridated Hydroxyapatite. Int J Mol Sci 19.

19. De Smet E, Jaecques SV, Wevers M, et al. 2013. Constant strain rate and peri-implant bone modeling: an in vivo longitudinal micro-CT analysis. Clin Implant Dent Relat Res 15:358-366.

20. Carli AV, Ross FP, Bhimani SJ, et al. 2016. Developing a Clinically Representative Model of Periprosthetic Joint Infection. J Bone Joint Surg Am 98:1666-1676.

21. Carli AV, Bhimani S, Yang X, et al. 2017. Quantification of Peri-Implant Bacterial Load and in Vivo Biofilm Formation in an Innovative, Clinically Representative Mouse Model of Periprosthetic Joint Infection. J Bone Joint Surg Am 99:e25.

22. Taha M, Abdelbary H, Ross FP, et al. 2018. New Innovations in the Treatment of PJI and Biofilms-Clinical and Preclinical Topics. Current reviews in musculoskeletal medicine 11:380-388.

23. Bargon R, Bruenke J, Carli A, et al. 2019. General Assembly, Research Caveats: Proceedings of International Consensus on Orthopedic Infections. J Arthroplasty 34:S245-S253 e241.

24. Apostu D, Lucaciu O, Berce C, et al. 2018. Current methods of preventing aseptic loosening and improving osseointegration of titanium implants in cementless total hip arthroplasty: a review. The Journal of international medical research 46:2104-2119.

25. Mavrogenis AF, Dimitriou R, Parvizi J, et al. 2009. Biology of implant osseointegration. Journal of musculoskeletal & neuronal interactions 9:61-71.

26. Parithimarkalaignan S, Padmanabhan TV. 2013. Osseointegration: an update. Journal of Indian Prosthodontic Society 13:2-6.

27. Vasconcellos LM, Leite DO, Oliveira FN, et al. 2010. Evaluation of bone ingrowth into porous titanium implant: histomorphometric analysis in rabbits. Brazilian oral research 24:399-405.

28. Hahn H, Palich W. 1970. Preliminary evaluation of porous metal surfaced titanium for orthopedic implants. Journal of biomedical materials research 4:571-577.

29. Castellini I, Andreani L, Parchi PD, et al. 2016. Hydroxyapatite in total hip arthroplasty. Our experience with a plasma spray porous titanium alloy/hydroxyapatite double-coated cementless stem. Clinical cases in mineral and bone metabolism : the official journal of the Italian Society of Osteoporosis, Mineral Metabolism, and Skeletal Diseases 13:221-227.

30. Batailler C, Fary C, Servien E, et al. 2018. Influence of femoral broach shape on stem alignment using anterior approach for total hip arthroplasty: A radiologic comparative study of 3 different stems. PLoS One 13:e0204591.

31. Kapadia BH, Berg RA, Daley JA, et al. 2016. Periprosthetic joint infection. Lancet (London, England) 387:386-394.

32. Lamagni T. 2014. Epidemiology and burden of prosthetic joint infections. The Journal of antimicrobial chemotherapy 69 Suppl 1:i5-10.

33. Ciofu O, Rojo-Molinero E, Macià MD, et al. 2017. Antibiotic treatment of biofilm infections. APMIS : acta pathologica, microbiologica, et immunologica Scandinavica 125:304-319.

34. Kandel CE, Jenkinson R, Daneman N, et al. 2019. Predictors of Treatment Failure for Hip and Knee Prosthetic Joint Infections in the Setting of 1- and 2-Stage Exchange Arthroplasty: A Multicenter Retrospective Cohort. Open forum infectious diseases 6:ofz452.

35. Morris JL, Letson HL, Grant A, et al. 2019. Experimental model of peri-prosthetic infection of the knee caused by Staphylococcus aureus using biomaterials representative of modern TKA. Biology open 8.

36. Jie K, Deng P, Cao H, et al. 2019. Prosthesis design of animal models of periprosthetic joint infection following total knee arthroplasty: A systematic review. PLoS One 14:e0223402.

37. Nilsdotter-Augustinsson A, Briheim G, Herder A, et al. 2007. Inflammatory response in 85 patients with loosened hip prostheses: a prospective study comparing inflammatory markers in patients with aseptic and septic prosthetic loosening. Acta orthopaedica 78:629-639.

38. Guyen O. 2019. Hemiarthroplasty or total hip arthroplasty in recent femoral neck fractures? Orthopaedics & traumatology, surgery & research : OTSR 105:S95-s101.

39. Stevenson JD, Kumar VS, Cribb GL, et al. 2018. Hemiarthroplasty proximal femoral endoprostheses following tumour reconstruction: is acetabular replacement necessary? The bone & joint journal 100-b:101-108.

40. Hernigou P, Quiennec S, Guissou I. 2014. Hip hemiarthroplasty: from Venable and Bohlman to Moore and Thompson. Int Orthop 38:655-661.

41. Parker MJ, Cawley S. 2020. Cemented or uncemented hemiarthroplasty for displaced intracapsular fractures of the hip: a randomized trial of 400 patients. The bone & joint journal 102-b:11-16.

42. Sato T, Tanino H, Nishida Y, et al. 2017. Dynamic femoral head translations in dysplastic hips. Clinical biomechanics (Bristol, Avon) 46:40-45.

43. Yamaguchi S, Sasho T, Kato H, et al. 2009. Ankle and subtalar kinematics during dorsiflexion-plantarflexion activities. Foot & ankle international 30:361-366.

44. Tinga S, Kim SE, Banks SA, et al. 2018. Femorotibial kinematics in dogs with cranial cruciate ligament insufficiency: a three-dimensional in-vivo fluoroscopic analysis during walking. BMC veterinary research 14:85.

45. Banks SA, Hodge WA. 1996. Accurate measurement of three-dimensional knee replacement kinematics using single-plane fluoroscopy. IEEE transactions on bio-medical engineering 43:638-649.

46. Dennis DA, Komistek RD, Northcut EJ, et al. 2001. "In vivo" determination of hip joint separation and the forces generated due to impact loading conditions. J Biomech 34:623-629.

Appendix A – Animal Use Protocols

AUP 2013_027 was obtained for animal use in Chapter 2.

AUP 2017_156 was obtained for animal use in Chapters 3 and 4.

Due to the page length of the AUP only partial content of initial sections are attached for reference in this appendix. For a complete version of the approved AUPs, please contact ADMP or Animal Care and Veterinary services at Western University.

AUP 2013_027

1. Investigator Contact Information

PI_FULL_NAME El Warrak, Alex
AUP NUMBER 2013-027
AUP TYPE
Primary Role Principal Investigator
1. PI Full Name
El Warrak, Alex

2. Primary Institution&Department
Research Western / Animal Care &Veterinary Services

3. Office Location
- Building &Room #

4. Weekday Phone #

5. PI After-Hours
Emergency Contact#

6. Pager – Phone &Pager #

7. Primary Email [redacted]

8. Other Email

9. Lab Campus Location, if different from Q.3 Medical &Dental Sciences Buildings

10. Lab Phone #, if different from Q.4

1.1 PI Designate Contact Information
Primary Role On This Protocol

PI Student
1. PI Representative
Paish, Adam

2. Primary Institution &Department
Schulich School Of Medicine &Dentistry

3. Office Location - Building &Room #
[redacted]

4. Weekday Phone [redacted]

5. After-Hours Emergency Contact #
[redacted]

6. Pager – Phone &Pager #

7. Primary Email
[redacted]

Submit - Animal Use Protocol - AUP Form 3

8. Other Email

9. This is a Primary Contact on this Protocol

10. Include Primary Contact on all E-mail Correspondence

11. This is the Requestor on this Protocol
Yes

2. Protocol Title &Project Type
1. Animal Use Protocol Title Rat partial hip replacement (Pilot)

2. Application Type, Pick One
Pilot

3. If 'Full Renewal' or 'Post-Pilot Full Protocol' provide Associated Previous Protocol Number

4. If Post-Pilot Full Protocol or Full Renewal, Provide a PROGRESS REPORT SUMMARY that outlines progress relating to the scientific question asked in this AUP, as well as to the REPLACEMENT of animals, REDUCTION of animal use numbers AND REFINEMENT of experimental technique.

5. If Post-Pilot Full Protocol or Full Renewal, provide previous Protocol Year's animal

use number.

6. Proposed Start Date (mm/dd/yy)
07/01/2013

Attachments List
File Spec Description Created
3. Lay Summary &Glossary
1. Using non-scientific language, please describe the project's purpose, expected benefit, and a brief summary of your work with the animal model(s). Please be aware that in the event of communications with Western Media Relations and the PI is not available, this summary will be sent to Western Media Relations.

Purpose: To demonstrate the ability to successfully perform a partial hip-joint replacement in a rat, using a novel, custom rat orthopaedic hip component. 1) Using 3D metal printing, fabricate a working prototype of a femoral orthopaedic hip component made of surgical-grade titanium alloy (Ti6Al4V), and designed specifically to be used in a rat. 2) Perform a partial hip replacement surgery using the prototype implants. 3) Evaluate surgical success using gait analysis to determine whether the rats' hips are functionally stable (no dislocation) and that the animals have been restored to normal locomotion. 4) Using micro-computed tomography (micro-CT), investigate the bone-metal interphase for signs of osseointegration.

Expected benefit: This project will demonstrate the first cost-effective, functional hip hemiarthroplasty component in a rat model, leading to a new tool for basic scientists. Compared to the traditional large animal model (pig, goat, sheep, etc.), the use of a rat model will reduce variability, and future studies can be carried out with increased throughput and statistical power, through the use of existing live-animal micro-imaging systems to assess osseointegration.

2. GLOSSARY OF TERMS - Identify each individual scientific term and abbreviation using CAPITAL LETTERS, and then briefly define each term to be referenced in any section of this protocol. e.g. ALLELE - The genetic variant of a gene responsible for the different traits of certain characteristics and genetic diseases.

partial hip-joint replacement: referred to surgically as a hemiarthroplasty, this procedure involves replacing one-half of the hip joint, in this case, the femoral side.

3D metal printing: a new additive manufacturing technique that can fabricate custom objects based on instructions from computer-aided design software

Ti6Al4V: titanium alloy with 6% aluminum and 4% vanadium, used in human orthopaedic components

gait analysis: technique for assessing movement during normal walking or running

micro-CT: a small CT machine, made specifically for imaging small animals

osseointegration: the functional integration of a surgical implant into the bone cell matrix, allowing for proper fixation and function of the implant over time

4. CCAC Animal Procedural Outline
CCAC PROCEDURAL OVERVIEW - Use this field to convey in simple terms using approximately 40 words or less the nature of the procedures conducted on the animals. Please use KEY WORDS provided through the above link.

General: pilot study; medical research
Procedures: micro-CT imaging (whole-body radiation); gait analysis (rat treadmill, cameras); surgery

Agents: iso-fluorine (anesthesia); CO2 gas (euthanasia); buprenorphine (analgesic)

Surgery: major surgery (partial joint replacement)

AUP 2017_156

PI :
Truscott, Emily

Protocol #
2017-156

Status :
Approved (w/o Stipulation)

Approved :
04/01/2018

Expires :
04/01/2022
Title:
Rat partial hip replacement study

Add/Update/Remove Species Used on this Protocol
Species Agents Drugs Restraint Breeding
Rat
Yes Yes No No
TOC

Animal Use Protocol Overview
Animal Use Protocol Title
Rat partial hip replacement study

Application Type. If this is a post-pilot project, please attach the Pilot Report to this section, below.
Post-pilot

Provide Associated Previous Protocol Number

Please provide a report detailing the previous AUP's use of Animals
2013_027

Using non-scientific language, please describe the project's purpose, expected benefit, and a brief summary of your work with the animal model(s).

Please be aware that in the event of communications with Western Media Relations and the PI is not available, this summary will be sent to Western Media Relations.

Purpose: To assess the bone-metal and metal-cartilage interfaces of custom 3D-printed metal functional orthopaedic implants, in a rat model of partial hip replacement. 1) Implants will be manufactured via 3D metal printing, and made of surgical-grade titanium alloy (Ti6Al4V) and/or surgical grade cobalt-chrome (F75). Components have been designed specifically to be used in a rat. 2) Perform a partial hip replacement surgery using 3D-printed metal implants. 3) Evaluate surgical success using gait analysis to determine whether the rats' hips are functionally stable (no dislocation) and that the animals have been restored to normal locomotion. 4) Using micro-computed tomography (micro-CT), investigate the bone-metal interphase for signs of osseointegration. 5) Postmortem histology will be performed to evaluate cartilage wear. Expected benefit: This project will demonstrate the first cost-effective, functional hip component in a rat model, leading to a new tool for basic scientists. Compared to the traditional large animal model (pig, goat, sheep, etc.), the use of a rat model will reduce variability, and future studies can be carried out with increased throughput and statistical power, through the use of existing live-animal micro-imaging systems to assess osseointegration.

GLOSSARY OF TERMS - Identify each individual scientific term and abbreviation using CAPITAL LETTERS, and then briefly define each term to be referenced in any section of this protocol. e.g. ALLELE - The genetic variant of a gene responsible for the different traits of certain characteristics and genetic diseases.

Osseointegration - the growth of new bone with the surface of an implant, which ensures the long-term stability of
the component

3D-printing (metal) - Selective laser melting of metal powder in a layer by layer fashion

Here is the link to CCAC's Policy on Scientific Merit and Ethical Review of Animal-based Research:
http://www.ccac.ca/Documents/Standards/Policies/Scientific_merit_and_ethical_review_of_animal-based_research.pdf

Has the work outlined in this AUP received favourable scientific peer review?
Yes No

Do you wish to provide a funding peer review assessment, which may be considered in lieu of internal scientific peer review? If 'YES', please attach the funding assessment.
Yes No

If this is a RESEARCH AUP, please provide a list of one to three publications relevant to the work outlined in this
AUP.

If this is a research AUP, attach an OUTLINE for scientific merit reviewers that provides sufficient information that another scientist working in the same field of study could effectively review this AUP's scientific merit, below. PIs may utilize whichever format best describes its scientific merit, e.g. background, rationale, hypothesis, objectives, experimental procedures

Using only key words, specify the animal models and procedures described within this AUP.

General: medical research Procedures: micro-CT & x-ray imaging (whole-body radiation); gait analysis (rat treadmill, cameras); surgery Agents: iso-fluorine (anesthesia); CO2 gas (euthanasia); buprenorphine (analgesic) Surgery: major surgery (partial joint replacement)
TOC

Funding Source List
Fund Source Grant Title Funded? Grant
Number Start Date Grant Holder
Canadian Institutes Of Health Research
Dynamic Imaging of the Musculoskeletal
System: From Cell Yes R1896A46 02/01/2017

Canadian Institutes Of Health Research
Dynamic micro-computed tomography for pre-clinical muscular Yes R1896A41 04/09/2014
UWO Bone And Joint Institute
Adam Paish - CMHR Award Yes R1896A47 02/01/2017

Funding Source Name
Canadian Institutes Of Health Research
Proposal Title
Dynamic Imaging of the Musculoskeletal System: From Cell
Is this award currently funded?
Please provide the associated GRANT #

R1896A46

Funding START date mm/dd/yy
02/01/2017

PI on Grant (if different than PI on Protocol)
David W. Holdsworth

Funding Source Name
Canadian Institutes Of Health Research
Proposal Title
Dynamic micro-computed tomography for pre-clinical muscular

Is this award currently funded?
Please provide the associated GRANT #
R1896A41

Funding START date mm/dd/yy
04/09/2014
PI on Grant (if different than PI on Protocol)
Funding Source Name
UWO Bone And Joint Institute
Proposal Title
Adam Paish - CMHR Award
Is this award currently funded?
Please provide the associated GRANT #
R1896A47
Funding START date mm/dd/yy
02/01/2017
PI on Grant (if different than PI on Protocol)
TOC

Purpose of Animal Use
Identify PRIMARY purpose of animal use
2-Medical or Veterinary Research
TOC
Hazardous Materials
Microorganism, Biological Agent or Hazardous Species Used?
Yes No

Institute Biosafety Committee #
Recombinant DNA or Viral Vector Directly into Animals Used?
Yes No

Experimental Agents or Veterinary Drug Used?
Yes No

Nuclear Substance, Radiation, or Imaging Device Used?
Yes No

Radiation Permit #

2342-RRI-807

Appendix B – Copyright Permissions

Will you be
translating? No

Title A Clinically Representative Rat Model of Hip Hemiarthroplasty
Institution name Western University

Expected presentation date May 2020

Requestor Location

Adam D.M. Paish
[redacted]
Attn: Adam D.M. Paish

Publisher Tax ID EU826007151

Total 0.00 CAD

TERMS AND CONDITIONS

OR ENTITY FOR ANY SPECIAL, CONSEQUENTIAL, INCIDENTAL, INDIRECT, EXEMPLARY OR PUNITIVE DAMAGES, HOWEVER CAUSED, ARISING OUT OF OR IN CONNECTION WITH THE DOWNLOADING, PROVISIONING, VIEWING OR USE OF THE MATERIALS REGARDLESS OF THE FORM OF ACTION, WHETHER FOR BREACH OF CONTRACT, BREACH OF WARRANTY, TORT, NEGLIGENCE, INFRINGEMENT OR OTHERWISE (INCLUDING, WITHOUT LIMITATION, DAMAGES BASED ON LOSS OF PROFITS, DATA, FILES, USE, BUSINESS OPPORTUNITY OR CLAIMS OF THIRD PARTIES), AND WHETHER OR NOT THE PARTY HAS BEEN ADVISED OF THE POSSIBILITY OF SUCH DAMAGES. THIS LIMITATION SHALL APPLY NOTWITHSTANDING ANY FAILURE OF ESSENTIAL PURPOSE OF ANY LIMITED REMEDY PROVIDED HEREIN.

Should any provision of this Agreement be held by a court of competent jurisdiction to be illegal, invalid, or unenforceable, that provision shall be deemed amended to achieve as nearly as possible the same economic effect as the original provision, and the legality, validity and enforceability of the remaining provisions of this Agreement shall not be affected or impaired thereby. The failure of either party to enforce any term or condition of this Agreement shall not constitute a waiver of either party's right to enforce each and every term and condition of this Agreement. No breach under this agreement shall be deemed waived or excused by either party unless such waiver or consent is in writing signed by the party granting such waiver or consent. The waiver by or consent of a party to a breach of any provision of this Agreement shall not operate or be construed as a waiver of or consent to any other or subsequent breach by such other party. This Agreement may not be assigned (including by operation of law or otherwise) by you without WILEY's prior written consent. Any fee required for this permission shall be non-refundable after thirty (30) days from receipt by the CCC.

These terms and conditions together with CCC's Billing and Payment terms and conditions (which are incorporated herein) form the entire agreement between you and WILEY concerning this licensing transaction and (in the absence of fraud) supersedes all prior agreements and representations of the parties, oral or written. This Agreement may not be amended except in writing signed by both parties. This Agreement shall be binding upon and inure to the benefit of the parties' successors, legal representatives, and authorized assigns. In the event of any conflict between your obligations established by these terms and conditions and those established by CCC's Billing and Payment terms and conditions, these terms and conditions shall prevail. WILEY expressly reserves all rights not specifically granted in the combination of (i) the license details provided by you and accepted in the course of this licensing transaction, (ii) these terms and conditions and (iii) CCC's Billing and Payment terms and conditions.

This Agreement will be void if the Type of Use, Format, Circulation, or Requestor Type was misrepresented during the licensing process. This Agreement shall be governed by and construed in accordance with the laws of the State of New York, USA, without regards to such state's conflict of law rules. Any legal action, suit or

proceeding arising out of or relating to these Terms and Conditions or the breach thereof shall be instituted in a court of competent jurisdiction in New York County in the State of New York in the United States of America and each party hereby consents and submits to the personal jurisdiction of such court, waives any objection to venue in such court and consents to service of process by registered or certified mail, return receipt requested, at the last known address of such party.

WILEY OPEN ACCESS TERMS AND CONDITIONS
Wiley Publishes Open Access Articles in fully Open Access Journals and in Subscription journals offering Online Open. Although most of the fully Open Access journals publish open access articles under the terms of the Creative Commons Attribution (CC BY) License only, the subscription journals and a few of the Open Access Journals offer a choice of Creative Commons Licenses. The license type is clearly identified on the article.

The Creative Commons Attribution License
The Creative Commons Attribution License (CC-BY) allows users to copy, distribute and transmit an article, adapt the article and make commercial use of the article. The CC-BY license permits commercial and non-
Creative Commons Attribution Non-Commercial License
The Creative Commons Attribution Non-Commercial (CC-BY-NC) License permits use, distribution and reproduction in any medium, provided the original work is properly cited and is not used for commercial purposes.(see below)
Creative Commons Attribution-Non-Commercial-NoDerivs License

The Creative Commons Attribution Non-Commercial-NoDerivs License (CC-BY-NC ND) permits use, distribution and reproduction in any medium, provided the original work is properly cited, is not used for commercial purposes and no modifications or adaptations are made. (see below)

Use by commercial "for-profit" organizations

Use of Wiley Open Access articles for commercial, promotional, or marketing purposes requires further explicit permission from Wiley and will be subject to a fee. Further details can be found on Wiley Online Library
http://olabout.wiley.com/WileyCDA/Section/id-410895.html
Other Terms and Conditions: v1.10 Last updated September 2015
Questions? customercare@copyright.com or +1-855-239-3415 (toll free in the US) or +1-978-646-2777.

Appendix C - Curriculum Vitae

ADAM D.M. PAISH

Academic CV

PhD Candidate, Dept. of Medical Biophysics, Western University

---

EDUCATION

WESTERN UNIVERSITY – London, ON, Canada

PhD Candidate in Medical Biophysics May 2014 – Present

- Research focus on orthopaedic implant development for small animal models using micro-computed tomography analysis and 3D metal printing
- 2016 AC Groom Award Winner for Top PhD Seminar in Medical Biophysics

WESTERN UNIVERSITY – London, ON, Canada

Medical Innovation Fellowship Jul. 2019 – May 2020

- Tasked with identifying unmet needs within the healthcare system and creating novel solutions
- One of six applicants selected for program, unique to Canada, out of international applicant pool

UNIVERSITY OF MINNESOTA – Minneapolis, MN, USA

Earl Bakken Medical Device Center Bootcamp Jul. 2019 – Aug. 2019

- Medical Alley course in entrepreneurship, medical innovation, engineering and health policy
- Top bio-design project in mach pitch competition

IVEY INTERNATIONAL CENTRE FOR HEALTH INNOVATION – London, ON, Canada

Health Leadership Training Program Jan. 2013 – Apr. 2014

- Completed MBA level course in healthcare analytics

- Participated in strategic training sessions for future leaders in health innovation and knowledge translation

WESTERN UNIVERSITY – London, ON, Canada

MSc in Medical Biophysics (Reclassified) Sep. 2012 – Apr. 2014
- Joint Motion Program (JuMP) and Collaborative Program in Musculoskeletal Health Research (CMHR) funded trainee.

WESTERN UNIVERSITY – London, ON, Canada

Hon. BSc Spec. Kinesiology Sep. 2008 – Apr. 2012
- Additional Minor in Medical Science
- Achieved Dean's Honours List status in all four years of study
- Graduated with "Western Scholars" distinction

SCHOLARSHIPS AND AWARDS

PROTEUS INNOVATION COMPETITION – London, ON, Canada

Pitch Competition Winner Jan. 2018 – Mar. 2018
- Award of $5,000 for top business plan and pitch: Force-Guided Navigation system for surgery.

WORLDISCOVERIES – London, ON, Canada

Graduate Student Innovation Scholar Jan. 2017 – May 2017
- Award of $1,500 for participation in the program, which included training medical innovation, patenting and entrepreneurship.

WESTERN BONE AND JOINT INSTITUTE – London, ON, Canada

Transdisciplinary Bone and Joint Training Award Sep. 2015 – 2018
- Award of $10,000 annually for three years

DEPARTMENT OF MEDICAL BIOPHYSICS, UWO – London, ON, Canada
Alan C. Groom Award Sep. 2016
- Award of $1,000, presented to the PhD student who presents the most effective research seminar.

CANADIAN BONE AND JOINT CONFERENCE – London, ON, Canada

Top Presenter Apr. 2016

- Presented for the most effective podium presentation in Novel Applications of MSK Imaging

THE UNIVERSITY OF WESTERN ONTARIO – London, ON, Canada

Western Graduate Research Scholarship Sep. 2012 – 2017

- Award of $4,500 annually for duration of graduate studies

LAWSON HEALTH RESEARCH INSTITUTE – London, ON, Canada

Internal Research Fund Grant Jan 2013 – Dec 2015

- Assisted in writing grant that was funded for $15,000 to conduct pilot projects for novel technologies

CANADIAN INSTITUES OF HEALTH RESEARCH (CIHR) - Ottawa, ON, Canada

Travel Award May 2015

- $1000 for travel and expenses at the Canadian Health Research Forum

SCHULICH SCHOOL OF MEDICINE AND DENTISTRY – London, ON, Canada

Graduate Research Scholarship Jan. 2015

- $2000 award
- Administered through the Joint Motion Program (JuMP), a CIHR training program in musculoskeletal health research and leadership

CANADIAN INSTITUES OF HEALTH RESEARCH (CIHR) - Ottawa, ON, Canada

Strategic Training Initiative in Health Research (STIHR) Fellowship Sep. 2012 – Aug. 2014

- Award of $11,500 annually including a stipend enhancement of $2000
- Administered through the Joint Motion Program (JuMP), a CIHR training program in musculoskeletal health research and leadership

THE UNIVERSITY OF WESTERN ONTARIO – London, ON, Canada

Western Scholarship of Excellence Mar. 2008

- Entrance Scholarship of $2000
- Award for achieving a high school average between 90.0-94.9% entering university

THESIS MANUSCRIPTS

1. A.D.M. Paish, H.N. Nikolov, I.D. Welch, A.O. El-Warrak, M.G. Teeter, D.D.R. Naudie, D.W. Holdsworth. Image-Based Design and 3D-metal Printing of a Rat Hip Implant for use in a Clinically Representative Model of Joint Replacement. *J Orthop Res.* 2020 May 5. doi: 10.1002/jor.24706.

2. A.D.M. Paish, E.A. Truscott, H. Abdelbary, M.G. Teeter, D.D. Naudie, D.W. Holdsworth. A Rat Model of Hip Hemiarthroplasty Using 3D-printed Titanium Implants. *In preparation for the Journal of Orthopaedic Research.*

3. A.D.M. Paish, E.A Truscott, S.I. Pollmann, H. Abdelbary, M.G. Teeter, D.D. Naudie, D.W. Holdsworth. Rat hind limb gait following a hip-hemiarthroplasty. *In preparation for the Journal of Orthopaedic Research.*

ADDITIONAL WORKS IN PREPARATION

1. A.D.M. Paish, T. Chmiel, B. Salt, L.L Pederson D.W. Holdsworth, A.O. El-Warrak. 3D design and fabrication of a custom titanium bone plate for ulnar fracture repair in a peregrine falcon wing. *In preparation for the Journal of Avian Medicine and Surgery.*

CONFERENCE PRESENTATIONS

1. A.D.M. Paish, E.A. Truscott, S.I. Pollmann, H. Abdelbary, M.G. Teeter, D.D. Naudie, D.W. Holdsworth. A Rat Model of Hip Hemiarthroplasty Using 3D-printed Titanium Implants. Orthopaedic Research Society Annual Meeting 2020, Phoenix, AZ, 2020-02-08.

2. A.D.M. Paish, H.N Nikolov, E.A. Truscott, A.O. El-Warrak, I.D. Welch, M.G. Teeter, D.D. Naudie, D.W. Holdsworth. Iterative design of a small-animal hip-hemiarthroplasty model for preclinical research. Imaging Network Ontario, London, ON. 2019-03-29. Award Winning Podium Presentation.

3. A.D.M. Paish, T. Chmiel H.N. Nikolov, A.O. El-Warrak, I.D. Welch, M.G. Teeter, D.D. Naudie, D.W. Holdsworth. A 3D-Metal Printed Implant System for a Small Animal Model of Hip Hemiarthroplasty. Orthopedic Research Society, New Orleans, LA. 2018-03-10. Poster Presentation.

4. Rapid prototyping of a lightweight bone plate for complex fracture fixation in a peregrine falcon. A.D.M. Paish, T. Chmiel, B. Salt, A.O. El-Warrak, D.W. Holdsworth. Imaging Network Ontario, London, ON. 2017-03-15. Poster Presentation.

5. A.D.M. Paish, H.N. Nikolov, A.O. El-Warrak, I.D. Welch, M.G. Teeter, D.D. Naudie, D.W. Holdsworth. Towards optimizing a custom small animal model of partial joint replacement

system created via additive manufacturing. 10th World Biomaterials Congress, Montreal QC. 2016-05-17. Poster Presentation

6. A.D.M. Paish, T. Chmiel, S.I. Pollmann, H.N. Nikolov, A.O. El-Warrak, M.G. Teeter, D.D. Naudie, D.W. Holdsworth. A Radiolucent Treadmill for X-ray Fluoroscopic Kinematic Analysis of a Small-Animal Model of Partial Hip Replacement Arthroplasty. Canadian Bone and Joint Conference 2016-04-08. Platform Presentation (Top Prize)

7. A.D.M. Paish, T. Chmiel, S.I. Pollmann, D.W. Holdsworth. A micro-CT-integrated radiolucent treadmill for fluoroscopic gait assessment in small animal models. Imaging Network Ontario 2016-03-30. Platform Presentation

8. A.D.M. Paish, T. Chmiel, S.I. Pollmann, D.W. Holdsworth. A Novel Radiolucent Treadmill for X-ray Fluoroscopy Kinematic Analysis in Small-Animal Models of Musculoskeletal Disease. London Health Research Day 2016-03-29. Platform Presentation

9. A.D.M. Paish, H.N. Nikolov, I.D. Welch, D.W. Holdsworth. Design and installation of a rat hip implant for a small animal orthopaedic model of joint replacement. London Imaging Discovery. 2015-06-11. Poster Presentation (Award Winning)

10. A.D.M. Paish, H.N. Nikolov, I.D. Welch, D.W. Holdsworth. Image-based design of a rat hip prosthesis. Canadian Student Health Research Forum. 2015-06-03. Poster Presentation, Faculty Nominated Presenter (Top 5% of Schulich Medicine and Dentistry PhD Trainees 2015)

11. A.D.M. Paish, H.N. Nikolov, I.D. Welch, D.W. Holdsworth. Image-based design of a rat hip prosthesis. London Health Research Day. 2015-04-01. Platform Presentation (Award Winning)

12. A.D.M. Paish H.N. Nikolov, I.D. Welch, D.W. Holdsworth. Design of a novel functional hip prosthesis created through additive manufacturing for use in a small animal model of osseointegration. Orthopaedic Research Society Annual Meeting. 2015-03-28. Poster Presentation

13. A.D.M. Paish H.N. Nikolov, I.D. Welch, D.W. Holdsworth. The use of micro-CT image data and additive manufacturing to create a functional hip implant for small animal studies. SPIE Medical Imaging, 2015-02-24. Poster Presentation

14. A.D.M. Paish, H.N. Nikolov, I.D. Welch, D.W. Holdsworth. Development of a functional metal hip implant for a small animal model of osseointegration. London Imaging Discovery. 2014-06-26. Platform Presentation

15. A.D.M. Paish, H.N Nikolov, I.D. Welch, D.W. Holdsworth. Development of a novel functional orthopaedic implant for use in a rodent model of partial hip replacement.

Imaging Network Ontario Symposium. 2014-03-25. Platform Presentation, Poster Presentation (Award Winning)

16. A.D.M. Paish, I.D. Welch, D.W. Holdsworth. Development of a functional orthopaedic implant for a small animal model. London Health Research Day. 2014-03-18. Poster Presentation

17. A.D.M. Paish, H.N Nikolov, I.D. Welch, D.W. Holdsworth. Development of a novel functional orthopaedic implant for use in a rodent model of partial hip replacement. Imaging Network Ontario Symposium. 2013-06-13. Poster Presentation

18. A.D.M. Paish, H.N. Nikolov, S.I. Pollmann, J.U. Umoh, I.D. Welch, D.W. Holdsworth. Functional orthopaedic implants for small animal models. London Health Research Day. 2013-03-19. Poster Presentation

ADDITONAL WRITTEN CONTRIBUTIONS

1. Lawson Internal Research Fund Grant Fall 2012 Competition ($15,000 Awarded).

2. M. Guiler, S. Tian, A.D.M. Paish. Mustang Athlete Student Council Constitution. 2014-10-10. Supervising Author of the Official Constitution the Mustang Athlete Student Council at Western University

3. M. Guiler, S. Tian, Adam D.M. Paish, M. Bryant, T. Flaxman. Editors: C. Mathies, B. Emery, B. Cooper; Student Athlete Code of Conduct. Student-Athlete Handbook 2014-2015. Western Mustangs Athletics. 2014-09-04

4. A.D.M. Paish, A. Scarffe. What It Means To Be A Mustang: A Forum Discussion With The Mustangs Athlete Student Council. University of Western Ontario. 2014-03-06

CLINICAL SHADOWING

LONDON HEALTH SCIENCES CENTRE / ST JOSEPH'S HEALTH – London, Ontario, Canada

Clinical Fellow Aug. 2019 – Mar. 2020

- Shadowed orthopaedic surgeons in the operating room and in the clinic
- Identified 145 of unmet medical needs within Surgery, Paediatrics, Neuro-rehab and Internal Medicine

UNIVERSITY OF TEXAS MD ANDERSON CANCER CENTER – Houston, Texas, U.S.A.

Observer May 2013
- Shadowed physicians and surgeons in variety of fields, including G.I. oncology, interventional radiology, endoscopy, bronchoscopy, general surgery and thoracic surgery
- Gained a clinical understanding of various types of cancer treatments and interventions

LONDON HEALTH SCIENCES CENTRE – London, Ontario, Canada

Observer Feb. 2013
- Shadowed orthopaedic surgeons in the operating room and in the clinic
- Gained an understanding of a variety of lower limb orthopaedic interventions and care

FOWLER KENNEDY SPORTS MEDICINE CLINIC – London, Ontario, Canada

Volunteer Jan. 2009 – Mar. 2009
- Shadowed physiotherapists and assisted in administrative work at the clinic
- Gained an understanding of several specific tests and techniques for assessing musculoskeletal injuries

CREDIT VALLEY HOSPITAL – Mississauga, Ontario, Canada

Co-op Student/Volunteer Sep. 2007 – Aug. 2008
- Obtained over 500 hours of clinical experience observing care, treatment and medical procedures in ICU/CCU.
- Shadowed surgeons and anaesthesiologists in the OR during surgical procedures including total-knee replacement, arthroscopic ACL replacement, pulmonary resection, cataract removal, thyroid resection, total mastectomy and arthroscopic gall bladder removal

EXTRACURRICULAR AND COMMUNITY INVOLVEMENT

WESTERN UNIVERSITY - London, Ontario, Canada

Varsity Baseball Assistant Coach Jan. 2016 – Present
- Coach and mentor for elite level student athletes
- Design and order on field uniform apparel

WESTERN UNIVERSITY - London, Ontario, Canada

President – UWO Baseball Alumni Jan. 2016 – Present
- Connect team alumni with current players
- Organize annual alumni golf tournament and fundraiser

LONDON BADGERS BASEBALL – London, ON, Canada

Assistant Coach Mar. 2011 – Aug. 2017

- Coach youth AAA baseball players, specializing in pitching instruction
- Won Intercountry Baseball Association League Championship in 2011 and 2014

MUSTANGS ATHLETE STUDENT COUNCIL - London, ON, Canada

Founding President/Executive Advisor Apr. 2013 – Apr. 2014

- Aim is to ensure the success of student-athlete community outreach programs and social initiatives, in addition to advocacy for the student athlete community
- Plan future directions of the Council as it grows to become a leading voice for student-athletes

LONDON MAJORS BASEBALL – London, ON, Canada

Semi-Professional Athlete Jan. 2011 – Sept. 2011, Jan. 2015 – Aug. 2015

- Starting pitcher
- Led the Intercounty Baseball League (IBL) in 'complete games' during 2011 season, won IBL 'rookie pitcher of the year' and runner-up for 'rookie of the year' during 2011 season.

WESTERN UNIVERSITY – London, ON, Canada

Sr. Captain Nov. 2010 – Oct. 2015

- Varsity captain of 'Western Mustangs' baseball
- Assisted coaching staff in developing and executing team fundraising initiatives

JOINT MOTION PROGRAM (JuMP) - London, ON, Canada

Workshop Leader Jun. 2015

- Co-organized and lead a workshop about effective communication in a transdisciplinary research environment for JuMP summer students

JOINT MOTION PROGRAM (JuMP) - London, ON, Canada

Outreach Co-ordinator Feb. 2013 – 2014

- Involved in organising events involving JuMP and the Arthritis Society of Canada as well as social events for JuMP trainees

ROBARTS RESEARCH INSTITUTE – London, ON, Canada

Network of Imaging Students (NOISe) Representative Oct. 2012 – 2014

- Student society for graduate researchers working in the field of medical imaging

THE UNIVERSITY OF WESTERN ONTARIO – London, ON, Canada

Varsity Leaders Circle Vice-president Sep. 2012 – Apr. 2013

- Currently oversee Western's varsity student athlete council
- Aim is to ensure the success of student-athlete community outreach programs and social initiatives
- Plan future directions of the Circle as it expands on its impact within the Western student-athlete community and local London area

BOYS AND GIRLS CLUB OF PEEL REGION – Mississauga, ON, Canada

Youth Program Leader Jun. 2012 – Aug. 2012

- Planned and organized games and activities for the summer children's program at the Salvation Army's Peel Family Shelter
- Worked with 'high risk' children undergoing moderate to severe family issues

THE UNIVERSITY OF WESTERN ONTARIO – London, ON, Canada

Kinesiology School Advisory Council Member Sep. 2011 – Jun. 2012

- Student representative for Varsity Athletics and Student Health and Recreation Services
- Held a vote on all issues presented to the council by the School of Kinesiology including curriculum changes and procedural amendments

THE UNIVERSITY OF WESTERN ONTARIO – London, ON, Canada

Varsity Leaders Circle Social Committee Co-chair Sep. 2011 – Jun. 2012

- Created and hosted events designed to increase networking within the varsity student-athlete community

THE UNIVERSITY OF WESTERN ONTARIO – London, ON, Canada

Athletics Fundraising Ambassador Jun. 2011 – Sept. 2011

- Represented Western at the Canadian Baseball Hall of Fame induction
- Met with and contacted local business personnel to generate donations to the 'Adopt a Mustang' fundraising program

VOLUNTEER ECO STUDENTS ABROAD – Cornwall, ON, Canada

Volunteer May 2011 – Jun. 2011

- Worked with the 'Kichwa' native community in the Amazon, Ecuador as a construction worker and as an educational assistant

THE UNIVERSITY OF WESTERN ONTARIO – London, ON, Canada

Varsity Captains Circle Member Sep. 2010 – Aug. 2011

- Represented 'Western Mustangs Baseball' on the council of varsity captains (later became the Varsity Leaders Circle)
- Helped to plan and organize social events designed to increase networking within the varsity student-athlete community

EXTRACURRICULAR AWARDS AND RECOGNITIONS

THE UNIVERSITY OF WESTERN ONTARIO – London, ON, Canada

Top 10 Student Athlete Dec. 2014

- Selected to meet and run 4km with the Hon. Kathleen Wynne, Premier of Ontario and Matthew Brown, Mayor of London, Ontario as one of the top 10 highest achieving student athletes at Western

ONTARIO UNIVERSITY ATHLETICS – Hamilton, ON, Canada

Academic Achievement Award Winner Dec. 2008 - 2014

- 8-time award winner
- Awarded annually to student-athletes who achieve dean's honours list status while competing in a varsity sport for their respective university

BASEBALL CANADA – Ottawa, ON, Canada

National Baseball Championships Aug. 2010, Aug. 2013 and Aug. 2014

- As a starting pitcher for Ontario, won a silver (2010) and two bronze (2013, 2014) medal
- 2010 National Championship Game MVP

WESTERN MUSTANGS ATHLETICS – London, ON, Canada

Purple Blanket Award Winner Apr. 2013

- Awarded to the student athletes who, in the opinion of the Selection Committee at Western University, achieved superior distinction at the Provincial/National level of competition as representatives of Western
- Signifies a student athlete at Western who is amongst the top 1%, all-time

ONTARIO UNIVERSITY ATHLETICS – Hamilton, ON, Canada

Ontario University Pitcher of the Year Oct. 2010, 2012

- Awarded to the top university baseball pitcher in the Province of Ontario
- Selection based on a vote by all Ontario university baseball Managers

ONTARIO UNIVERSITY ATHLETICS – Hamilton, ON, Canada

First Team All-Star Oct. 2010, 2012

- Awarded to the top university student-athlete at his or her position in a particular varsity sport in the Province of Ontario
- Selection based on a vote by all Ontario university baseball Managers

COMMUNITY LIVING LONDON NIGHT OF HEROES– London, ON, Canada

Community Heroes Honouree Mar. 2012

- Recognition for contributions to the London, Ontario community through baseball and through work done to grow the Varsity Leader's Circle at Western University

ONTARIO UNIVERSITY ATHLETICS – Hamilton, ON, Canada

Second Team All-Star Oct. 2011

- Awarded to a university student-athlete to is one of the top players at his or her position in a particular varsity sport in the Province of Ontario